Arnab Majumdar

Master Thesis

A continuum shell formulation for anisotropic graphene structures and its comparison to molecular dynamics results

Arnab Majumdar

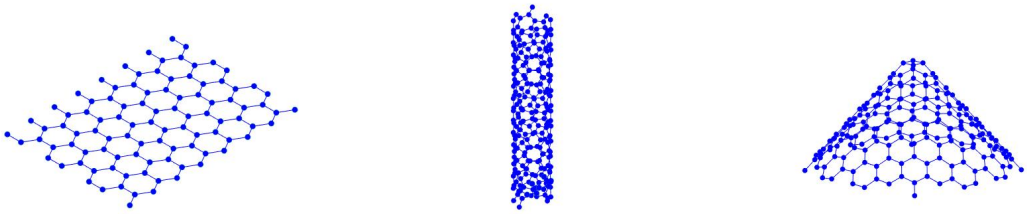

This thesis was supervised by:
Research assistant: Reza Ghaffari
Responsible professor: Prof. Roger A. Sauer
Aachen Institute for Advanced Study in Computational Engineering Science (AICES)
Rheinisch-Westflische Technische Hochschule, Aachen

Aachen Institute for Advanced Study in Computational Engineering Science | RWTH AACHEN UNIVERSITY

Abstract

Graphene is considered as one of the wonder materials of this century. Although it was first proposed in 1947 by P.R. Wallace for understanding the electronic properties of 3D graphite it came into physical existence only after Konstantin Novoselov and Andre Geim extracted a single-atom-thick crystalline from a bulk graphite in 2004. It is recognized as a semi metal, which has unique mechanical, thermal and electrical properties. Due to these unique properties, a lot of its potential applications have been discussed, like the early detection of cancer cells, space elevator, conversion of ocean water to drinkable water and so on. However, in order to have a good engineered solution for its application, a good mathematical model is required for prediction of its response under different conditions. In this work, the mechanical properties of graphene structure are studied and a hyper-elastic continuum model is used in order to predict its response under different loading condition. The continuum model is based on three invariants, two of which contributes to the isotropic deformation and the third one contributes to anisotropic response. The model is then implemented in a membrane formulation using Lagrange shape function and its response is studied under different loading condition. Finally, a molecular dynamic simulation for graphene structure is performed on a Carbon Nano Tube (CNT) structure created through MATLAB and its result is compared with the continuum mechanical result.

Acknowledgements

This work is conducted by the department of Aachen Institute for Advanced Study in Computational Engineering Science (AICES) and Rheinisch-Westflische Technische Hochschule Aachen (RWTH). I would like to give a special thank to the research group of Professor Roger A. Sauer, my supervisor Mr. Reza Ghaffari and my parents for their support.

List of Figures

Contents

Chapter 1

Introduction

Graphene has the potential of becoming the material that will open the gateway for our future. This is due to the fact that graphene and graphene based structures like Carbon Nano Tube (CNT) and Carbon Nano Cone (CNC) [3, 4, 5, 6, 7, 8] exhibit some exceptional mechanical [9, 10, 11], thermal [12, 13, 14, 15] and electrical [16, 17, 18, 19] behaviours. These material properties can be used for various applications like the development of sensors [20], energy storage devices [21] and healthcare facilities [22]. Graphene can also be used in the fight against corrosion with the development of corrosion resistant coating [23]. Another potential area of application is the design of composites. Graphene can be used for the improvement of mechanical, thermal and electrical properties of composites [24, 25, 26, 27, 28]. Graphene based structures like CNT and CNC can also be used for different applications because of their superior material properties. These structures are manufactured through the rolling of graphene sheets [29, 30]. However all these applications can be achieved to their full potential only if we can have good analysis methods for the simulation of such structures. Therefore in this work an effort has been made to obtain a good analysis method to describe the mechanical properties of graphene.

There are different approaches in trial for modelling the mechanical properties of graphene. The Cauchy-Born rule applied to inter molecular potential is one them. Arroyo and Belytschko [31] applied exponential Cauchy-Born rule for CNT structures, whereas Guo et.al. [32] and Wang et. al. [33] used higher order Cauchy-Born rule for the same problem. For Single Walled Carbon Nano Tube (SWCNC), Yan et. al. proposed [34] a higher order gradient continuum theory and Tersoff-Brenner potential. Shenoy et. al. [35] and Yan et. al. [36] used Quasi-Continuum approach for the simulation of buckling and post-buckling behaviour for CNCs. This approach was further extended with temperature dependency within the work of Wang et. al. [37], where a CNC structure is subjected to uni-axial compression. Apart from Molecular and quasi continuum, classical continuum mechanical approaches are also considered for modelling within different works. Considering linear isotropy, these approaches gained popularity. For example, Firouz-Abadi et. al. [38] analyse the natural frequencies of nano cones assuming linear isotropy and using classical continuum theories. This work is further extended to stability analysis, when subjected to external pressure and axial loads within the work of R. Firouz-Abadi et. al. [39]. Furthermore, Gandomani et. al. [40] worked on the stability analysis of a CNC

conveying fluid. In the work of Lee and Lee [29], FE methods are employed to find out the natural frequencies of CNC and CNT structures, where the interaction of carbon atoms are modelled with continuum frame elements. Although the assumption of linear isotropy works for small deformation, graphene and graphene related structures also exhibit anisotropic behaviour under large deformation. Sfyris et. al. [41, 41] use Taylor series expansion and propose a set of invariants based on lattice structure to formulate the strain energy functional. Delfani et. al. [42, 43, 44] use the symmetry operator to elasticity tensor along with the Taylor series expansion in order to reduce the number of independent variables. Kumar and Parks [45] develop a membrane model with logarithmic strain, which is further improved by Ghaffari et. al. [46], where it is formulated based on right Cauchy-Green tensor. In this work, the material from Ghaffari et. al. [46] is implemented in the membrane formulation.

Within this document, chapter 2 discusses the theory of membrane formulation. Chapter 3 discusses the material model of graphene that incorporates the anisotropic behaviour of graphene under large deformation. Chapter 4 discusses the basics of molecular dynamic simulation as well as the algorithms for the generation of Graphene based structures, like sheet, CNT and CNC. Finally the Molecular Dynamic result is compared with the continuum result.. Finally, chapter 5 the results of both simulations and comparison of result.

Chapter 2

Shell Formulation

In this section the continuum mechanical approach of modelling the behaviour of graphene is discussed. Within this approach, materials are assumed to be continuous in space. Since graphene is a 2D material, its efficient to model it as shell. Shell structures are computationally different than 3D bodies. In this section, the geometry, kinematics and balance laws for shell structures are discussed. The finite element discretization is then applied on these formulations.

2.1 Geometry of shell structure

Figure 2.1 shows a shell structure is being deformed from a configuration $\mathcal{S}_0$ to a configuration $\mathcal{S}$. As shown in this figure, the shell structures denoted by surface $\mathcal{S}_0$ and surface $\mathcal{S}$ can be seen as mappings from a master domain $\mathcal{P}$ and therefore can be parametrically denoted by

$$\boldsymbol{x} = \boldsymbol{x}\left(\xi^1, \xi^2\right), \tag{2.1}$$

$$\boldsymbol{X} = \boldsymbol{X}\left(\xi^1, \xi^2\right) \tag{2.2}$$

respectively. Here, (ξ^1, ξ^2) corresponds to a point in the parameter domain $\mathcal{P}$, which is mapped by equation 2.1 and 2.2 to material points $\boldsymbol{x} \in \mathcal{S}$ and $\boldsymbol{X} \in \mathcal{S}_0$ respectively. $\mathcal{S}$ refers to the deformed configuration of the surface, i.e. the current configuration and $\mathcal{S}_0$ refers to the undeformed one, i.e. the reference configuration. In further text, Latin letters (e.g. i, j, k. ...) will be used for the components of 3 dimensional vectors and tensors and will take a value of 1,2 and 3. Likewise, Greek letters (e.g. α, β, ...) will be used for the components of 2 dimensional vectors and tensors and will take a value of 1 and 2. Considering Einstein's notation, repeated indices imply summation over indices, see [47]. Therefore, the tangent vectors at a point $\boldsymbol{x}$ and $\boldsymbol{X}$ are expressed as

$$\boldsymbol{a}_{\boldsymbol{\alpha}} = \frac{\partial \boldsymbol{x}}{\partial \xi^{\alpha}}, \tag{2.3}$$

$$\boldsymbol{A}_{\boldsymbol{\alpha}} = \frac{\partial \boldsymbol{X}}{\partial \xi^{\alpha}} \tag{2.4}$$

for the current configuration and reference configuration respectively. These sets of two tangent vectors form a basis for the tangent plane at a particular location in

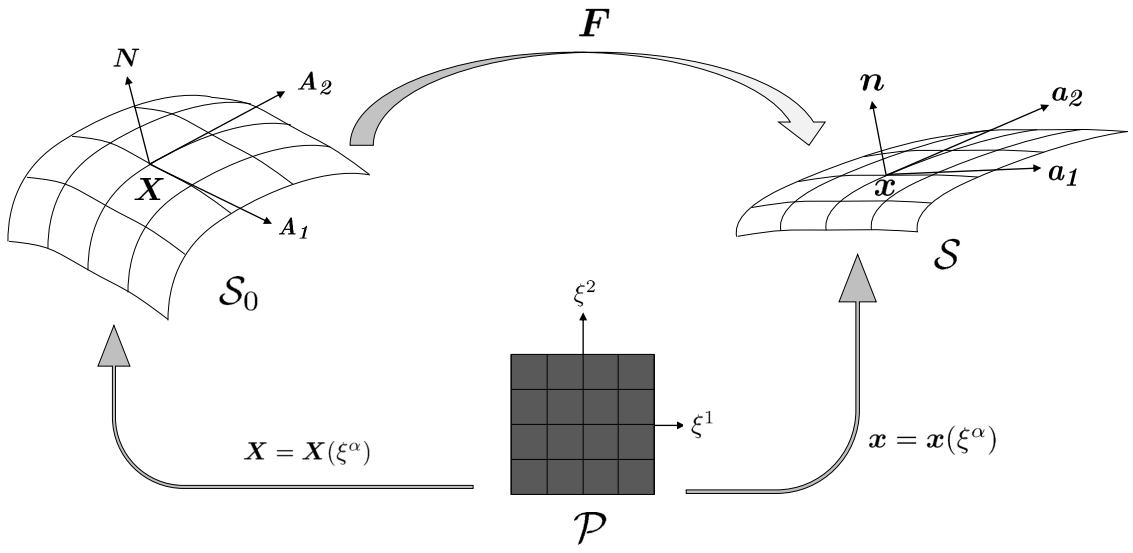

Figure 2.1: Mapping of parameter domain $\mathcal{P}$ to reference surface $\mathcal{S}_0$ and current surface $\mathcal{S}$

their respective configuration. However, they are not orthonormal in general. The co-variant components of these metric tensors are

$$a_{\alpha\beta} = \boldsymbol{a_\alpha} \cdot \boldsymbol{a_\beta}, \tag{2.5}$$
$$A_{\alpha\beta} = \boldsymbol{A_\alpha} \cdot \boldsymbol{A_\beta}. \tag{2.6}$$

This contra-variant components can be obtained through the inversion of metric tensors.

$$\left[a^{\alpha\beta}\right] = \left[a_{\alpha\beta}\right]^{-1}, \tag{2.7}$$
$$\left[A^{\alpha\beta}\right] = \left[A_{\alpha\beta}\right]^{-1}. \tag{2.8}$$

Using these contra-variant components, we obtain the dual basis of the aforementioned tangent plane as

$$\boldsymbol{a^\alpha} = a^{\alpha\beta}\boldsymbol{a_\beta}, \tag{2.9}$$
$$\boldsymbol{A^\alpha} = A^{\alpha\beta}\boldsymbol{A_\beta}. \tag{2.10}$$

It may be noted that the following condition has to be satisfied

$$\boldsymbol{a_\alpha} \cdot \boldsymbol{a^\beta} = \boldsymbol{A_\alpha} \cdot \boldsymbol{A^\beta} = \delta^\beta_\alpha, \tag{2.11}$$

where δ^β_α is the Kronecker delta.

The normal vectors of the tangent plane of the current and reference configuration can then be represented as

$$\boldsymbol{n} = \frac{\boldsymbol{a_1} \times \boldsymbol{a_2}}{||\boldsymbol{a_1} \times \boldsymbol{a_2}||} = \frac{\boldsymbol{a_1} \times \boldsymbol{a_2}}{\sqrt{\det a_{\alpha\beta}}}, \tag{2.12}$$
$$\boldsymbol{N} = \frac{\boldsymbol{A_1} \times \boldsymbol{A_2}}{||\boldsymbol{A_1} \times \boldsymbol{A_2}||} = \frac{\boldsymbol{A_1} \times \boldsymbol{A_2}}{\sqrt{\det A_{\alpha\beta}}}. \tag{2.13}$$

Therefore $\{\boldsymbol{a_1}, \boldsymbol{a_2}, \boldsymbol{n}\}$ and $\{\boldsymbol{A_1}, \boldsymbol{A_2}, \boldsymbol{N}\}$ represent the sets of basis vectors in the current and reference configuration, respectively. The corresponding dual bases are $\{\boldsymbol{a^1}, \boldsymbol{a^2}, \boldsymbol{n}\}$ and $\{\boldsymbol{A^1}, \boldsymbol{A^2}, \boldsymbol{N}\}$. General vectors $\boldsymbol{v}$ on $\mathcal{S}$ can be represented as

$$\boldsymbol{v} = v^\alpha \boldsymbol{a}_\alpha + v_n \boldsymbol{n} = v_\alpha \boldsymbol{a}^\alpha + v_n \boldsymbol{n} \tag{2.14}$$

Here v^α, v_α are co-variant and contra-variant components, respectively. The parametric derivative of a vector $\boldsymbol{v}$ can be represented by

$$\boldsymbol{v}_{,\alpha} = \frac{\partial \boldsymbol{a}_\alpha}{\partial \xi^\alpha}. \tag{2.15}$$

Apart from the parametric derivative, one more derivative is required for further calculations. It is named the co-variant derivative and is defined by

$$\boldsymbol{v}_{;\alpha} = (\boldsymbol{n} \otimes \boldsymbol{n})\, \boldsymbol{v}_{,\alpha}. \tag{2.16}$$

For example the co-variant derivative of tangent vector $\boldsymbol{a_\alpha}$ can be computed as

$$\boldsymbol{a_\alpha}_{;\beta} = \boldsymbol{a_\alpha}_{,\beta} - \Gamma^\gamma_{\alpha\beta} \boldsymbol{a_\gamma}. \tag{2.17}$$

$\Gamma^\gamma_{\alpha\beta}$ introduced in equation 2.17, is known as the Christoffel symbol of second kind and can be computed as $\Gamma^\gamma_{\alpha\beta} = \boldsymbol{a_\alpha}_{,\beta} \cdot \boldsymbol{a}^\gamma$. The out-of-plane component of the derivative is known as the curvature tensor and is denoted as $b_{\alpha\beta}$.

$$b_{\alpha\beta} = \boldsymbol{n} \cdot \boldsymbol{a_\alpha}_{;\beta} = \boldsymbol{n} \cdot \boldsymbol{a_\alpha}_{,\beta} \tag{2.18}$$

The eigenvalues of this tensor are the principle curvatures of the surface $\mathcal{S}$, which can be given as

$$\kappa_{1,2} = H \pm \sqrt{H^2 - \kappa}, \tag{2.19}$$

where $H = a^{\alpha\beta} b_{\alpha\beta}$ is the mean curvature and $\kappa = \det[b_{\alpha\beta}] / \det[a_{\alpha\beta}] = b/a$ is the Gaussian curvature.

The identity tensor on the surface $\mathcal{S}$ is different from the 3D identity tensor and can be computed as

$$\mathbf{1} = \boldsymbol{a_\alpha} \otimes \boldsymbol{a^\alpha} = \boldsymbol{a^\alpha} \otimes \boldsymbol{a_\alpha} = \tilde{\mathbf{1}} - \boldsymbol{n} \otimes \boldsymbol{n}. \tag{2.20}$$

$\tilde{\mathbf{1}}$ introduced in equation 2.20 denotes the 3D identity tensor.

2.2 Kinematics of shell structure

In this section deformation of a shell structure is discussed and a relation is developed between the current and reference configuration, mentioned in section 2.1. As a starting point, let us consider a small line element $d\boldsymbol{X}$ in the reference configuration, which deforms to the current configuration and becomes $d\boldsymbol{x}$. Using equation 2.1, 2.2, 2.3 and 2.4 we may say

$$d\boldsymbol{X} = \frac{\partial \boldsymbol{X}}{\partial \xi^\alpha} d\xi^\alpha = \boldsymbol{A_\alpha} d\xi^\alpha, \tag{2.21}$$

$$d\boldsymbol{x} = \frac{\partial \boldsymbol{x}}{\partial \xi^\alpha} d\xi^\alpha = \boldsymbol{a_\alpha} d\xi^\alpha. \tag{2.22}$$

Further using equation 2.21, we may say,

$$\begin{aligned} d\boldsymbol{X} \cdot \boldsymbol{A}^{\boldsymbol{\beta}} &= \boldsymbol{A}_{\boldsymbol{\alpha}} d\xi^{\alpha} \cdot \boldsymbol{A}^{\boldsymbol{\beta}} \\ &= \delta^{\beta}_{\alpha} d\xi^{\alpha} \\ \Rightarrow d\boldsymbol{X} \cdot \boldsymbol{A}^{\boldsymbol{\alpha}} &= d\xi^{\alpha}. \end{aligned} \tag{2.23}$$

Now inserting equation 2.23 into equation 2.22, we get

$$\begin{aligned} d\boldsymbol{x} &= \boldsymbol{a}_{\boldsymbol{\alpha}} \left(d\boldsymbol{X} \cdot \boldsymbol{A}^{\boldsymbol{\alpha}} \right) \\ &= \left(\boldsymbol{a}_{\boldsymbol{\alpha}} \otimes \boldsymbol{A}^{\boldsymbol{\alpha}} \right) d\boldsymbol{X}. \end{aligned} \tag{2.24}$$

Equation 2.24 shows the relationship between the reference and the current configuration, where the tensor

$$\mathbf{F} = \boldsymbol{a}_{\boldsymbol{\alpha}} \otimes \boldsymbol{A}^{\boldsymbol{\alpha}} \tag{2.25}$$

is the surface deformation gradient that maps $\boldsymbol{x} \rightarrow \boldsymbol{X}$. The inverse mapping $\mathbf{F}^{-1} = \boldsymbol{A}_{\alpha} \otimes \boldsymbol{a}^{\alpha}$ can be found through a similar approach. Therefore, the tangent vectors for both configurations, described in equation 2.5, 2.4, 2.9 and 2.10 can be related as

$$\begin{aligned} \boldsymbol{a}_{\boldsymbol{\alpha}} &= \mathbf{F}\, \boldsymbol{A}_{\boldsymbol{\alpha}}, \\ \boldsymbol{A}_{\boldsymbol{\alpha}} &= \mathbf{F}^{-1} \boldsymbol{a}_{\boldsymbol{\alpha}}, \\ \boldsymbol{a}^{\boldsymbol{\alpha}} &= \mathbf{F}^{-T} \boldsymbol{A}^{\boldsymbol{\alpha}}, \\ \boldsymbol{A}_{\boldsymbol{\alpha}} &= \mathbf{F}^{T} \boldsymbol{a}_{\boldsymbol{\alpha}}. \end{aligned} \tag{2.26}$$

The right and left Cauchy-Green tensors and their inverses can be written as

$$\begin{aligned} \mathbf{C} &= \mathbf{F}^{T}\mathbf{F} = a_{\alpha\beta} \boldsymbol{A}^{\alpha} \otimes \boldsymbol{A}^{\beta}, \\ \mathbf{C}^{-1} &= a^{\alpha\beta} \boldsymbol{A}_{\alpha} \otimes \boldsymbol{A}_{\beta}, \\ \mathbf{B} &= \mathbf{F}\mathbf{F}^{T} = A^{\alpha\beta} \boldsymbol{a}_{\alpha} \otimes \boldsymbol{a}_{\beta}, \\ \mathbf{B}^{-1} &= A_{\alpha\beta} \boldsymbol{a}^{\alpha} \otimes \boldsymbol{a}^{\beta}. \end{aligned} \tag{2.27}$$

In order to understand the stretching of the surface between $\mathcal{S}_0$ and $\mathcal{S}$, an area element $da \subset \mathcal{S}$ is taken whose area can be calculated as

$$da = \left|\left| \left(\boldsymbol{a_1} d\xi^1 \right) \times \left(\boldsymbol{a_2} d\xi^2 \right) \right|\right| = ||\boldsymbol{a_1} \times \boldsymbol{a_2}||\, d\square = \sqrt{\det a_{\alpha\beta}}\, d\square. \tag{2.28}$$

$d\square = d\xi^1 d\xi^2$ introduced here, represents the corresponding area element in master domain $\mathcal{P}$. Same kind of relation can be written for $dA \subset \mathcal{S}_0$. Therefore considering equations 2.12, 2.13 and 2.28, we may write

$$\begin{aligned} dA &= J_A d\square, \quad J_A = \sqrt{\det A_{\alpha\beta}}, \\ da &= J_a d\square, \quad J_a = \sqrt{\det a_{\alpha\beta}}, \\ da &= J dA, \quad J = \frac{J_a}{J_A}. \end{aligned} \tag{2.29}$$

2.3 Equilibrium of Shells

In this section, the balance laws of forces and moments for a shell as shown in figure 2.2 are discussed.

In order to identify the section forces or moments let's start with an infinitesimal small element da located at $\boldsymbol{x}$ as shown in figure 2.2. Edges of this small element are aligned along $\boldsymbol{a_1}$ and $\boldsymbol{a_2}$. On the cut surface, the in-plane and out-of-plane components of section forces are denoted as $N^{\alpha\beta}$ and S^{α} respectively. These components are shown in the right hand inset of figure 2.2 Therefore collecting all the section forces, the stress tensor can be written as

$$\boldsymbol{\sigma} = N^{\alpha\beta}\boldsymbol{a_\alpha} \otimes \boldsymbol{a_\beta} + S^{\alpha}\boldsymbol{a_\alpha} \otimes \boldsymbol{n}. \tag{2.30}$$

Now applying Cauchy's formula, we can say that the traction vector $\boldsymbol{T}$ for a section cut normal to $\boldsymbol{\nu}$ can be given as

$$\boldsymbol{T} = \boldsymbol{\sigma}^{\mathrm{T}}\boldsymbol{\nu} \tag{2.31}$$

In figure 2.2, the section is cut perpendicular to $\boldsymbol{a^\alpha}$. Therefore, $\boldsymbol{\nu} = \nu_\alpha \boldsymbol{a^\alpha}$ is the vector normal to the cut surface and the components of the traction vector is

$$\boldsymbol{T}^{\alpha} = \boldsymbol{\sigma}^{\mathrm{T}}\boldsymbol{a^\alpha} = N^{\alpha\beta}\boldsymbol{a_\beta} + s^{\alpha}\boldsymbol{n}. \tag{2.32}$$

Similarly, distributed section moments $M^{\alpha\beta}$ are collected to create the moment tensor

$$\boldsymbol{\mu} = -M^{\alpha\beta}\boldsymbol{a_\alpha} \otimes \boldsymbol{a_\beta}. \tag{2.33}$$

Components of $-\mathbf{M}^{\alpha}$ is shown in the middle inset of figure 2.2. The distributed moment vector at the section can be defined as

$$\boldsymbol{M} = \boldsymbol{\mu}^{\mathrm{T}}\boldsymbol{\nu}, \tag{2.34}$$

whose components are

$$\boldsymbol{M}^{\alpha} = -M^{\alpha\beta}\boldsymbol{a_\beta}. \tag{2.35}$$

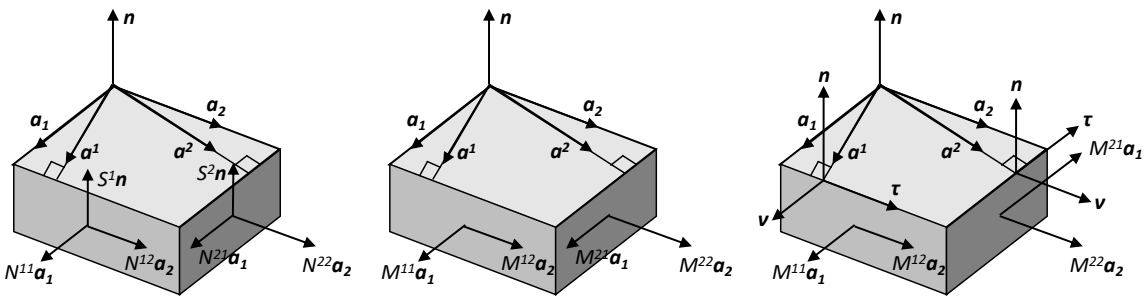

Figure 2.2: Mapping of parameter domain $\mathcal{P}$ to reference surface $\mathcal{S}_0$ and current surface $\mathcal{S}$

However $\boldsymbol{M}$ is introduced here only for convenience. The moment physically acting on the element is given by a rotated quantity

$$\boldsymbol{m} = \boldsymbol{n} \times \boldsymbol{M}. \tag{2.36}$$

Breaking $\boldsymbol{m}$ into components, it can be expressed as

$$\boldsymbol{m} = m_\nu \boldsymbol{\nu} + m_\tau \boldsymbol{\tau}. \tag{2.37}$$

These components are shown in the right hand inset of figure 2.2. m_ν and m_τ are in-plane and out-of-plane components, respectively. Considering the identity

$$\boldsymbol{a_\beta} \times \boldsymbol{n} = \tau_\beta \boldsymbol{\nu} - \nu_\beta \boldsymbol{\tau}, \tag{2.38}$$

m_ν and m_τ can be formulated as

$$\begin{aligned} m_\nu &= M^{\alpha\beta} \nu_\alpha \tau_\beta \\ m_\tau &= -M^{\alpha\beta} \nu_\alpha \nu_\beta \end{aligned} \tag{2.39}$$

The vector $\boldsymbol{M}$ can also be written in terms of m_ν and m_τ as

$$\boldsymbol{M} = m_\tau \boldsymbol{\nu} - m_\nu \boldsymbol{\tau}. \tag{2.40}$$

In order to construct the equation for balance of momentum, let us consider a part of surface $\mathcal{S}$, which is denoted by $d\mathcal{S}$. The body force acting per unit surface area of $d\mathcal{S}$ is denoted as $\boldsymbol{f}$. For the balance of momentum we assume that the boundary of $d\mathcal{S}$ should be smooth. As per Newton's first law of motion the change of momentum for $d\mathcal{S}$ can be equated to the summation of forces acting on $d\mathcal{S}$. Hence,

$$\frac{D}{Dt} \int_{d\mathcal{S}} \rho \boldsymbol{v} da = \int_{d\mathcal{S}} \boldsymbol{f} da + \int_{\partial d\mathcal{S}} \boldsymbol{T} ds \quad \forall d\mathcal{S} \subset \mathcal{S}. \tag{2.41}$$

In the local form, equation 2.41 can be written as

$$\boldsymbol{T^\alpha}_{;\alpha} + \boldsymbol{f} = \rho \dot{\boldsymbol{v}} \quad \forall \boldsymbol{x} \in \mathcal{S}. \tag{2.42}$$

This is also known as the strong form of momentum balance at $\boldsymbol{x} \in d\mathcal{S}$. This can be further decomposed into in-plane and out-of-plane components. considering $\boldsymbol{f} = f^\alpha \boldsymbol{a_\alpha} + p\boldsymbol{n}$ and $\dot{\boldsymbol{v}} = a = a^\alpha \boldsymbol{a_\alpha} + a_n \boldsymbol{n}$ the in-plane and out-of-plane equilibrium equation for momentum can be expressed as

$$\begin{aligned} N^{\gamma\alpha}{}_{;\gamma} - b^\alpha_\gamma S^\gamma + f^\alpha &= \rho a^\alpha, \\ S^\gamma{}_{;\gamma} + N^{\alpha\gamma} b_{\alpha\gamma} + p &= \rho a_n \end{aligned} \tag{2.43}$$

respectively. For the derivation, see [48].

Similar to the balance of linear momentum, the balance of angular momentum can be formulated by equating the change in angular momentum and sum of all

external moments acting on $d\mathcal{S}$. The equation for the balance of momentum can therefore be expressed as

$$\frac{D}{Dt}\int_{\mathcal{S}} \rho \boldsymbol{x} \times \boldsymbol{v} da = \int_{\mathcal{S}} \boldsymbol{x} \times \boldsymbol{f} da + \int_{\partial\mathcal{S}} \boldsymbol{x} \times \boldsymbol{T} ds + \int_{\partial\mathcal{S}} \boldsymbol{m} ds \quad \forall d\mathcal{S} \subset \mathcal{S}. \tag{2.44}$$

Equation 2.44 can also be written as

$$\int_{\mathcal{S}} \boldsymbol{a_\alpha} \times \left[\left(N^{\alpha\beta} - b^\beta_\gamma M^{\gamma\alpha} \right) \boldsymbol{a_\beta} + \left(S^\alpha + M^{\beta\alpha}{}_{;\beta} \right) \boldsymbol{n} \right] da = \boldsymbol{0}. \tag{2.45}$$

For the derivation of this form, interested readers are referred to [48]. It can clearly be understood that equation 2.45 can be true if and only if

$$\sigma^{\alpha\beta} = N^{\alpha\beta} - b^\beta_\gamma M^{\gamma\alpha}, \tag{2.46}$$

$$S^\alpha = -M^{\beta\alpha}{}_{;\beta}\,. \tag{2.47}$$

Equations 2.46 and 2.46 show that $\sigma^{\alpha\beta}$ and $M^{\alpha\beta}$ are symmetric. This means that the in-plane components of Cauchy stress, i.e. $N^{\alpha\beta}$ are generally not symmetric. This is due to the fact that the in-plane components of Cauchy stress are affected by the bending as well. However in some cases, the in-plane components are also symmetric.

At the boundary of the shell, two types of boundary condition can be applied. One is the Dirichlet boundary condition for displacement and another is the Neumann boundary condition for tractions and bending moments. However, the Kirchhoff-Love theory does not allow the forces and the bending moments to be applied independently. This is due the fact that the component m_ν introduced in equation 2.37 is actually part of traction force $\mathbf{T}$. Therefore considering $\boldsymbol{\nu} = \boldsymbol{\tau} \times \mathbf{n}$ and $\boldsymbol{\tau} = \frac{\partial \boldsymbol{x}}{\partial s}$, it can be formulated that

$$m_\nu \boldsymbol{\nu} = (m_\nu \times \boldsymbol{n})' - \boldsymbol{x} \times (m_\nu \boldsymbol{n})'\,, \tag{2.48}$$

where $(...)' = \frac{\partial}{\partial s}$. Now inserting equation 2.48 into the last two terms of equation 2.44 and considering that the first part of equation 2.48 integrates to zero over a smooth boundary we get

$$\int_{\partial d\mathcal{S}} (\boldsymbol{x} \times \boldsymbol{T} + \boldsymbol{m})\, ds = \int_{\partial d\mathcal{S}} (\boldsymbol{x} \times \boldsymbol{t} + m_\tau \boldsymbol{\tau})\, ds. \tag{2.49}$$

So $\boldsymbol{t}$ introduced in equation 2.49 can be termed as the effective traction, which can be formulated as

$$\boldsymbol{t} = \boldsymbol{T} - (m_\nu \boldsymbol{n})'\,. \tag{2.50}$$

Therefore, the boundary conditions on the shell boundary $\partial\mathcal{S} = \partial_x\mathcal{S} \cup \partial_t\mathcal{S} \cup \partial_m\mathcal{S}$ can be specified as

$$\begin{aligned} &\boldsymbol{x} = \bar{\boldsymbol{\varphi}} \text{ on } \partial_x\mathcal{S}, \\ &\boldsymbol{t} = \bar{\boldsymbol{t}} \text{ on } \partial_t\mathcal{S}, \\ &\boldsymbol{m_\tau} = \bar{\boldsymbol{m}}_{\boldsymbol{\tau}} \text{ on } \partial_m\mathcal{S}, \end{aligned} \tag{2.51}$$

where $\bar{\boldsymbol{\varphi}}(\boldsymbol{X})$, $\bar{\boldsymbol{t}}(\boldsymbol{X})$ and $\bar{\boldsymbol{m}}_{\boldsymbol{\tau}}(\boldsymbol{X})$ are the boundary conditions.

In this work, graphene is considered as a membrane, not a shell. In case of a membrane $M^{\alpha\beta}$ and S^{α} is zero. Therefore, $N^{\alpha} = \sigma^{\alpha\beta}$ and $\boldsymbol{t} = \boldsymbol{T}$. The stress and traction can then be expressed as

$$\boldsymbol{\sigma} = \sigma^{\alpha\beta}\boldsymbol{a}_{\boldsymbol{\alpha}} \otimes \boldsymbol{a}_{\boldsymbol{\beta}}, \tag{2.52}$$

$$\boldsymbol{T}^{\boldsymbol{\alpha}} = \sigma^{\alpha\beta}\boldsymbol{a}_{\boldsymbol{\beta}}. \tag{2.53}$$

The equation 2.42 for balance of linear momentum can be used for membrane also but equation 2.43 can be simplified. The equations discussed hereafter will be applicable for more specific case of membrane.

2.4 Constitution of the membrane

In this section, the first and second law of thermodynamics will be applied to the membrane structure respectively.Consider hyperelasticity the constitution of the membrane structure will be discussed.

The first law of thermodynamics talks about energy conservation. In our case, this enforces the balance of mechanical power for the membrane structure. This is formulated by contracting equation 2.42 with velocity $\boldsymbol{v}$ and thereafter integrating over $\boldsymbol{d\mathcal{S}} \subset \mathcal{S}$, we get

$$\int_{d\mathcal{S}} \boldsymbol{v}.\left(\boldsymbol{T}^{\boldsymbol{\alpha}}{}_{;\alpha} + \boldsymbol{f} - \rho\dot{\boldsymbol{v}}\right) da = 0 \quad \forall d\mathcal{S} \in \mathcal{S}. \tag{2.54}$$

Equation 2.54 can be rewritten in the form of energy conservation as

$$\dot{K} + P_{\text{int}} = P_{\text{ext}}, \tag{2.55}$$

where K is kinetic energy, P_{int} is the internal energy of the membrane structure and P_{ext} is the energy due to the external forces and moments. These quantities can be formulated as

$$K = \frac{1}{2}\int_{d\mathcal{S}} \rho\boldsymbol{v}.\boldsymbol{v}da, \tag{2.56}$$

$$P_{\text{int}} = \frac{1}{2}\int_{d\mathcal{S}} \sigma^{\alpha\beta}\dot{a}_{\alpha\beta}da, \tag{2.57}$$

$$P_{\text{ext}} = \int_{d\mathcal{S}} \boldsymbol{v}.\boldsymbol{f}da + \int_{\partial d\mathcal{S}} \boldsymbol{v}.\boldsymbol{T}ds. \tag{2.58}$$

A detailed derivation of equations 2.56 to 2.58 can be found in [48].

The second law of thermodynamics state that energy input to an isolated system is always greater than or equal to the energy output retrieved out of it, i.e. there is no system with more than 100% efficiency. In order to formulate this in our case, we need to covert equation 2.57 to the reference configuration. That means, equation 2.57 becomes

$$P_{\text{int}} = \frac{1}{2}\int_{d\mathcal{S}_0} \tau^{\alpha\beta}\dot{a}_{\alpha\beta}dA, \tag{2.59}$$

where

$$\tau^{\alpha\beta} = J\sigma^{\alpha\beta}. \tag{2.60}$$

Therefore the second law of thermodynamics is expressed by the inequality

$$\frac{1}{2}\tau^{\alpha\beta}\dot{a}_{\alpha\beta} - \dot{\Psi} \geq 0, \tag{2.61}$$

where ψ is the Helmholtz free energy of the membrane. In our case, we consider a conservative system, which is going through a cyclic process at a fixed temperature. That means $\dot{\psi} = \dot{W}$ and there will be no mechanical dissipation. Equation 2.61 can therefore be amended as

$$\frac{1}{2}\tau^{\alpha\beta}\dot{a}_{\alpha\beta} - \dot{W} = 0. \tag{2.62}$$

In the case of a membrane, the strain energy function W can be represented as a function of $a_{\alpha\beta}$. That means,

$$W = W\left(a_{\alpha\beta}\right). \tag{2.63}$$

Chapter 3 discusses about the function W for graphene structure in detail. However, substituting equation 2.63 into equation 2.62 we get,

$$\tau^{\alpha\beta} = 2\frac{\partial W}{\partial a_{\alpha\beta}}. \tag{2.64}$$

Equation 2.64 can be considered as the equation of membrane constitution. For the implementation of a finite element formulation we further require a variation of W, i.e. δW and a linearization of δW. These can be written,

$$\delta W = \frac{1}{2}\tau^{\alpha\beta}\delta a_{\alpha\beta}, \tag{2.65}$$

$$\Delta\delta W = c^{\alpha\beta\gamma\delta}\delta\frac{1}{2}a_{\alpha\beta}\frac{1}{2}\Delta a_{\gamma\delta}, \tag{2.66}$$

where

$$c^{\alpha\beta\gamma\delta} = 4\frac{\partial^2 W}{\partial a_{\alpha\beta}\partial a_{\gamma\delta}}. \tag{2.67}$$

2.5 Finite element formulation

In this section, the finite element formulation of the equilibrium equation 2.42 is discussed. However before we apply the finite element formulation on equation 2.42, it needs to be converted into its weak form. In order to do so, we need to contract it with variation of displacement $\boldsymbol{\delta x} \in \mathcal{V}$ and integrate over the whole domain. The procedure is same as equation 2.54 but the difference is, $\boldsymbol{v}$ will be replaced with $\boldsymbol{\delta x}$. Therefore, the weak form can be written as

$$G_{\text{in}} + G_{\text{int}} - G_{\text{ext}} = 0, \tag{2.68}$$

where

$$G_{in} = \int_{\mathcal{S}_0} \boldsymbol{\delta x}.\rho_0 \dot{\boldsymbol{v}} dA, \tag{2.69}$$

$$G_{\text{int}} = \int_{\mathcal{S}_0} \frac{1}{2} \delta a_{\alpha\beta} \tau^{\alpha\beta} dA, \tag{2.70}$$

$$G_{\text{ext}} = \int_{\mathcal{S}} \boldsymbol{\delta x}.\boldsymbol{f} da + \int_{\partial \mathcal{S}} \boldsymbol{\delta x}.\boldsymbol{T} da \tag{2.71}$$

In this work, we consider only a static case. Therefore, G_{in} can be ignored for our case. This means, equation 2.68 becomes

$$G_{\text{int}} - G_{\text{ext}} = 0. \tag{2.72}$$

For the implementation of a finite element formulation, the surface $\mathcal{S}_0$ is divided into discrete elements denoted by Ω_0^e. These elements are mathematically defined by their corner points or nodal points, which are denoted by $\boldsymbol{X}_I$. The deformation of a membrane is denoted by a mapping of $\boldsymbol{X}_I$ into the deformed configuration. This mapping can be mathematically describes as $\boldsymbol{X}_I \leftarrow \boldsymbol{x}_I$. $\mathcal{S}_0$ are mapped into the deformed configuration as Ω^e. In this work, only quadrilateral elements are considered, since it is easier to relate them to the master element in the parameter domain $\xi^\alpha \in [-1, 1]$. The position vectors $\boldsymbol{X}$ and $\boldsymbol{x}$ can be approximated as $\boldsymbol{X}^h$ and $\boldsymbol{x}^h$ within the elements Ω_0^e and Ω^e respectively. The approximation can be formulated as

$$\boldsymbol{X} \approx \boldsymbol{X}^h = \sum_I N_I \boldsymbol{X}_I, \tag{2.73}$$

$$\boldsymbol{x} \approx \boldsymbol{x}^h = \sum_I N_I \boldsymbol{x}_I, \tag{2.74}$$

where $N_I\left(\xi^1, \xi^2\right)$ are shape functions, which is defined on the parameter space of the master element and $\boldsymbol{X}$ and $\boldsymbol{x}$ are the position vectors at the nodes in the reference configuration and current configuration respectively. The summation coefficient I varies from 1 to n_{ne}, where n_{ne} is the total number of nodes. The shape functions are formulated based on the nodes of master elements. Some types of master elements are the 4-noded linear Lagrange elements, 9-noded quadratic Lagrange elements, quadratic NURBS elements and cubic T-spline elements. In our case, we will consider the 4-noded linear Lagrange elements. Therefore, the shape functions can be written as

$$\begin{aligned} N_1 &= \frac{\left(1-\xi^1\right)\left(1-\xi^2\right)}{4}, \\ N_2 &= \frac{\left(1+\xi^1\right)\left(1-\xi^2\right)}{4}, \\ N_3 &= \frac{\left(1+\xi^1\right)\left(1+\xi^2\right)}{4}, \\ N_4 &= \frac{\left(1-\xi^1\right)\left(1+\xi^2\right)}{4}. \end{aligned} \tag{2.75}$$

Furthermore, the variation $\boldsymbol{\delta x}$ can be expressed as

$$\boldsymbol{\delta x} \approx \sum_I N_I \boldsymbol{\delta x}_I \tag{2.76}$$

The internal and external energy in equation 2.70 and 2.71 can be shown as the summation of energy for each element. Therefore,

$$G_{\text{int}} = \sum_{e=1}^{n_{el}} G^e_{\text{int}}, \tag{2.77}$$

$$G_{\text{ext}} = \sum_{e=1}^{n_{el}} G^e_{\text{ext}} \tag{2.78}$$

Now, inserting equation 2.73 to 2.76 into equation 2.70 and 2.71, we get

$$G_{\text{int}} = \boldsymbol{\delta x_e} \boldsymbol{f}^{\boldsymbol{e}}_{\text{int}}, \tag{2.79}$$

$$G_{\text{ext}} = \boldsymbol{\delta x_e} \boldsymbol{f}^{\boldsymbol{e}}_{\text{ext}}, \tag{2.80}$$

where

$$\boldsymbol{f}^{\boldsymbol{e}}_{\text{int}} = \int_{\Omega^e_0} \tau^{\alpha\beta} \mathbf{N}^T_{,\alpha} \boldsymbol{a_\beta} dA, \tag{2.81}$$

$$\boldsymbol{f}^{\boldsymbol{e}}_{\text{ext}} = \int_{\Omega^e_0} \mathbf{N}^T \boldsymbol{f_0} da + \int_{\delta_t \Omega^e_0} \mathbf{N}^T \bar{\boldsymbol{t}} ds + \int_{\Omega^e_0} \mathbf{N}^T p \boldsymbol{n} da. \tag{2.82}$$

However in our case, there is no body force. Therefore 2.82 becomes

$$\boldsymbol{f}^{\boldsymbol{e}}_{\text{ext}} = \int_{\delta_t \Omega^e_0} \mathbf{N}^T \bar{\boldsymbol{t}} ds. \tag{2.83}$$

Now inserting 2.79 and 2.80 into equation 2.72, we get

$$\boldsymbol{\delta x_e} \left[\boldsymbol{f}_{\text{int}} - \boldsymbol{f}_{\text{ext}} \right] = 0. \tag{2.84}$$

Considering $\boldsymbol{\delta x_e}$ as arbitrary we get,

$$\begin{aligned} & \boldsymbol{f}_{\text{int}} - \boldsymbol{f}_{\text{ext}} = 0 \\ \Rightarrow \quad & \boldsymbol{f(u)} = 0, \end{aligned} \tag{2.85}$$

where $\boldsymbol{u} = \boldsymbol{x} - \boldsymbol{X}$. Equation 2.85 is solved using Newton-Raphson method. Following algorithm is followed within the Newton-Raphson method for going from k$^{\text{th}}$ step to (k+1)$^{\text{th}}$ step.

1. Make an initial guess of $\boldsymbol{u_0}$.
2. Solve $\dfrac{\partial f}{\partial \boldsymbol{u}} \Delta \boldsymbol{u_{k+1}} = -\boldsymbol{f(u_k)}$.
3. Update the value of $\boldsymbol{u_{k+1}} = \boldsymbol{u_k} + \Delta \boldsymbol{u_{k+1}}$.

4. Decide a tolerance value for $\Delta \boldsymbol{u_{k+1}}$ or $\boldsymbol{f(u_k)}$ for convergence of the iteration scheme.

$\partial f/\partial \boldsymbol{u}$ introduced here, can be termed as stiffness matrix $\mathbf{K}$. So for an element the stiffness matrix $\mathbf{K^e}$ becomes

$$\mathbf{k^e} = \mathbf{K^{mat}} + \mathbf{K^{geo}} + \mathbf{K}^{\text{ext}}, \tag{2.86}$$

where

$$\mathbf{K^{mat}} = \int_{\Omega_0^e} c^{\alpha\beta\gamma\delta} \mathbf{N}_{,\alpha}^T \left(\boldsymbol{a_\beta} \otimes \boldsymbol{a_\gamma}\right) \mathbf{N}_{,\delta} dA, \tag{2.87}$$

$$\mathbf{K^{geo}} = \int_{\Omega_0^e} \mathbf{N}_{,\alpha}^T \tau^{\alpha\beta} \mathbf{N}_{,\beta} dA, \tag{2.88}$$

$$\mathbf{K}^{\text{ext}} = \mathbf{0}. \tag{2.89}$$

Chapter 3

Membrane Energy

As mentioned in chapter 2, graphene is modelled as a membrane structure in this work. The formulation of the corresponding membrane energy is discussed in this chapter. Furthermore, this chapter discusses about the Neo-Hookean model and the results for both models will be compared in the next sections.

3.1 Material model of Graphene

Graphene is a highly stretchable material. Large strains of 12.5% [49], 20%[50] and 25% [51, 52] have been observed during experiments. These experimental results are further confirmed by results obtained through simulation, which include atomistic simulations [53, 54, 55] and first principle simulations [45, 56, 57, 58]. The material remains elastic within large range of strains, i.e. there is no dissipation of energy. Therefore, graphene can be modelled with a hyperelastic model. However, graphene is also known to have anisotropic behaviour at large deformation. In order to model this anisotropic behaviour for a membrane, some models are proposed, that are based on Taylor series expansion of elastic tensors. However, these models require a lot of parameters, which are to be determined by numerous experiments and multi dimensional optimization algorithms, as conducted in [42, 43, 44]. On the other hand, material models based on invariants, as proposed in [45] require the determination of fewer constants.

3.1.1 Strain energy function based on invariants

Kumar and Parks [45] propose a material model based on logarithmic strain $\mathbf{E^{(0)}} = \ln(\mathbf{U})$, see appendix A. Usually in hyper-elastic models, the strain energy function is expressed in terms of $\mathbf{F}$ or $\mathbf{C}$ but in this case $\mathbf{E^{(0)}}$ is chosen, since it can be decomposed into a shape preserving but area changing part and a pure isochoric part. The membrane energy can be expressed as

$$W = W\left(\mathbf{E^{(0)}}\right), \tag{3.1}$$

where $\mathbf{E^{(0)}}$ can be termed as one of the Seth-Hill strain measures $\mathbf{E^{(m)}}$, see appendix A. $\mathbf{E^{(m)}}$ can be mathematically realised as

$$\mathbf{E}^{(m)} = \begin{cases} \frac{1}{m}\left(\mathbf{U}^m - \mathbf{I}\right) & \forall\ r \neq 0, \\ \ln(\mathbf{U}) & \forall\ r = 0. \end{cases} \tag{3.2}$$

Putting $m = 0$, we get $\mathbf{E^{(0)}} = \ln(\mathbf{U})$, as shown in [59, 60]. However, from continuum mechanics we know that the second Kirchhoff-Piola stress $\mathbf{S}$ and half of the right Cauchy-Green tensor are work conjugates. We have to use a chain rule in order to calculate the stress tensor. That means,

$$\mathbf{S} = 2\frac{\partial W}{\partial \mathbf{C}} = 2\frac{\partial W}{\partial \mathbf{E^{(0)}}} : \frac{\partial \mathbf{E^{(0)}}}{\partial \mathbf{C}}. \tag{3.3}$$

This increases the computational time for finite element formulation.This model is based on $\mathbf{C}$. Ghaffari and Sauer [61] also compare the computational time with the model of [46]. The comparison shows that the model with $\mathbf{C}$ is 1.5 times faster. Therefore, equation 3.1 can be changed to

$$W = W(\mathbf{C}). \tag{3.4}$$

Due to material symmetry, equation 3.4 has satisfy

$$W = W(\mathbf{C}) = W(\mathbf{Q}\mathbf{C}\mathbf{Q}^{\mathbf{T}}) \forall \mathbf{Q} \in \mathcal{G}, \tag{3.5}$$

where $\mathbf{Q}$ denotes rigid body rotation and $\mathcal{G} \subseteq \mathbf{Orth}^n$ is the set of material symmetry group. $\mathbf{Orth}^n$ is the set of all orthogonal transformations. In the case of an isotropic material $\mathcal{G} = \mathbf{Orth}^n$ but in our case, i.e. the anisotropic materials, $\mathcal{G} \subset \mathbf{Orth}^n$. Zheng [62] proposes the anisotropic function of tensors, that can be represented in terms of invariants ($\mathcal{J}_1$, $\mathcal{J}_2$, $\mathcal{J}_3$, ... $\mathcal{J}_n$), which are functions of $\mathbf{C}$ and the structural tensor $\mathbb{H}$ [60, 63, 64]. Therefore, equation 3.4 can be written as

$$W = W(\mathbf{C}) = W(\mathcal{J}_1, \mathcal{J}_2, \mathcal{J}_3, ...\mathcal{J}_n), \tag{3.6}$$

where

$$\mathcal{J}_i\left(\mathbf{C}; \mathbb{H}\right) = \mathcal{J}_i\left(\mathbf{Q}\mathbf{C}\mathbf{Q}^{\mathbf{T}}; \mathbb{P}_{\mathbf{Q}}\mathbb{H}\right) \forall \mathbf{Q} \in \mathbf{Orth}^n. \tag{3.7}$$

$\mathbb{P}_{\mathbf{Q}}$ introduced here, denotes the transformation of a structural tensor and $\mathcal{J}_i$ are the symmetry invariants. Equation 3.7 can further be verified by the work of Smith [65, 66]. According to Smith, a finite set of irreducible invariants forms a basis through which a scalar function of tensors can be represented.

3.1.2 Strain energy function based on invariants of logarithmic strain

Graphene has 6 fold rotational symmetry because the structure repeats itself 6 times within a span of 360°. Figure 3.1 shows that there are no changes in the structure of graphene for a rotation of 60° in either direction. For such structures, the invariants

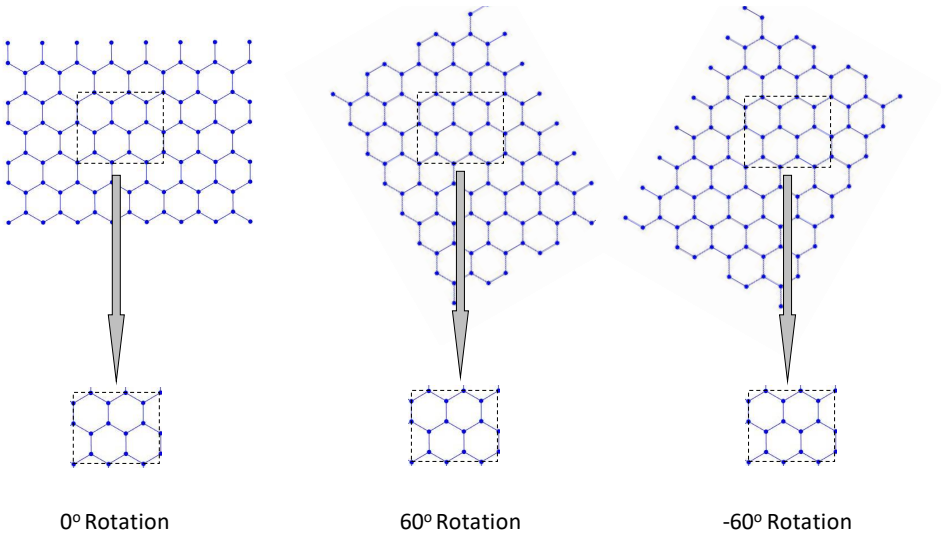

Figure 3.1: Graphene sheet rotated with 60° and -60° angle without any change in the internal structure

can be formulated as per equation C.10 from appendix C. Therefore, the equations for the invariants are

$$\begin{aligned}
\mathcal{J}_{1\mathbf{E}^{(0)}} &= \epsilon_a = \ln(J), \\
\mathcal{J}_{2\mathbf{E}^{(0)}} &= \left(\frac{\gamma_i}{2}\right)^2 = \frac{1}{2}\mathbf{E}^{(\mathbf{0})}_{\mathbf{dev}} : \mathbf{E}^{(\mathbf{0})}_{\mathbf{dev}} = \left(\ln(\lambda)\right)^2, \\
\mathcal{J}_{3\mathbf{E}^{(0)}} &= \left(\frac{\gamma_\theta}{2}\right)^3 = \frac{1}{8}\mathbb{H}\left(\mathbf{E}^{(\mathbf{0})}, \mathbf{E}^{(\mathbf{0})}, \mathbf{E}^{(\mathbf{0})}\right) = \left(\ln(\lambda)\right)^3 \cos(6\theta),
\end{aligned} \tag{3.8}$$

where $\lambda = \sqrt{\lambda_1/\lambda_2}$, considering λ_α for $\alpha = 1, 2$ as principle stretches and $\theta = \arccos(\boldsymbol{N}_1.\hat{\boldsymbol{x}})$ is the angle between the maximum stretch direction ($\boldsymbol{N}_1$) and the armchair direction ($\hat{\boldsymbol{x}}$), shown in figure 3.2. It can be observed in equation 3.8 that first two invariants are isotropic invariants, where ϵ_a is related to dilation and γ_i is related to shear. However, the third invariant γ_θ is related to anisotropy.

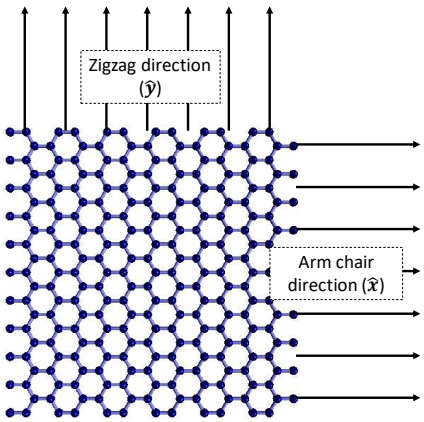

Figure 3.2: Armchair and zigzag direction in a graphene structure, where the structure is generated in Nanotube Modeler [1]

The material response of graphene can be divided into two parts. This can be done because logarithmic strain can be decomposed into an area changing and shape changing part. Therefore the strain energy can divided into

1. pure dilation,
2. shape changing deformation.

The dilation part can be formulated based on Universal Binding Energy Relation (UBER), which was first proposed by Rose et.al. [67, 68]. The UBER formulation can be expressed as

$$W^{\text{Dil}}_{\mathbf{E}^{(0)}}(\epsilon_a) = \varepsilon\left[1 - (1 + \hat{\alpha}\epsilon_a)\exp(-\hat{\alpha}\epsilon_a)\right], \tag{3.9}$$

where ε and $\hat{\alpha}$ are material constants, which are obtained through fitting of the ab initio energies, that are calculated through Generalized Gradient Approximation (GGA) and Local density approximation (LDA) method. The values of these constants can be obtained from table 3.1. The shape changing part is dependent on γ_i and γ_θ. However, the energy associated with shape change is also dependent on the current state of dilation. i.e. the initial area. Therefore, the shape changing or the deviatoric part can be formulated as

$$W^{\text{Dev}}_{\mathbf{E}^{(0)}}(\gamma_i, \gamma_\theta; \epsilon_a) = \frac{1}{2}\mu(\epsilon_a)\gamma_i^2 + \frac{1}{8}\eta(\epsilon_a)\gamma_\theta^3, \tag{3.10}$$

where $\mu(\epsilon_a)$ and $\eta(\epsilon_a)$ are constants dependent on the current dilatory state. μ is well fit with the ab initio calculation by the following exponential function

$$\mu(\epsilon_a) = \mu_0 - \mu_1 e^{\hat{\beta}\epsilon_a}, \tag{3.11}$$

where the values of μ_0 and μ_1 can be obtained from table 3.1. The function $\eta(\epsilon_a)$ is well fit by an even quadratic function of ϵ_a

$$\eta(\epsilon_a) = \eta_0 - \eta_1\epsilon_a^2, \tag{3.12}$$

where η_0 and η_1 are material constants, whose values can be obtained from table 3.1. Therefore, the strain energy function can be written as

$$W_{\mathbf{E}^{(0)}} = \varepsilon\left[1 - (1 + \hat{\alpha}\epsilon_a)\exp(-\hat{\alpha}\epsilon_a)\right] + \frac{1}{2}(\mu_0 - \mu_1 e^{\hat{\beta}\epsilon_a})\gamma_i^2 + \frac{1}{8}(\eta_0 - \eta_1\epsilon_a^2)\gamma_\theta^3, \tag{3.13}$$

where the values of the seven constants are given in table 3.1.

	$\hat{\alpha}$	ε[N/m]	μ_0[N/m^{-1}]	μ_1[N/m^{-1}]	$\hat{\beta}$	η_0[N/m^{-1}]	η_1[N/m^{-1}]
GGA	1.53	93.84	172.18	27.03	5.16	94.65	4393.26
LDA	1.38	116.43	164.17	17.31	6.22	86.9	3611.5

Table 3.1: Material constants obtained through Generalized Gradient Approximation (GGA) and Local Density Approximation (LDA) method

3.1.3 Strain energy function based on invariants of right Cauchy-Green tensor

As pointed out in section 3.1.1, the model based on logarithmic strain has some significant disadvantage in terms of computational effort. Therefore a model based on the right Cauchy-Green tensor is proposed in Ghaffari et. al. [46], where the need for application of chain rule is overcomed. The basic logic of model development remains similar to the model discussed in the previous section, i.e. the 6-fold rotational symmetry. However, the invariants for right Cauchy-Green tensor $\mathbf{C}$ can be realised as

$$\begin{aligned}
\mathcal{J}_{1\mathbf{C}} &= \sqrt{\det(\mathbf{C})} = J, \\
\mathcal{J}_{2\mathbf{C}} &= \frac{1}{2}\bar{\mathbf{C}}^{\perp} : \bar{\mathbf{C}}^{\perp} = \frac{1}{4}\left(\frac{\Lambda_1}{\Lambda_2} + \frac{\Lambda_2}{\Lambda_1} - 2\right), \\
\mathcal{J}_{3\mathbf{C}} &= \frac{1}{8}\mathbb{H}\left(\bar{\mathbf{C}}, \bar{\mathbf{C}}, \bar{\mathbf{C}}\right) = \frac{1}{8}\left[\left(\hat{\mathbf{M}} : \bar{\mathbf{C}}\right)^3 - 3\left(\hat{\mathbf{M}} : \bar{\mathbf{C}}\right)\left(\hat{\mathbf{N}} : \bar{\mathbf{C}}\right)^2\right] \\
&= \frac{1}{8}\left(\frac{\lambda_1}{\lambda_2} + \frac{\lambda_2}{\lambda_1}\right)^3 \cos(6\theta),
\end{aligned} \tag{3.14}$$

where $J = \det(\mathbf{F})$, considering $\mathbf{F}$ is the deformation gradient, $\bar{\mathbf{C}}$ is the area-invariant part of $\mathbf{C}$, $\bar{\mathbf{C}}^{\perp}$ is the deviatoric part of $\bar{\mathbf{C}}$, Λ_α and λ_α are the eigenvalues of $\mathbf{C}$ and $\mathbf{U}$ respectively ($\mathbf{U} = \sqrt{\mathbf{C}}$, see appendix A), $\hat{\mathbf{M}}$ and $\hat{\mathbf{N}}$ are two traceless tensors related to direction of lattice, see equation C.2 of appendix C and $\mathbb{H}$ is the structural tensor defined through equation C.1 of appendix C within θ is the angle between maximum stretch direction and armchair direction $\hat{\boldsymbol{x}}$. Additionally considering $\bar{\mathbf{F}}$ the area-invariant part of the deformation gradient, we get

$$\begin{aligned}
\bar{\mathbf{F}} &= J^{-\frac{1}{2}}\mathbf{F}, \\
\bar{\mathbf{C}} &= \bar{\mathbf{F}}^T\bar{\mathbf{F}} = \frac{1}{J}\mathbf{C}, \\
\bar{\mathbf{C}}^{\perp} &= \frac{1}{J}\left(\mathbf{C} - \frac{1}{2}\mathrm{tr}(\mathbf{C})\mathbf{I}\right).
\end{aligned} \tag{3.15}$$

Right Cauchy-Green tensor and stretch tensor can be expressed as

$$\begin{aligned}
\mathbf{C} &= \sum_{\alpha=1}^{2} \Lambda_\alpha \boldsymbol{N}_{\boldsymbol{\alpha}} \otimes \boldsymbol{N}_{\boldsymbol{\alpha}}, \\
\mathbf{U} &= \sum_{\alpha=1}^{2} \lambda_\alpha \boldsymbol{N}_{\boldsymbol{\alpha}} \otimes \boldsymbol{N}_{\boldsymbol{\alpha}}
\end{aligned} \tag{3.16}$$

respectively, where $\boldsymbol{N}_{\boldsymbol{\alpha}}$ for $\alpha = 1, 2$ are the eigenvectors of $\mathbf{C}$. $\boldsymbol{N}_{\boldsymbol{1}}$ is the direction of maximum stretch. Therefore θ can be formulated as

$$\theta = \arccos(\boldsymbol{N}_{\boldsymbol{1}}.\hat{\boldsymbol{x}}). \tag{3.17}$$

The dilatoric part of the strain energy can be formulated exactly similar to the previous section, see equation 3.9. Therefore the dilatoric part can be formulated as

$$W^{\mathrm{Dil}}(\mathcal{J}_{1\mathbf{C}}) = \varepsilon\left[1 - (1 + \hat{\alpha}\ln(\mathcal{J}_{1\mathbf{C}}))\exp(-\hat{\alpha}\ln(\mathcal{J}_{1\mathbf{C}}))\right], \tag{3.18}$$

where constants are given in table 3.1. The deviatoric part needs to be amended. Considering equation 3.10, the functions μ and η remains unchanged. However instead of invariants a function of invariants is included. Therefore the deviatoric part becomes

$$W^{\text{Dev}}(\mathcal{J}_{2\mathbf{C}}, \mathcal{J}_{3\mathbf{C}}; \mathcal{J}_{1\mathbf{C}}) = 2\mu(\mathcal{J}_{1\mathbf{C}})f_1(\mathcal{J}_{2\mathbf{C}}) + \eta(\mathcal{J}_{1\mathbf{C}})f_2(\mathcal{J}_{2\mathbf{C}}, \mathcal{J}_{3\mathbf{C}}), \tag{3.19}$$

where

$$\begin{aligned} \mu(\mathcal{J}_{1\mathbf{C}}) &= \mu_0 - \mu_1 \mathcal{J}_{1\mathbf{C}}^{\hat{\beta}}, \\ \eta(\mathcal{J}_{1\mathbf{C}}) &= \eta_0 - \eta_1 (\ln \mathcal{J}_{1\mathbf{C}})^2. \end{aligned} \tag{3.20}$$

The values of material constants can be found from table 3.1. The function f_1 can be formulated as the Taylor series expansion of $\mathcal{J}_{2\mathbf{C}}$ and the function f_2 can be formulated as a second order expansion of $\mathcal{J}_{2\mathbf{C}}$ and $\mathcal{J}_{3\mathbf{C}}$, where $\mathcal{J}_{2\mathbf{C}}$ and $\mathcal{J}_{2\mathbf{C}}^2$ are omitted because they don't have a periodicity of 60° and $\mathcal{J}_{2\mathbf{C}}$ is omitted because it includes $\cos(12\theta)$, which has too high periodicity. Therefore the functions f_1 and f_2 can be formulated as

$$f_1(\mathcal{J}_{2\mathbf{C}}) = e_1 \mathcal{J}_{2\mathbf{C}} - e_2 \mathcal{J}_{2\mathbf{C}}^2, \tag{3.21}$$

$$f_2(\mathcal{J}_{2\mathbf{C}}, \mathcal{J}_{3\mathbf{C}}) = \mathcal{J}_{3\mathbf{C}} \left(g_1 - g_2 \mathcal{J}_{2\mathbf{C}}\right), \tag{3.22}$$

where e_1, e_2, g_1 and g_2 are material constants, whose values can be taken from table below.

e_1	e_2	g_1	g_2
0.25	0.0811	0.125	0.06057

Table 3.2: contants introduced in equation 3.21 and 3.22

Therefore the strain energy function, formulated in terms of invariants of right Cauchy-Green tensor can be realised as

$$\begin{aligned} W \;=\; & \varepsilon \left[1 - (1 + \hat{\alpha} \ln(\mathcal{J}_{1\mathbf{C}})) \exp(-\hat{\alpha} \ln(\mathcal{J}_{1\mathbf{C}}))\right] + 2\mu(\mathcal{J}_{1\mathbf{C}}) f_1(\mathcal{J}_{2\mathbf{C}}) \\ & + \eta(\mathcal{J}_{1\mathbf{C}}) f_2(\mathcal{J}_{2\mathbf{C}}, \mathcal{J}_{3\mathbf{C}}), \end{aligned} \tag{3.23}$$

where the constants are given in table 3.1 and 3.2. In this work, the strain energy function from equation 3.23 is used.

3.1.4 Stress and elasticity tensor

In this work, the second Kirchoff-Piola stress, see appendix B is selected as the stress measure to be calculated and it is calculated from the strain energy function using equation 3.3. However using equation 2.27 and 2.64, it can be shown that when expressed in terms of $\boldsymbol{A}^{\boldsymbol{\alpha}}$ for $(\alpha = 1, 2)$ the components of $\mathbf{S}$ is equal to $\tau^{\alpha\beta}$.

$$\begin{aligned} \mathbf{S} = S^{\alpha\beta} \left(\boldsymbol{A}_{\boldsymbol{\alpha}} \otimes \boldsymbol{A}_{\boldsymbol{\beta}}\right) \;&=\; 2 \frac{\partial W}{\partial a^{\alpha\beta}} \left(\boldsymbol{A}_{\boldsymbol{\alpha}} \otimes \boldsymbol{A}_{\boldsymbol{\beta}}\right) \\ &=\; \tau^{\alpha\beta} \left(\boldsymbol{A}_{\boldsymbol{\alpha}} \otimes \boldsymbol{A}_{\boldsymbol{\beta}}\right). \end{aligned} \tag{3.24}$$

As shown in [69], $\tau^{\alpha\beta}$ will be used for FE formulation. In our model, the second Kirchhoff-Piola stress can be computed as

$$\begin{aligned}\mathbf{S} = \frac{\partial W}{\partial \mathbf{C}} &= \frac{\partial W}{\partial \mathcal{J}_{1\mathbf{c}}}\frac{\partial \mathcal{J}_{1\mathbf{c}}}{\partial \mathbf{C}} + \frac{\partial \mathcal{J}_{2\mathbf{c}}}{\partial \mathbf{C}}\frac{\partial W}{\partial \mathcal{J}_{2\mathbf{c}}} + \frac{\partial \mathcal{J}_{3\mathbf{c}}}{\partial \mathbf{C}}\frac{\partial W}{\partial \mathcal{J}_{3\mathbf{c}}} \\ &= H_1\mathbf{C}^{-1} + \frac{H_2}{J}\bar{\mathbf{C}}^{\perp} + \frac{H_3}{4J}\left(a_{\hat{\mathbf{M}}}\hat{\mathbf{M}} + a_{\hat{\mathbf{N}}}\hat{\mathbf{N}}\right),\end{aligned} \tag{3.25}$$

where

$$\begin{aligned}H_1 &= \varepsilon\hat{\alpha}^2\ln(J)e^{-\hat{\alpha}\ln(J)} - 2\mu_1\hat{\beta}J^{\hat{\beta}}f_1 - 2\eta_1\ln(J)f_2 - H_2\mathcal{J}_{2\mathbf{C}} - 3H_3\mathcal{J}_{3\mathbf{C}}, \\ H_2 &= 2\left(2\mu\left(e_1 - 2e_2\mathcal{J}_{2\mathbf{C}}\right) - g_2\eta\mathcal{J}_{3\mathbf{C}}\right), \\ H_3 &= \eta\left(g_1 - g_2\mathcal{J}_{2\mathbf{C}}\right)\end{aligned} \tag{3.26}$$

are the coefficients, see appendix D. In component form, using equations 2.27 and D.2, $\mathbf{C}^{-1}$, $\bar{\mathbf{C}}^{\perp}$, $\hat{\mathbf{M}}$ and $\hat{\mathbf{N}}$ tensors of equation can be represented as

$$\begin{aligned}\mathbf{C}^{-1} &= a^{\alpha\beta}\boldsymbol{A}_{\boldsymbol{\alpha}} \otimes \boldsymbol{A}_{\boldsymbol{\beta}}, \\ \bar{\mathbf{C}}^{\perp} &= \frac{1}{J}\left(\mathbf{C} - \frac{1}{2}\mathrm{tr}(\mathbf{C})\mathbf{I}\right) \\ &= \frac{1}{J}\left(A^{\alpha\gamma}a_{\gamma\delta}A^{\delta\beta} - \frac{1}{2}\mathrm{tr}(\mathbf{C})A^{\alpha\beta}\right)\boldsymbol{A}_{\boldsymbol{\alpha}} \otimes \boldsymbol{A}_{\boldsymbol{\beta}}, \\ \hat{\mathbf{M}} &= \hat{M}^{\alpha\beta}\boldsymbol{A}_{\boldsymbol{\alpha}} \otimes \boldsymbol{A}_{\boldsymbol{\beta}}, \\ \hat{\mathbf{N}} &= \hat{N}^{\alpha\beta}\boldsymbol{A}_{\boldsymbol{\alpha}} \otimes \boldsymbol{A}_{\boldsymbol{\beta}},\end{aligned} \tag{3.27}$$

where $A^{\alpha\beta}$ and $a^{\alpha\beta}$ are covariant components of metric tensor, $A^{\alpha\beta}$ and $a^{\alpha\beta}$ are contra-variant components of metric tensor, which can be formulated as per equation 2.5 to 2.8.

$$\begin{aligned}\mathbf{I} &= A^{\alpha\beta}\boldsymbol{A}_{\boldsymbol{\alpha}} \otimes \boldsymbol{A}_{\boldsymbol{\beta}}, \\ \mathrm{tr}(\mathbf{C}) &= \mathbf{C} : \mathbf{I} = a_{\alpha\beta}A^{\alpha\beta}.\end{aligned} \tag{3.28}$$

$\hat{M}^{\alpha\beta}$ and $\hat{N}^{\alpha\beta}$ are covariant components of $\hat{\mathbf{M}}$ and $\hat{\mathbf{N}}$ respectively. The co and contra-variant components can be obtained as

$$\begin{aligned}\hat{M}^{\alpha\beta} &= \boldsymbol{A}_{\boldsymbol{\alpha}} \cdot \hat{\mathbf{M}} \cdot \boldsymbol{A}_{\boldsymbol{\beta}}, \\ \hat{N}^{\alpha\beta} &= \boldsymbol{A}_{\boldsymbol{\alpha}} \cdot \hat{\mathbf{N}} \cdot \boldsymbol{A}_{\boldsymbol{\beta}}, \\ \hat{M}_{\alpha\beta} &= \boldsymbol{A}^{\boldsymbol{\alpha}} \cdot \hat{\mathbf{M}} \cdot \boldsymbol{A}^{\boldsymbol{\beta}}, \\ \hat{N}_{\alpha\beta} &= \boldsymbol{A}^{\boldsymbol{\alpha}} \cdot \hat{\mathbf{N}} \cdot \boldsymbol{A}^{\boldsymbol{\beta}}.\end{aligned} \tag{3.29}$$

So finally using equation 3.24, 3.25 to **??**, the stress in component form can be realized as

$$\tau^{\alpha\beta} = H_1 a^{\alpha\beta} + \frac{H_2}{J^2}\left(A^{\alpha\gamma}a_{\gamma\delta}A^{\delta\beta} - \frac{1}{2}\mathrm{tr}(\mathbf{C})\right) + \frac{H_3}{4J}\left(a_{\hat{\mathbf{M}}}\hat{M}^{\alpha\beta} + a_{\hat{\mathbf{N}}}\hat{N}^{\alpha\beta}\right). \tag{3.30}$$

Refer to appendix D for $a_{\hat{\mathbf{M}}}$, $a_{\hat{\mathbf{N}}}$ The elasticity tensor can be formulated by differentiating the strain energy function twice with respect to right Cauchy-Green tensor. As per Kintzel [70] and Kintzel and Baar [71] mathematically elasticity tensor can be expressed as

$$\mathbb{C} = \frac{\partial^2 W}{\partial \mathbf{C} \otimes \partial \mathbf{C}}, \tag{3.31}$$

where $\mathbb{C}$ is given in appendix D.

3.2 Neo-Hookean model of material

The Neo-Hookean model is one of the most popular models for describing elasticity. Peter Wriggers [72] proposed expression of the 3D Neo-Hookean strain energy function in two different forms, which can be realised as

$$W_{NH1} = \frac{\Lambda}{4}(J^2 - 1 - 2\ln J) + \frac{\mu}{2}(I_1 - 2 - 2\ln J), \tag{3.32}$$

$$\begin{aligned} W_{\mathrm{NH2}} &= \frac{\Lambda}{4}(J^2 - 1 - 2\ln J) + \frac{\mu}{2}\left(\frac{I_1}{J} - 2\right) \\ &= \frac{\kappa}{4}(J^2 - 1 - 2\ln J) + \frac{\mu}{2}(\tilde{I}_1 - 2). \end{aligned} \tag{3.33}$$

Here, Λ and μ are material constants and $\kappa = \Lambda + \mu$. κ and μ are given in per table 3.3.

Table 3.3: material constants obtained through generalized gradient approximation (GGA) and local density approximation (LDA) method

	κ	μ
Generalized Gradient Approximation (GGA)	219	145
Local Density Approximation (LDA)	222	147

Therefore $\mathbf{S}_{\mathrm{NH1}}$ and $\mathbf{S}_{\mathrm{NH2}}$ are the 2nd K-P stress tensor corresponding to W_{NH1} and W_{NH2} respectively.

$$
\begin{aligned}
\mathbf{S}_{\mathrm{NH1}} &= 2\frac{\partial W_1}{\partial \mathbf{C}} \\
&= 2\frac{\partial}{\partial \mathbf{C}}\left[\frac{\Lambda}{4}(J^2-1-2\ln J)+\frac{\mu}{2}(I_1-2-2\ln J)\right] \\
&= 2\left[\frac{\Lambda}{4}\left(J^2\mathbf{C}^{-1}-\mathbf{C}^{-1}\right)+\frac{\mu}{2}\left(\mathbf{I}-\mathbf{C}^{-1}\right)\right] \\
&= \frac{\Lambda}{2}\left(J^2\mathbf{C}^{-1}-\mathbf{C}^{-1}\right)+\mu\left(\mathbf{I}-\mathbf{C}^{-1}\right) \qquad (3.34)\\
\mathbf{S}_{\mathrm{NH2}} &= 2\frac{\partial W_2}{\partial \mathbf{C}} \\
&= 2\frac{\partial}{\partial \mathbf{C}}\left[\frac{\kappa}{4}\left(J^2-1-2\ln J\right)+\frac{\mu}{2}\left(\tilde{I}_1-2\right)\right] \\
&= 2\left[\frac{\kappa}{4}\left(J^2\mathbf{C}^{-1}-\mathbf{C}^{-1}\right)+\frac{\mu}{2}\frac{1}{J}\left(\mathbf{I}-\frac{1}{2}I_1\mathbf{C}^{-1}\right)\right] \\
&= \frac{\kappa}{2}\left(J^2\mathbf{C}^{-1}-\mathbf{C}^{-1}\right)+\frac{\mu}{J}\left(\mathbf{I}-\frac{1}{2}I_1\mathbf{C}^{-1}\right) \qquad (3.35)
\end{aligned}
$$

Now referring appendix B, the Cauchy stress can be formulated in terms of the right Cauchy-Green tensor as

$$\boldsymbol{\sigma}=\frac{1}{J}\mathbf{F}\mathbf{S}\mathbf{F}^{\mathrm{T}}, \qquad (3.36)$$

The Cauchy stresses corresponding to W_1 and W_2 can be expressed as

$$
\begin{aligned}
\boldsymbol{\sigma}_{\mathrm{NH1}} &= \frac{1}{J}\mathbf{F}\mathbf{S}_{\mathrm{NH1}}\mathbf{F}^{\mathrm{T}} \\
&= \frac{1}{J}\mathbf{F}\left[\frac{\Lambda}{2}\left(J^2\mathbf{C}^{-1}-\mathbf{C}^{-1}\right)+\mu\left(\mathbf{I}-\mathbf{C}^{-1}\right)\right]\mathbf{F}^{\mathrm{T}} \\
&= \frac{\Lambda}{2J}\left(J^2\mathbf{F}\mathbf{C}^{-1}\mathbf{F}^{\mathrm{T}}-\mathbf{F}\mathbf{C}^{-1}\mathbf{F}^{\mathrm{T}}\right)+\frac{\mu}{J}\left(\mathbf{F}\mathbf{F}^{\mathrm{T}}-\mathbf{F}\mathbf{C}^{-1}\mathbf{F}^{\mathrm{T}}\right), \qquad (3.37)\\
\boldsymbol{\sigma}_{\mathrm{NH2}} &= \frac{1}{J}\mathbf{F}\mathbf{S}_{\mathrm{NH2}}\mathbf{F}^{\mathrm{T}} \\
&= \frac{1}{J}\mathbf{F}\left[\frac{\kappa}{2}\left(J^2\mathbf{C}^{-1}-\mathbf{C}^{-1}\right)+\frac{\mu}{J}\left(\mathbf{I}-\frac{1}{2}I_1\mathbf{C}^{-1}\right)\right]\mathbf{F}^{\mathrm{T}} \\
&= \frac{\kappa}{2J}\left(J^2\mathbf{F}\mathbf{C}^{-1}\mathbf{F}^{\mathrm{T}}-\mathbf{F}\mathbf{C}^{-1}\mathbf{F}^{\mathrm{T}}\right)+\frac{\mu}{J^2}\left(\mathbf{F}\mathbf{F}^{\mathrm{T}}-\frac{1}{2}I_1\mathbf{F}\mathbf{C}^{-1}\mathbf{F}^{\mathrm{T}}\right). \qquad (3.38)
\end{aligned}
$$

In this work only equation 3.37 is considered for FEM implementation. The stress in the component form written as

$$\tau_{\mathrm{NH}}^{\alpha\beta}=\frac{\Lambda}{2J}\left(J^2-1\right)a^{\alpha\beta}+\frac{\mu}{J}\left(A^{\alpha\beta}-a^{\alpha\beta}\right). \qquad (3.39)$$

Referring to [48], the components of elasticity tensor can be written as

$$c_{\mathrm{NH}}^{\alpha\beta\gamma\delta}=\Lambda J^2 a^{\alpha\beta}a^{\gamma\delta}+\left(\Lambda(J^2-1)-2\mu\right)a^{\alpha\beta\gamma\delta}. \qquad (3.40)$$

Chapter 4

Molecular dynamic approach

In this section, the molecular dynamic approach for the behaviour of graphene will be discussed. In contrary to the continuum approach discussed in chapter 2, the molecular dynamic approach considers the material as a set of atoms. This section discusses the basic principles of molecular dynamic simulation of different structures of graphene, e.g. carbon nano tube (CNT) and carbon nano cone (CNC) structures.

4.1 Basic principles of molecular dynamics

In molecular dynamics, a computational method is employed for molecular systems to determine their time dependent behaviour. One of the first simulations in this

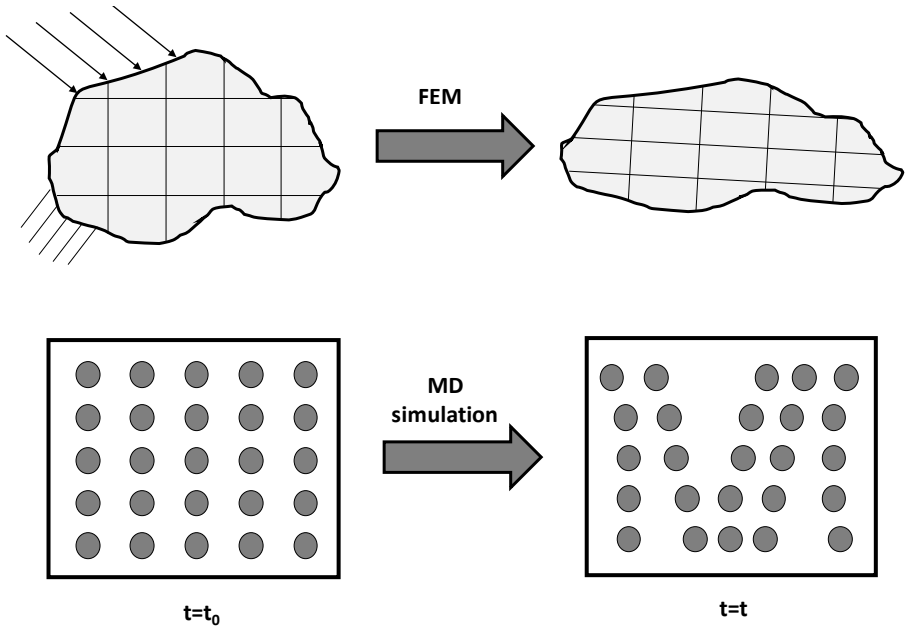

Figure 4.1: [Top inset] simple FEM simulation of an arbitrary body using continuum mechanical approach,
[bottom inset] simple molecular dynamic simulation

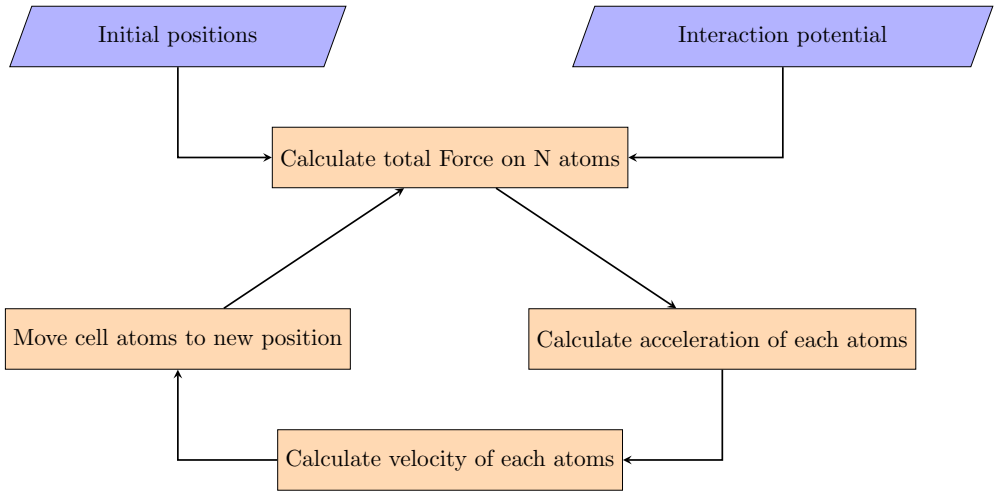

Figure 4.2: basic steps for molecular dynamic simulation

method was reported in the works of Alder and Wainwright [73] in 1957. As can be seen from figure 4.1, the basic difference between the continuum mechanical approach and the molecular dynamic simulation is that the continuum mechanical approach deals with a continuous body and solves the problem using energy conversion and the molecular dynamic approach deals with set of atoms and solves the problem using Newton's second law of motion.

A molecular dynamic simulation can be seen as an amalgamation of the following steps:

1. The system of interest or the simulation box is specified. In figure 4.1, this is shown in the bottom inset using the box with the dark boundary.

2. The initial conditions are defined, i.e. the initial position and the velocity of atoms.

$$\text{Coordinate of i}^{th} \text{ atom} = \boldsymbol{r_i}\left(t_0\right). \tag{4.1}$$

3. Inter atomic potential is defined between each pair of particles. Additionally for each step energy has to be minimized for the system. This potential energy is due to the bonds and non bond interactions. The potential energy can be written as

$$U\left(\boldsymbol{r_i}\right) = U_{\text{bonded}}\left(\boldsymbol{r_i}\right) + U_{\text{non-bonded}}. \tag{4.2}$$

4. The force on each particle is then calculated by taking the derivative of $U\left(\boldsymbol{r_i}\right)$, i.e.

$$\boldsymbol{F_i} = -\bigtriangledown_{\boldsymbol{r}} U\left(\boldsymbol{r_i}\right). \tag{4.3}$$

5. The force can be used to determine the new position of the particles using Newton's second law of motion, i.e.

$$\boldsymbol{F} = m_i \frac{d^2 \boldsymbol{r_i}}{dt^2} = - \bigtriangledown_r U(\boldsymbol{r_i}). \tag{4.4}$$

Equation 4.4 calculates the acceleration and by integration of acceleration we get the velocity, from which the new position of particles can be computed.

Figure 4.1 shows these steps in a flow chart form.

4.2 Generation of graphene structure

As mentioned in the section 4.1, the initial position has to be specified for molecular dynamic simulations. In this work, three different structures of graphene are created and these can be termed as

1. Sheet structure
2. Carbon Nano Tube (CNT)
3. Carbon Nano Cone (CNC)

In this work, MATLAB [2] is used to create these structures.

4.2.1 Sheet structure

As shown in Lee [29], for creation of a graphene sheet structure, a new coordinate system is generated with the basis of $\{\vec{a_1}, \vec{a_2}\}$, see figure 4.3. The basis vectors $\boldsymbol{a_1}$

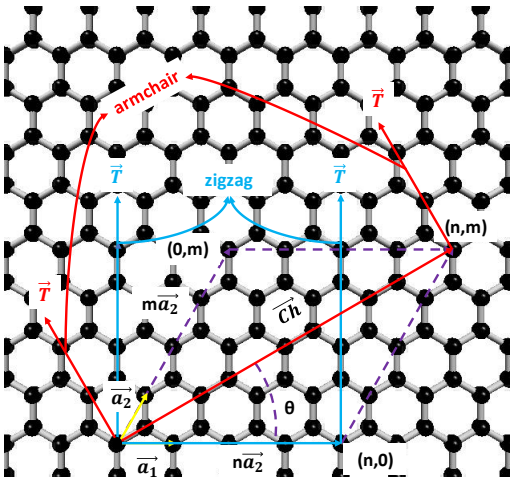

Figure 4.3: Geometry of graphene structure, where the sheet structure is using within Nano Tube Modeler [1]

and $\boldsymbol{a_2}$ can be defined as

$$\vec{\boldsymbol{a_1}} = \begin{Bmatrix} \sqrt{3} \\ 0 \end{Bmatrix} a_{c-c},$$
$$\vec{\boldsymbol{a_2}} = \begin{Bmatrix} \sqrt{3}/2 \\ 3/2 \end{Bmatrix} a_{c-c}, \tag{4.5}$$

where a_{c-c} is the carbon carbon bond length, which is equal to 0.1421 nm. The chiral vector, along which the sheet is cut, can be described as

$$\vec{\boldsymbol{Ch}} = m\vec{\boldsymbol{a_1}} + n\vec{\boldsymbol{a_2}}, \tag{4.6}$$

where m and n are two constants to be chosen such that the chiral angle θ, i.e. the angle in between the vector $\vec{\boldsymbol{Ch}}$ and $\vec{\boldsymbol{a_1}}$ satisfies the condition $0 \leq \theta \leq 30^o$. The chiral angle can be calculated as

$$\tan\theta = \sqrt{3}m/\left(2n+m\right)$$
or
$$\theta = \cos^{-1}\left[(2n+m)/2\sqrt{n^2+nm+m^2}\right]. \tag{4.7}$$

The translational vector $\vec{\boldsymbol{T}}$ is perpendicular to the direction of cutting. This can be calculated by

$$\vec{\boldsymbol{T}} = \left[(2m+n)/w\right]\vec{\boldsymbol{a_1}} - \left[(2n+m)/w\right]\vec{\boldsymbol{a_2}}. \tag{4.8}$$

Here w is the greatest common divisor of $(2m+n)$ and $(2n+m)$. The length of this vector shows a unit cell in the vertical direction, i.e. the structure repeats itself

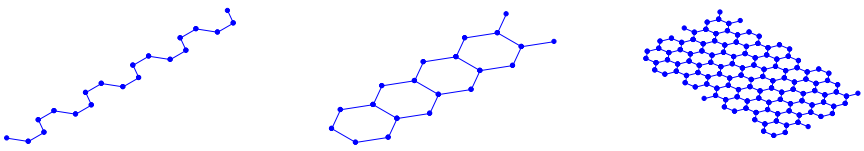

(a) m=5, n=5 (Armchair) (b) m=5, n=0 (Zigzag) (c) m=5, n=1

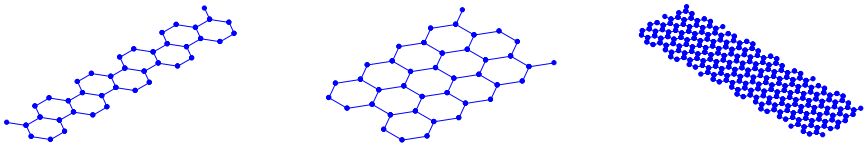

(d) m=5, n=5 (Armchair) with 2 unit cells in the vertical direction (e) m=5, n=0 (Zigzag) with 2 unit cells in the vertical direction (f) m=5, n=1 with 2 unit cells in the vertical direction

Figure 4.4: Graphene sheets with different cuts, created in MATLAB [2]. (a) to (c) is with only one unit cell in the vertical direction and (d) to (f) is with two unit cells in the vertical direction

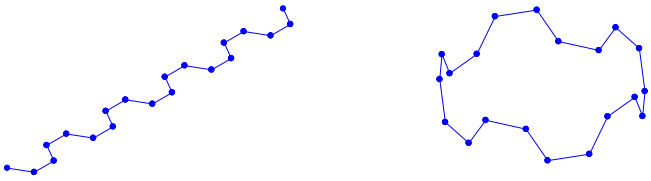

(a) Sheet structure (b) CNT structure

Figure 4.5: Conversion of sheet structure to a carbon Nano Tube (CNT) through bending

beyond this length. Finally, it can be concluded that for the creation of graphene structures, the required input is (m, n), where $(m \geq n)$. Two special cases are $n = 0$ and $m = n$, which are termed as zigzag and armchair respectively. Figure 4.4 shows graphene structures created for different cuts with 1 and 2 unit cells in the vertical direction.

4.2.2 Carbon Nano Tube structure (CNT)

For generation of Carbon Nano Tube (CNT) structure, the sheet structure is rolled as shown in figure 4.5 to form a CNT structure. The radius of the CNT can therefore

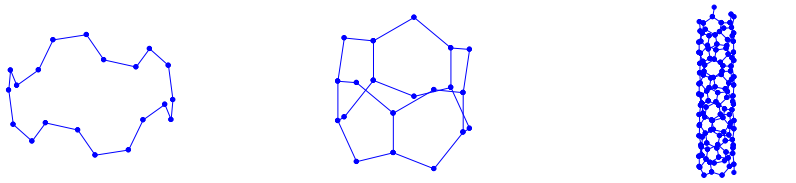

(a) m=5, n=5 (Armchair) (b) m=5, n=0 (Zigzag) (c) m=5, n=1

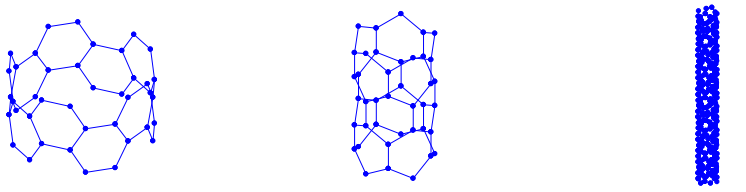

(d) m=5, n=5 (Armchair) with 2 unit cells in the vertical direction (e) m=5, n=0 (Zigzag) with 2 unit cells in the vertical direction (f) m=5, n=1 with 2 unit cells in the vertical direction

Figure 4.6: Carbon Nano Tube with different cuts, created in MATLAB [2]. In (a) to (c), it is shown with one unit cell in the vertical direction and in (d) to (f) with two unit cells in the vertical direction

be computed as

$$R = \text{Length of } \vec{\boldsymbol{Ch}}/2\pi = a_{c-c}\sqrt{3(n^2 + nm + m^2)}/2\pi. \tag{4.9}$$

The conversion of sheet structure to a CNT structure can be computed through the coordinate transformation, proposed by Koloczek et al. [74], which can be formulated as

$$\begin{aligned} X &= R\cos\left(G_x/R\right), \\ Y &= R\cos\left(G_x/R\right), \\ Z &= G_y, \end{aligned} \tag{4.10}$$

where (X, Y, Z) are the 3D coordinates of carbon atoms in the CNT structure and (G_x, G_y) are the 2D coordinates of carbon atoms in the sheet structure. Figure 4.6 shows the CNT structures of corresponding sheet structures shown in figure 4.4. Figure 4.6(a) and 4.6(b) shows the armchair and zigzag CNT respectively with one unit cell in the vertical direction. Figure 4.6(d) and 4.6(e) shows the same for the two unit cells.

4.2.3 Carbon Nano Cone structure (CNC)

Cone structures in general can have a wide variety of natural apex angles as per Jaszczak et al. [75]. However, in our case in order to satisfy the symmetry and the atom topology, only some specific apex angles are possible for Carbon Nano Cone (CNC) structures. Lin et al. [76] proposed 5 different apex angles, considering Euler's theorem and the symmetry of graphene. For the generation of CNC, a segment

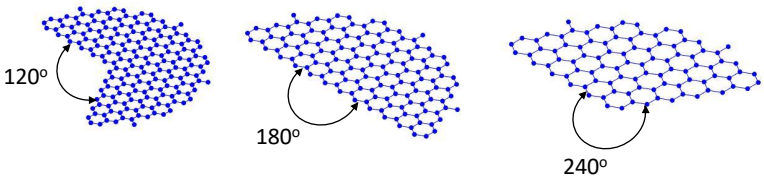

Figure 4.7: Cut graphene sheets from which CNC structure is generated

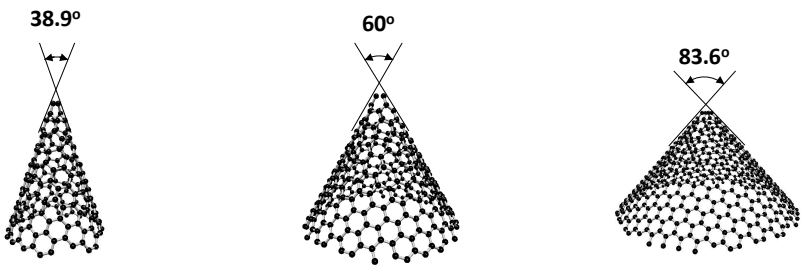

Figure 4.8: CNC structure, generated in Nano Tube Modeler [1], for different apex angles

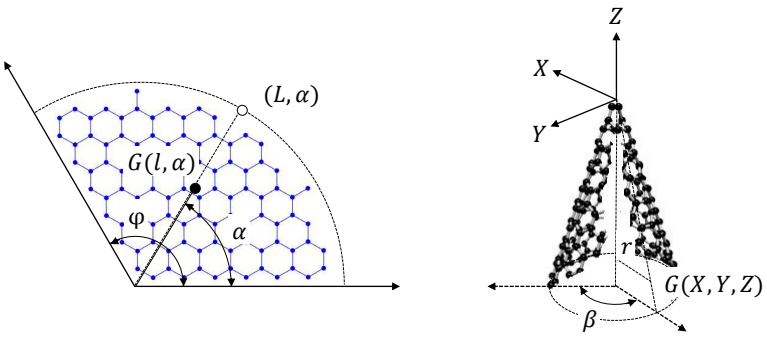

Figure 4.9: CNC structure, generated in Nano Tube Modeler [1], for different apex angles

is cut from the circular graphene sheet in a way shown in figure 4.7. The angle of the segment, which is termed as the disclination angle, can have a possible value of 60°, 120°, 180°, 240° or 300°. This work only investigates the case for 120°, 180° and 240°, whose corresponding apex angles are 38.9°, 60° and 83.6°, respectively, see 4.8. The co-ordinate transformation from sheet to the CNC structure can be realized as

$$\begin{aligned} X &= r\cos\beta, \\ Y &= r\sin\beta, \\ Z &= -\sqrt{l^2 - r^2}, \end{aligned} \tag{4.11}$$

where (l, α) are the coordinates of the sheet and $G(X, Y, Z)$ are the coordinates of CNC. l, α, β, r can be realised from figure 4.9 and can be calculated through the following relations.

$$\begin{aligned} \beta &= \alpha\,(2\pi/\varphi)\,, \\ r &= l\varphi/2\pi, \end{aligned} \tag{4.12}$$

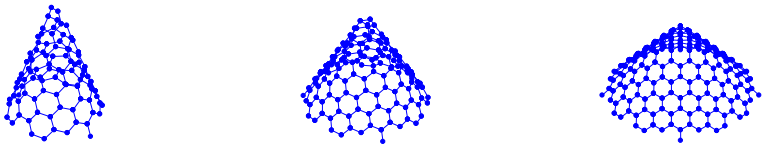

(a) Apex angle 38.9° (b) Apex angle 60° (c) Apex angle 83.6°

Figure 4.10: Carbon Nano Cube with 3 different apex angles, created in MATLAB [2]

where φ is as shown in figure 4.9. Inserting equation 4.12 into 4.11, the final relation is obtained as

$$\begin{aligned} X &= (l\varphi/2\pi)\cos\left[\alpha\left(2\pi/\varphi\right)\right], \\ Y &= (l\varphi/2\pi)\sin\left[\alpha\left(2\pi/\varphi\right)\right], \\ Z &= -l\sqrt{1-(\varphi/2\pi)}. \end{aligned} \tag{4.13}$$

Figure 4.10 shows 3 different CNCs generated in MATLAB, using the above mentioned algorithm.

4.3 Inter atomic potential

As mentioned section 4.1, the inter atomic potential has to be decided as well for the molecular dynamic simulation. For graphene, Bond Order potential is quite popular. Bond Order potential is calculated based on quantum mechanical theory. This incorporates both sigma and pi bonding. This was firstly developed by Pettifor et. al.[77, 78, 79] and later updated by Murdick [80] and Ward [81]. Referring to LAMMPS documentation [82], the equation of potential can be formulated as

$$E = \frac{1}{2}\sum_{i=1}^{N}\sum_{j=i_1}^{i_N}\phi_{ij}\left(r_i j\right) - \sum_{i=1}^{N}\sum_{j=i_1}\beta_{\sigma,ij}\left(r_{ij}\right)\cdot\Theta_{\sigma,ij} - \sum_{i=1}^{N}\sum_{j=i_1}\beta_{\pi,ij}\left(r_{ij}\right)\cdot\Theta_{\pi,ij} + U_{prom}, \tag{4.14}$$

where ϕ_{ij} is a short range two body function that takes care of the repulsion of two ion cores, $\beta_{\sigma,ij}\left(r_{ij}\right)$ and $\beta_{\pi,ij}\left(r_{ij}\right)$ are the sigma and pi bond integrals respectively, $\Theta_{\sigma,ij}$ and $\Theta_{\pi,ij}$ are the sigma and pi bond orders, respectively, U_{prom} is the promotional energy of the sp-valent systems. For details about these functions, the reader is referred to the work of Ward [81]. In this work, the inter atomic potential is implemented through the potential file available within the LAMMPS documentation [83].

Chapter 5

Results

In this section, results of the continuum mechanical and the molecular dynamic simulation of the graphene structures will be shown. In both cases, the result will be shown for a sheet structure undergoing uniaxial tension in the arm chair and Zigzag direction as well as bi axial tension. The continuum mechanical result for graphene structure is compared with the results from the Neo-Hookean material. In the molecular dynamic section, results for Carbon Nano Tube (CNT) structure is also shown under uniaxial tension and the evolution of the total energy (kinetic energy + potential energy) is studied. Finally both result is compared.

5.1 Continuum Mechanical Approach

The continuum mechanical approach, discussed in chapter 2 and3 is applied to a membrane structure of dimension 2 × 2 mm×mm. The membrane structure is shown in figure 5.1. Before application of forces, the membrane structure is subjected to 0.1% stretch to be stabilized. Thereafter the structure is subjected to uniaxial and biaxial tension with a force of 60 kN. The uniaxial tension is applied in the armchair and zigzag direction, see figure 5.2. As discussed in chapter 3, the constants of the material model can be determined either through Local Density Approximation method or through Generalized Gradient method. Based on the method employed, different results are obtained. Figure 5.3, 5.4 and 5.5 shows the stress-stretch relation in the direction of loading and in the transverse direction of loading for uniaxial tension in the arm chair direction, uniaxial tension in the zigzag direction and biaxial tension respectively. These results are obtained from equation 3.23 and validated with the results from Ghaffari et. al.[46]. The results

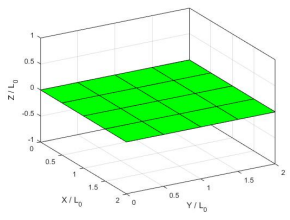

Figure 5.1: Undeformed membrane

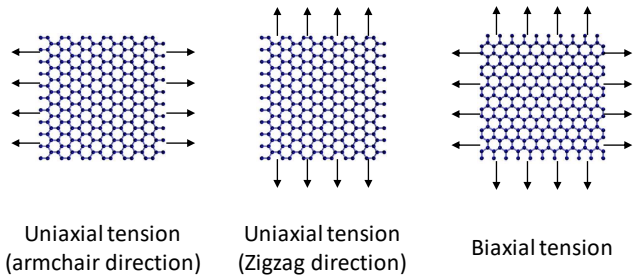

Figure 5.2: Different types of loading on a graphene

are different for uniaxial tension in the armchair direction and zigzag direction, which quite evidently shows the anisotropic behaviour. These figures show us that the stress builds up relatively quicker in case of uniaxial tension in the armchair direction in the direction of loading than in case of uniaxial tension in the zigzag direction. These figures show us that the stress builds up relatively quicker in case of uniaxial tension in the armchair direction, in the direction of loading than in case of uniaxial tension in the zigzag direction. These figures also include the corresponding behaviour for the Neo-Hookean material which shows isotropic behaviour. The Neo-hookean model approximates the behaviour of graphene at small deformation. However, at large deformation the difference is very big.

The peak stresses for both cases do not vary much with respect to the each other. The finite element results, obtained through MATLAB [2], for the membrane structure are shown in figure 5.6, figure 5.7 and figure 5.8. In figure 5.6, the material model constants are determined through Generalized Gradient Approxima-

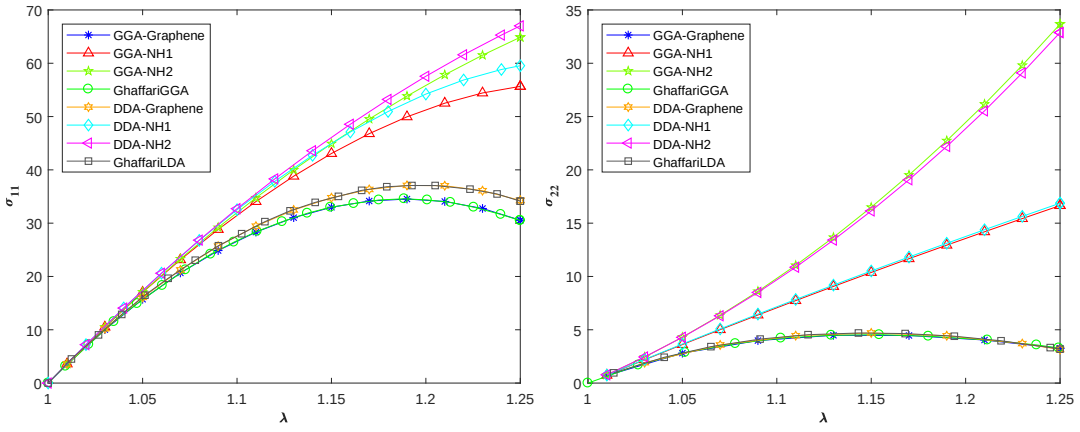

(a) Stress in the direction of loading

(b) Stress in the transverse direction of loading

Figure 5.3: Unaxial loading in the armchair direction and no stretching in the zigzag direction. GGA-Graphene, DDA-Graphene are for the anisotropic model corresponding to equation 3.23; GGA-NH1, DDA-NH1 are for the first Neo-Hookean model corresponding to equation 3.32 and GGA-NH2, DDA-NH2 are for the second Neo-Hookean model corresponding to equation 3.33

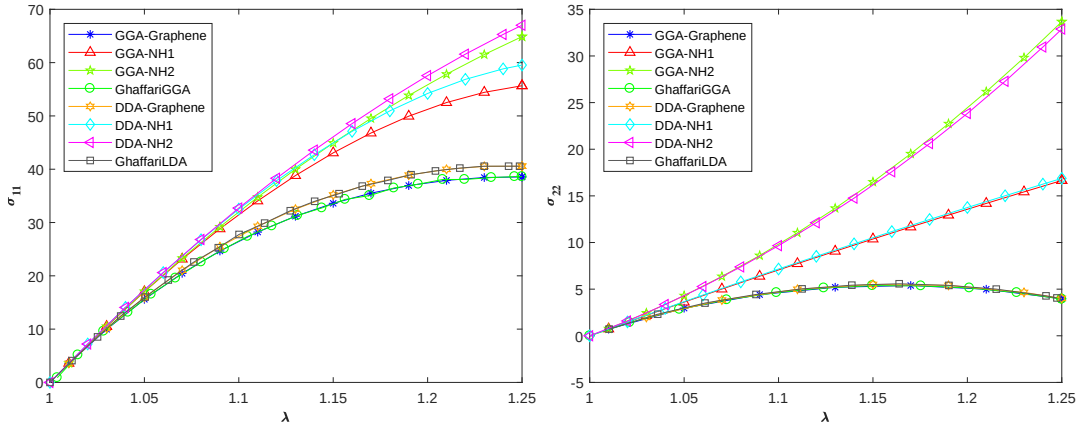

(a) Stress in the direction of loading

(b) Stress in the transverse direction of loading

Figure 5.4: Unaxial loading in the zigzag direction and no stretching in the armchair direction. GGA-Graphene, DDA-Graphene are for anisotropic model corresponding to equation 3.23; GGA-NH1, DDA-NH1 are for first Neo-Hookean model corresponding to equation 3.32 and GGA-NH2, DDA-NH2 are for the second Neo-Hookean model corresponding to equation 3.33

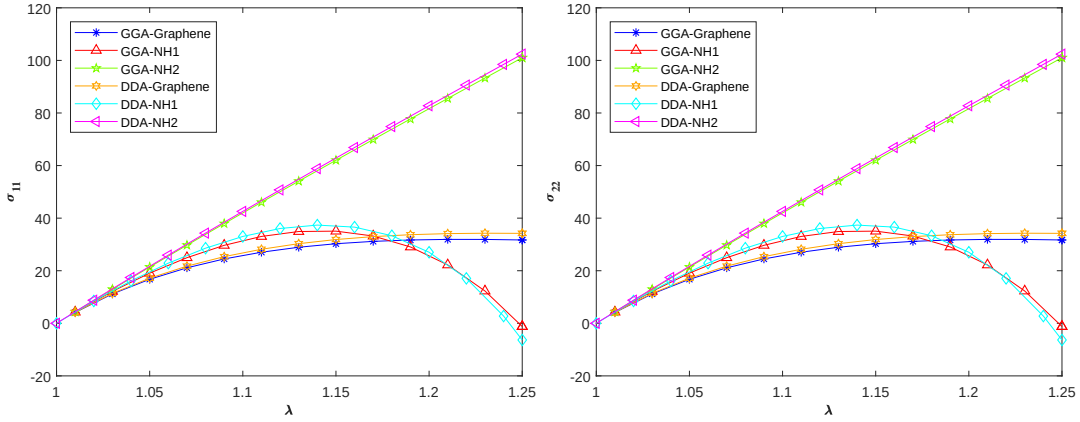

(a) Stress in the direction of loading

(b) Stress in the transverse direction of loading

Figure 5.5: Equi-biaxial loading. GGA-Graphene, DDA-Graphene are for anisotropic model corresponding to equation 3.23; GGA-NH1, DDA-NH1 are for the first Neo-Hookean model corresponding to equation 3.32 and GGA-NH2, DDA-NH2 are for the second Neo-Hookean model corresponding to equation 3.33

tion (GGA), wherein figure 5.6(a) to 5.6(c) shows the loading in armchair direction, zigzag direction and both directions respectively. Figure 5.7 shows the results in the same order for the material model of graphene, where the constants are determined through Local Density Approximation (LDA) method. Figure 5.8 shows the finite elementary implementation of Neo-Hookean model.

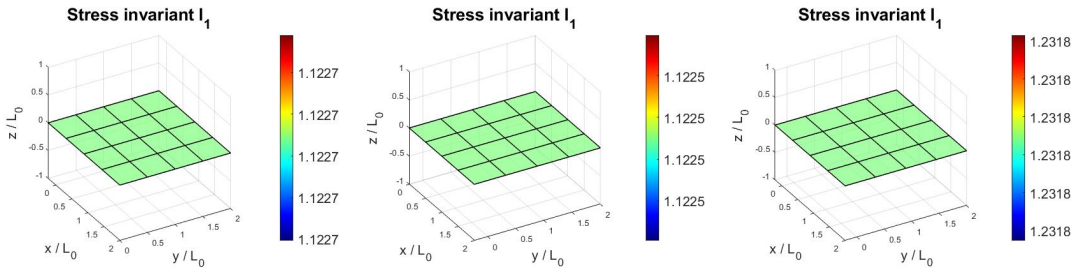

(a) Uniaxial loading in armchair direction (b) Uniaxial loading in zigzag direction (c) Equi-biaxial loading

Figure 5.6: Finite element implementation of the anisotropic model of Graphene, where the values of table 3.1 is taken considering generalized gradient approximation (GGA) method.

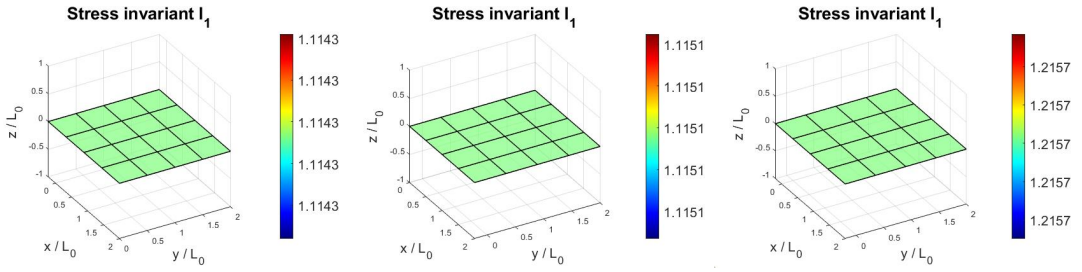

(a) Uniaxial loading in armchair direction (b) Uniaxial loading in zigzag direction (c) Equibiaxial loading

Figure 5.7: Finite element implementation of the anisotropic model of Graphene, where the values of table 3.1 is taken considering Local Density approximation (LDA) method.

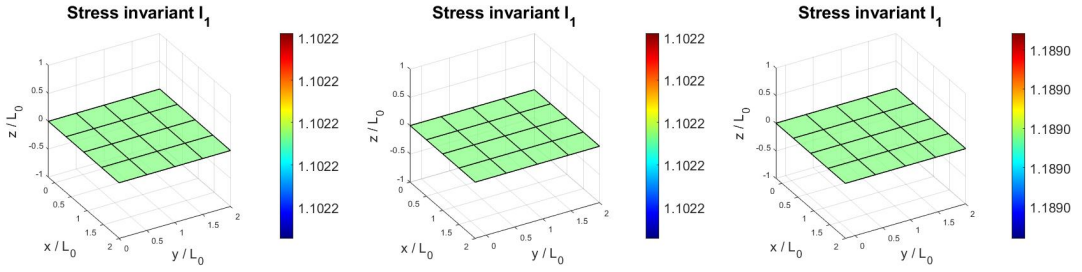

(a) Uniaxial loading in armchair direction (b) Uniaxial loading in zigzag direction (c) Equi-biaxial loading

Figure 5.8: Finite element implementation of Neo-Hookean model, where the constants are given in table 3.3 considering the local density approximation (LDA).

5.2 Molecular Dynamic simulation

In this section, stress-stretch behaviour is analysed using molecular dynamic approach. As described in chapter 5. Figure 4.4 shows different type of cuts for creation of a graphene sheet. For molecular dynamic simulation an armchair graphene

sheet is created with m=4 and n=4. Number of unit cells in the vertical direction is

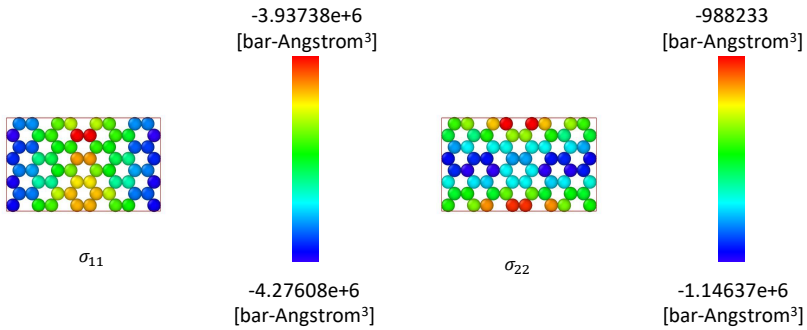

Figure 5.9: Initial stress distribution in the graphene sheet for molecular dynamic simulation with m=5 and n=5 with 4 unit cells [σ_{11} = xx component and σ_{22} = yy component].

4. Figure 5.9 shows the initial condition of the graphene sheet. Within LAMMPS, stress is calculated using `stress/atom` command. The stress is computed as

$$\begin{aligned} S_{ab} \;=\; -\Bigg[& m v_a v_b + \frac{1}{2}\sum_{n=1}^{N_p}\left(r_{1_a}F_{1_b} + r_{2_a}F_{2_b}\right) + \frac{1}{2}\sum_{n=1}^{N_b}\left(r_{1_a}F_{1_b} + r_{2_a}F_{2_b}\right) + \\ & \frac{1}{3}\sum_{n=1}^{N_b}\left(r_{1_a}F_{1_b} + r_{2_a}F_{2_b} + r_{3_a}F_{3_b}\right) + \frac{1}{4}\sum_{n=1}^{N_d}\left(r_{1_a}F_{1_b} + r_{2_a}F_{2_b} + r_{3_a}F_{3_b} + r_{4_a}F_{4_b}\right) + \\ & \frac{1}{4}\sum_{n=1}^{N_i}\left(r_{1_a}F_{1_b} + r_{2_a}F_{2_b} + r_{3_a}F_{3_b} + r_{4_a}F_{4_b}\right) + Kspace\left(r_{i_a}, F_{i_b}\right) + \sum_{n=1}^{N_f} r_{i_a}, F_{i_b} \Bigg], \end{aligned} \tag{5.1}$$

where the first term is the kinetic energy contribution, second term is a pairwise energy contribution, third term is the bond contribution, fourth term is the angle contribution, fifth term is the dihedral contribution, sixth term is the improper interaction contribution, seventh term is the long range Coulombic contribution and the final term is due to the internal constraints. N_p is the number of neighbour atoms for i$^{\text{th}}$ atom, N_b is the number of bonds for i$^{\text{th}}$ atom, N_a is the number of angles for i$^{\text{th}}$ atom, N_d is the number of dihedral for i$^{\text{th}}$ atom, N_i is the number of improper interactions for i$^{\text{th}}$ atom.r_i and F_i can be understood as the position and forces experienced by i$^{\text{th}}$ atom. However, the unit of this calculation is bar-Angstrom^3 (pressure$\times$volume). Therefore for the calculation purpose the value is divided by the volume to obtain the pressure and the pressure is divided by the hight of simulation box to get the force per unit length.

Figure 5.9 shows the initial distribution of stress calculated through equation 5.1. The colour bars show the stress distribution for the graphene sheet, subjected under

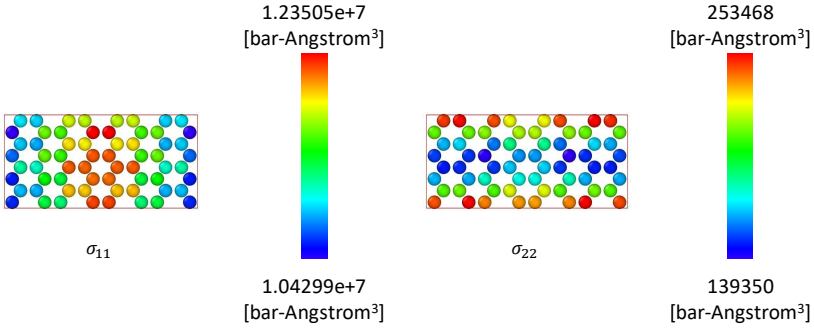

Figure 5.10: stress distribution in the graphene sheet under uniaxial tension in the arm chair direction [σ_{11} = xx component and σ_{22} = yy component].

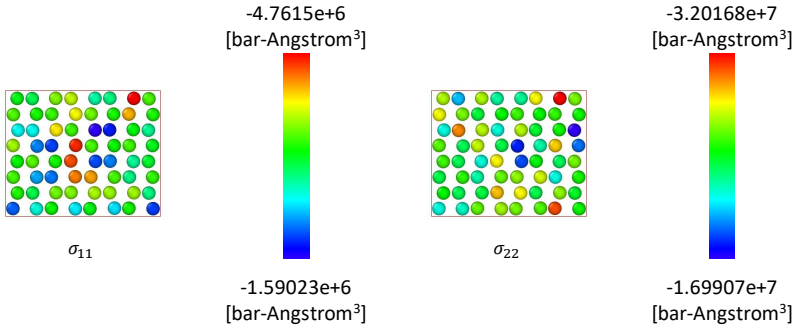

Figure 5.11: stress distribution in the graphene sheet under uniaxial tension in the zigzag direction [σ_{11} = xx component and σ_{22} = yy component].

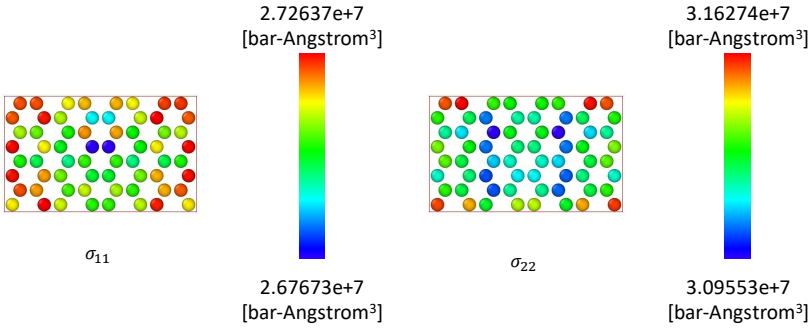

Figure 5.12: stress distribution in the graphene sheet under biaxial tension [σ_{11} = xx component and σ_{22} = yy component].

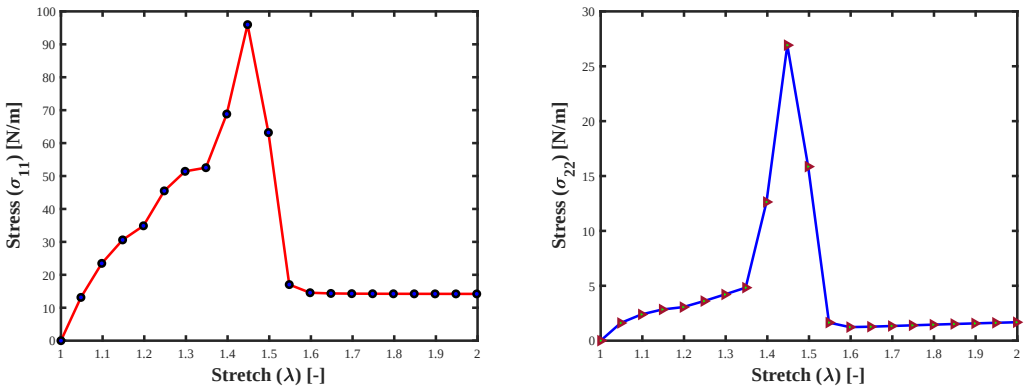

(a) Stress in the direction of loading.

(b) Stress in the transverse direction of loading.

Figure 5.13: Stretch vs stress curve for uniaxial tension in the arm chair direction.

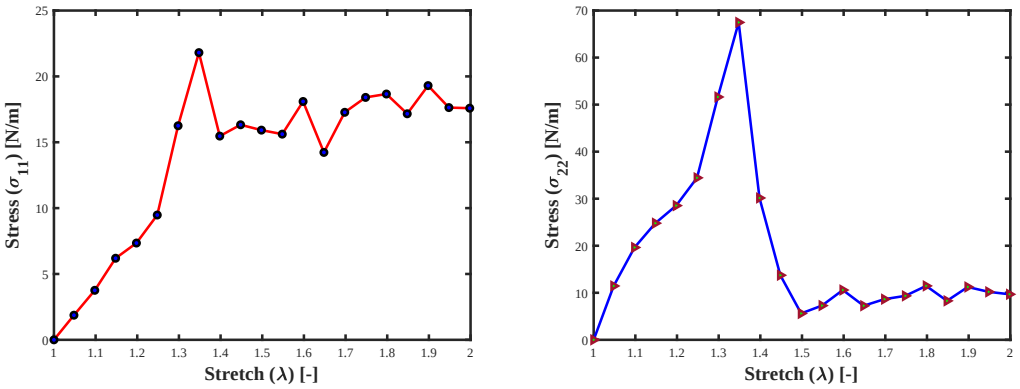

(a) Stress in the direction of loading.

(b) Stress in the transverse direction of loading.

Figure 5.14: Stretch vs stress curve for uniaxial tension in the zigzag direction.

uniaxial tension in the armchair direction, uniaxial tension in the zigzag direction (y direction) and biaxial tension. In this case, the x direction is the armchair direction and the is the zigzag direction. Stretch is calculated by dividing the initial length of the sheet in the loading direction by the final length of the sheet in the loading direction. Therefore,

$$\begin{aligned} \text{stretch for uniaxial tension in the armchair direction} &= \frac{[\max(x) - \min(x)]|_{\lambda=1}}{[\max(x) - \min(x)]|_{\lambda=\lambda_{\max}}}, \\ \text{stretch for uniaxial tension in the zigzag direction} &= \frac{[\max(y) - \min(y)]|_{\lambda=1}}{[\max(y) - \min(y)]|_{\lambda=\lambda_{\max}}}, \end{aligned}$$

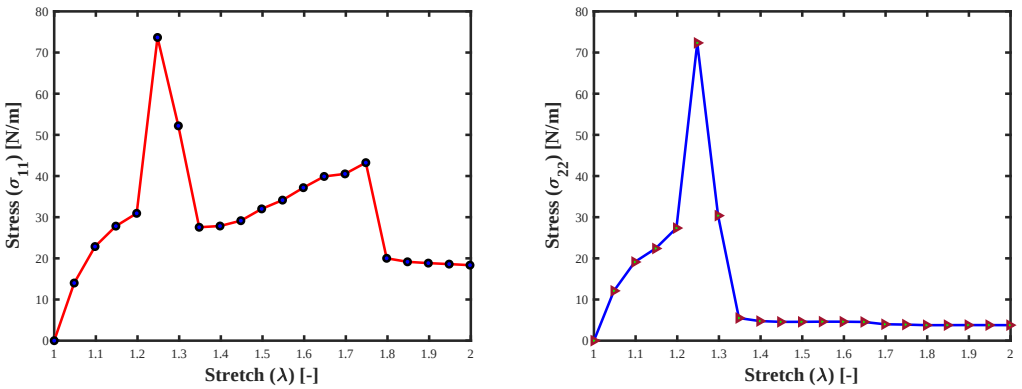

(a) Stress in the direction of loading.

(b) Stress in the transverse direction of loading.

Figure 5.15: Stretch vs stress curve for Biaxial tension.

$$\text{stretch for biaxial tension} \quad = \quad \frac{[\max(x) - \min(x)]|_{\lambda=1}}{[\max(x) - \min(x)]|_{\lambda=\lambda_{\max}}}. \tag{5.2}$$

Figure 5.13 shows the stress vs stretch curve for uniaxial tension in the armchair direction (i.e. x direction), figure 5.14 shows the same results for the uni axial tension in the Zigzag direction and 5.15 shows it for the biaxial tension. In all the cases the initial condition is considered as stress free, therefore the stress -stretch curve is shifted.

The molecular dynamic simulation is further implemented for different type of carbon nano tube (CNT) structures, as shown in figure 4.6. Figure 5.16 shows an armchair CNT with m=4,n=4. the number of unit cell the the vertical direction is 4. This structure is stretched in the z direction and the colours are given as per their zz component of stress. Likewise, figure 5.17 shows a zigzag CNT structure

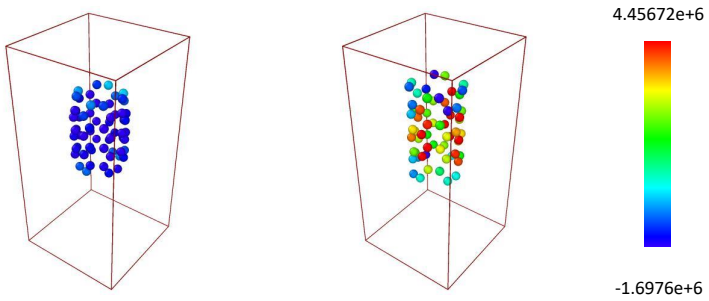

Figure 5.16: stress distribution in the armchair carbon nano tube (CNT) under uniaxial tension [σ_{33} = zz component].

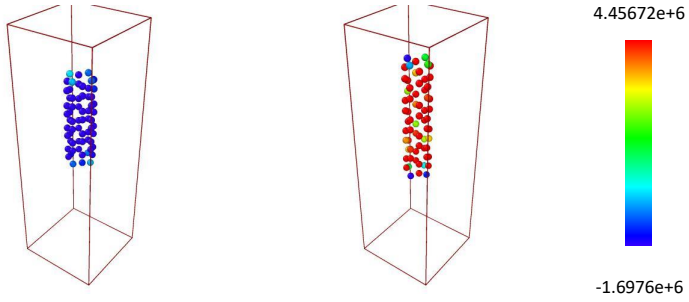

Figure 5.17: stress distribution in the zigzag carbon nano tube (CNT) under uniaxial tension [σ_{33} = zz component].

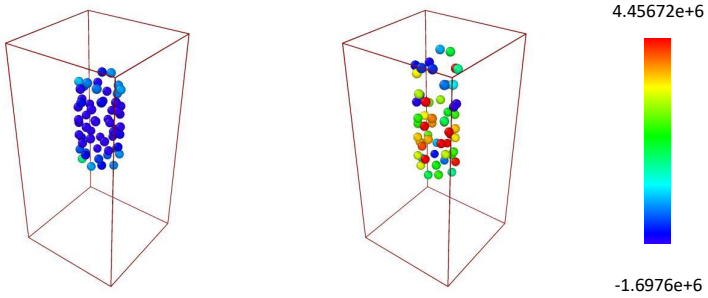

Figure 5.18: stress distribution in the carbon nano tube (CNT) with m=4, n=1 and i unit cell under uniaxial tension [σ_{33} = zz component].

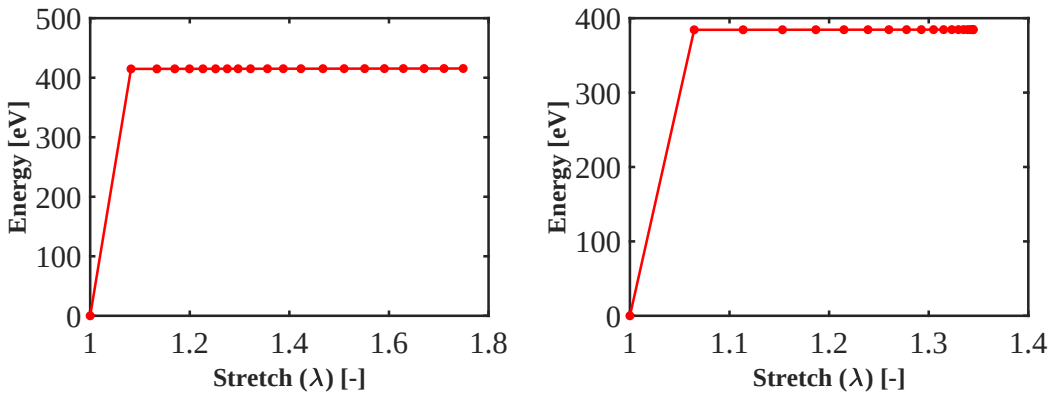

(a) Energy vs stretch for armchair CNT (m=4, n=4, number of unit cell=4).

(b) Energy vs stretch for armchair CNT (m=4, n=0, number of unit cell=4).

Figure 5.19: Energy vs stretch curve for standard CNT structures.

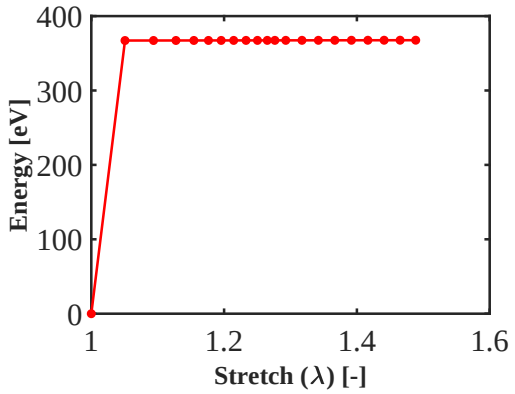

(a) Energy vs stretch for armchair CNT (m=4, n=4, number of unit cell=4.)

Figure 5.20: Energy vs stretch curve for general CNT structures.

with m=4, n=0, with 4 unit cells in the vertical direction. Figure 5.17 shows a CNT structure with m=4, n=2, with only one unit cell in the vertical direction. The evolution of total energy (potential energy + kinetic energy) is studied. Like the stress-stretch curves of sheet structures, in case of CNT also the initial conditions is considered as zero total energy and the curves are shifted accordingly. Figure 5.19 and 5.20 show the evolution of energy for standard CNT structures (armchair and zigzag) and general CNT structures.

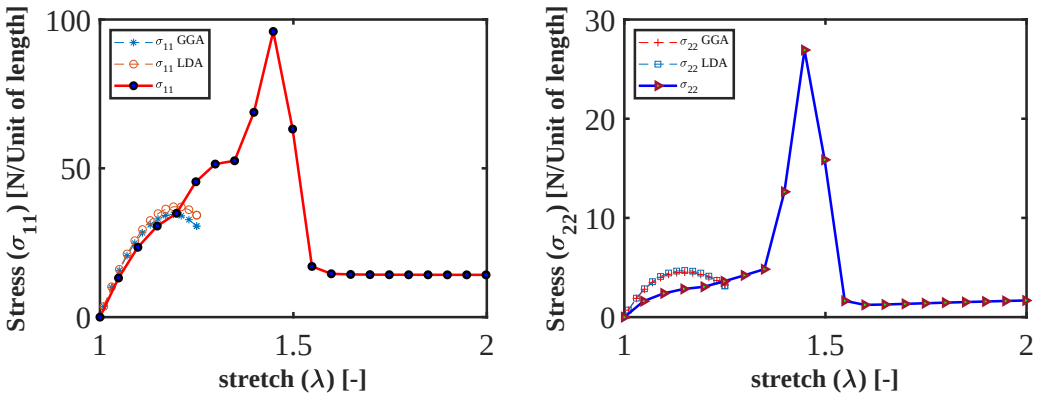

(a) Stress vs stretch in the direction of pulling. (b) Stress vs stretch in the transverse direction of pulling.

Figure 5.21: Comparison of continuum mechanical result (obtained through Generalized Gradient Approximation (GGA) and Local Density Approximation (LDA)) and molecular dynamic result for uni axial tension in the armchair direction.

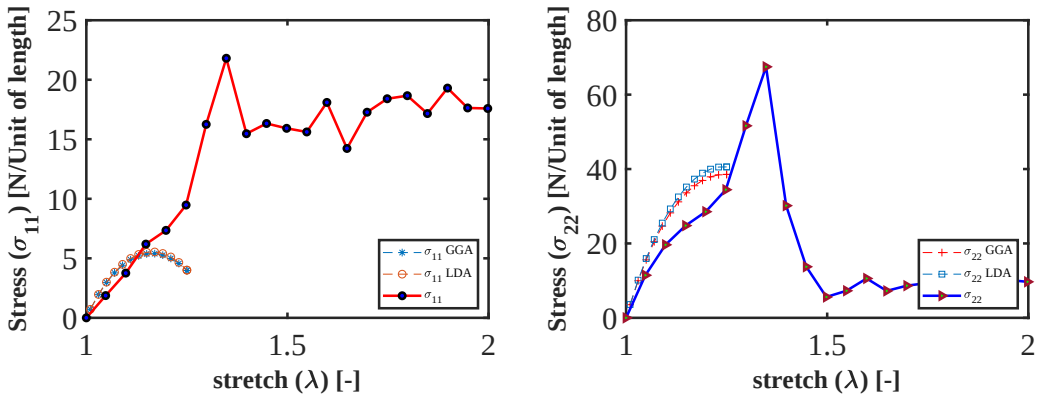

(a) Stress vs stretch in the transverse direction of pulling.

(b) Stress vs stretch in the direction of pulling.

Figure 5.22: Comparison of continuum mechanical result (obtained through Generalized Gradient Approximation (GGA) and Local Density Approximation (LDA)) and molecular dynamic result for uni axial tension in the zigzag direction.

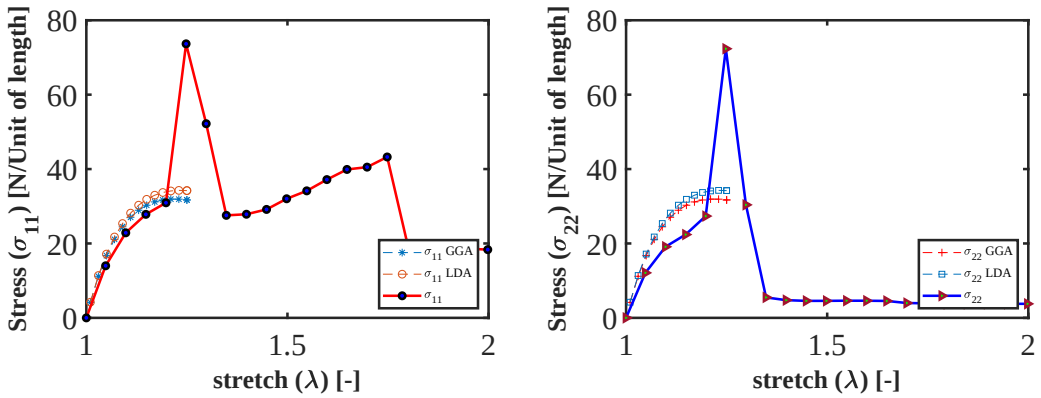

(a) Stress vs stretch in x direction.

(b) Stress vs stretch in the y direction.

Figure 5.23: Comparison of continuum mechanical result (obtained through Generalized Gradient Approximation (GGA) and Local Density Approximation (LDA)) and molecular dynamic result for biaxial tension.

5.3 Comparison of continuum mechanical result and molecular dynamic result

In this section the continuum mechanical and molecular dynamic results are compared. Figure 5.21, 5.22 and 5.23 shows the comparison of both results for uniaxial tension in the armchair direction, uniaxial tension in the zigzag direction and biaxial tension, respectively. The comparisons show that the continuum result and the molecular dynamic result match quite well.

5.4 Conclusion

It can be concluded that the continuum mechanical approach, proposed in this work can match stress-stretch behaviour of graphene sheet obtained based on ab-initio data. The molecular dynamic result is matching with the continuum mechanical result as well. Furthermore, the membrane formulation can be extended to a shell formulation and the continuum mechanical approach can be revised for application to a much complicated structure, like carbon nano tube (CNT) or carbon nano cone (CNC). Using the algorithms already discussed in this work, the CNT and CNC structures can be generated and a molecular dynamic simulation can be obtained for comparison with the continuum mechanical results.

Appendix A

Strain measures

Different kind of strain tensors can be taken as the basis of creation of a material model. This chapter will briefly discuss different strain measures and necessary background information about the path of development of these measures. Special attention will be given to the strain measure discussed in Kumar and parks [45], i.e. the logarithmic strain tensor and Cauchy-Green tensor which is taken as a basis of material modelling in this work.

A.1 Different Strain measures

Different kinds of strain measures are available in the literature. However, all of them may not be suitable for a particular model of material. As mentioned in section 2.2, deformation gradient $\mathbf{F}$ creates the bridge between the current and the reference configuration. Therefore it can be used as a basis of a material model development. The work conjugate of $\mathbf{F}$ is the first Kirchhoff-Piola stress, which can be obtained by differentiating the strain energy function (W) with respect to $\mathbf{F}$. However, for computational efficiency its better to use a as many symmetric tensors as possible for modelling of material behaviour. This gives the symmetric right Cauchy-Green Tensor $\mathbf{C}$ an edge over the previously introduced deformation gradient $\mathbf{F}$. The differentiation of strain energy function (W) with respect to $\mathbf{C}$ gives us the second Kirchhoff-Piola stress, which is work conjugate of $\mathbf{C}$ and symmetric as well.

Furthermore, deformation gradient can be further decomposed into two parts. These parts are separately responsible for rotation and stretch within the total deformation. This can be mathematically expressed as

$$\mathbf{F} = \mathbf{R}\mathbf{U}, \tag{A.1}$$

where $\mathbf{R}$ is responsible for rotation within the deformation and $\mathbf{U}$ is responsible of stretch. The stretch tensor $\mathbf{U}$ can be formulated using polar decomposition as

$$\mathbf{U} = \mathbf{C}^{\frac{1}{2}} = \sum_{i=1}^{2} \lambda_i \boldsymbol{N_i} \otimes \boldsymbol{N_i}, \tag{A.2}$$

where $\lambda_i = \sqrt{\Lambda_i}$ for $(i = 1, 2)$ are eigenvalues of $\mathbf{U}$. Λ_i is the eigenvalues of $\mathbf{C}$. $\boldsymbol{N_i}$ for $(i = 1, 2)$ are the eigenvectors of $\mathbf{C}$. The rotation tensor $\mathbf{R}$ can be formulated as

$$\mathbf{R} = \mathbf{F}\mathbf{U}^{-1}. \tag{A.3}$$

Now as already mentioned in section 3.1.1, using the stretch tensor $\mathbf{U}$ Bhoj Raj Seth developed the following strain measures.

$$\mathbf{E}^{(m)} = \begin{cases} \frac{1}{m}\left(\mathbf{U}^m - \mathbf{I}\right) & \forall\ r \neq 0, \\ \ln(\mathbf{U}) & \forall\ r = 0. \end{cases} \tag{A.4}$$

For different value of m we get different strain measures. For example, $m = 0$ gives the Hencky strain tensor, i.e. the logarithmic strain tensor. this can be formulated as

$$\mathbf{E}^{(0)} = \ln(\mathbf{U}). \tag{A.5}$$

Kumar and Parks [45] uses this for material modelling. This will be discussed in detail during further sections within this appendix. For $m = 1, 2$ we get

$$\mathbf{E}^{(1)} = \mathbf{U} - \mathbf{I}, \tag{A.6}$$

$$\mathbf{E}^{(2)} = \frac{1}{2}\left(\mathbf{C} - \mathbf{I}\right). \tag{A.7}$$

$\mathbf{E}^{(1)}$ and $\mathbf{E}^{(2)}$ can be termed as Biot tensor and Green-Lagrange tensor respectively.

A.2 Decomposition of logarithmic strain tensor in a area changing and shape changing part

Kumar and Parks [45] used Logarithmic strain tensor $\mathbf{E}^{(0)}$ for defining the material model. The major advantage of this is, we can decompose this in a purely dilatory (area changing) and shape changing part.

This can be done initially by decomposing the stretch tensor $\mathbf{U}$ as

$$\mathbf{U} = \mathbf{U}^a\tilde{\mathbf{U}} = \tilde{\mathbf{U}}\mathbf{U}^a, \tag{A.8}$$

where $\mathbf{U}^a$ and $\tilde{\mathbf{U}}$ are the area changing part and shape changing part of $\mathbf{U}$. Therefore it can be corroborated $\det(\mathbf{U}^a) = \det\mathbf{U}$ and $\det(\tilde{\mathbf{U}}) = 1$. Finally $\mathbf{U}^a$ and $\tilde{\mathbf{U}}$ can be formulated as

$$\mathbf{U}^a = J^{1/2}\mathbf{I}, \tag{A.9}$$

$$\tilde{\mathbf{U}} = \lambda \boldsymbol{N_1} \otimes \boldsymbol{N_1} + \lambda^{-1}\boldsymbol{N_2} \otimes \boldsymbol{N_2}, \tag{A.10}$$

where J can calculated as per equation 2.29 and $\lambda = \sqrt{\frac{\lambda_1}{\lambda_2}} \geq 1$. Finally using A.2, A.9 and A.10, $\mathbf{E}^{(0)}$ can be written as

$$\begin{aligned} \mathbf{E}^{(0)} &= \frac{1}{2}\ln J\mathbf{I} + \ln\lambda\left(\boldsymbol{N_1} \otimes \boldsymbol{N_1} - \boldsymbol{N_2} \otimes \boldsymbol{N_2}\right) \\ &= \frac{1}{2}\epsilon_a\mathbf{I} + \mathbf{E_0^{(0)}}, \end{aligned} \tag{A.11}$$

where

$$\epsilon_a = \ln J = \ln\left(\det \mathbf{U}\right) = \ln\left(\det \mathbf{U}^a\right), \tag{A.12}$$

$$\mathbf{E}_{\mathbf{0}}^{(\mathbf{0})} = \ln \tilde{\mathbf{U}} = \ln \lambda \left(\boldsymbol{N_1} \otimes \boldsymbol{N_1} - \boldsymbol{N_2} \otimes \boldsymbol{N_2}\right). \tag{A.13}$$

It can easily be concluded from the above two equation that the first part of equation A.11 denotes to the area changing part of $\mathbf{E}^{(\mathbf{0})}$. whereas the second part denotes the shape changing part of $\mathbf{E}^{(\mathbf{0})}$.

A.3 Advantages of right Cauchy-Green tensor

Although logarithmic strain $\mathbf{E}^{(\mathbf{0})}$ is a good candidate for material modelling, it has a big disadvantage in terms of computation. Since for anisotropic modelling a chain rule has to be used for calculation stress tensor, the material model becomes tedious in terms of computation. For this reason right Cauchy-Green tensor is used for modelling the behaviour of Graphene in this work.

Appendix B

Stress measures

For large deformation case, there are different proposition of stress measures. Different stress measures has different advantages and disadvantages in terms of computation. In this section, these stress measures and their physical significances are introduced.

Cautchy Stress: Cautchy stress is described in current configuration. It is first proposed by *Augustin-Louis Cautchy*. He introduced this as a linear mapping betwen traction vector($\boldsymbol{t}$) and normal vector($\boldsymbol{n}$). Cautchy stress is denoted by $\boldsymbol{\sigma}$ and can be formulated as

$$\boldsymbol{t} = \boldsymbol{\sigma}\boldsymbol{n} \tag{B.1}$$

All other stress are introduced as a conversion from cautchy stress in this document.

Kirchhoff Stress: Kirchhoff stress $\boldsymbol{\tau}$ is described as the stress on a weighted surface. This weighted surface is $\det(\mathbf{F})d\boldsymbol{a}$, where $d\boldsymbol{a}$ is the elemental surface area in current configuration and $\mathbf{F}$ is the deformation gradient. So, $\boldsymbol{\tau}$ can be formulated in terms of $\boldsymbol{\sigma}$ as

$$\boldsymbol{\tau} = J\boldsymbol{\sigma}, \tag{B.2}$$

where $J = \det(\mathbf{F})$ is defined as per equation 2.29.

First Kirchhoff-Piola Stress: First Kirchhoff-Piola stress $\mathbf{P}$ describes the stress in the reference configuration. $\mathbf{P}$ is formulated with respect to $\boldsymbol{\sigma}$ and $\boldsymbol{\tau}$ as following.

$$\mathbf{P} = \mathrm{J}\boldsymbol{\sigma}\mathbf{F}^{-T} = \boldsymbol{\tau}\mathbf{F}^{-T} \tag{B.3}$$

Second Kirchhoff-Piola Stress: Second Kirchhoff-Piola stress is detoned as $\mathbf{S}$. It has no physical significance. However, this is very popular for formulation because this is symmetric. In this document also, we mostly analyze with respect to $\mathbf{S}$.

$$\mathbf{S} = J\mathbf{F}^{-1}\boldsymbol{\sigma}\mathbf{F}^{-T} = \mathbf{F}^{-1}\mathbf{P} \tag{B.4}$$

Appendix C

symmetry invariants for 6 fold rotational symmetry

In this section, the symmetry invariants for a 6 fold rotational geometry is discussed. As mentioned in equation 3.7 of chapter 3, these invariants are functions of $\mathbf{C}$ and structural tensor. Therefore, firstly this section discusses the development of structural tensors for a n fold rotational symmetry. Thereafter as Kumar and Parks [45] suggested, the invariants for $\mathbf{E^{(0)}}$ are shown and finally the invariants for $\mathbf{C}$ are introduced.

C.1 Structural tensors and invariants for n-fold rotational symmetry

As mentioned in equation 3.5, the lattice structure of an anisotropic material can be left as indistinguishable compared to its initial configuration under some transformations. These transformations altogether form the symmetry group for the structure [84]. For a n fold rotational geometry, the symmetry group consists of identity mapping, inversion, rotation and reflection. The elements of the symmetry group can then be utilized to formulate the structural tensors, as shown by Zheng [62]. There for a n-fold symmetry the structural tensors can be realized as

$$\mathbb{H}_n = \mathfrak{R}\left[(\hat{\boldsymbol{x}} + i\hat{\boldsymbol{y}})^{(n)}\right] = \begin{cases} \mathfrak{R}\left[\left(\hat{\mathbf{M}} + i\hat{\mathbf{N}}\right)^{(m)}\right] & \text{for } n = 2m, \\ \mathfrak{R}\left[(\hat{\boldsymbol{x}} + i\hat{\boldsymbol{y}}) \otimes \left(\hat{\mathbf{M}} + i\hat{\mathbf{N}}\right)^{(m)}\right] & \text{for } n = 2m+1, \end{cases} \tag{C.1}$$

where $\hat{\boldsymbol{x}}$ and $\hat{\boldsymbol{y}}$ are two orthonormal vectors, amongst which at least one of them must be in the crystal symmetry plane. In case of graphene structure, these vectors are defined as shown in figure C.1. $\hat{\boldsymbol{x}}$ and $\hat{\boldsymbol{y}}$ represent the armchair and zigzag direction of graphene structure. The operator $(\bullet)^{(n)} = (\bullet) \otimes (\bullet)...(\bullet)$ can be realized as the tensor product of n times. $\mathfrak{R}[(\bullet)]$ indicates the real part of $(\bullet)$. The tensors $\hat{\mathbf{M}}$ and $\hat{\mathbf{N}}$ can be defines as

$$\begin{aligned} \hat{\mathbf{M}} &= \hat{\boldsymbol{x}} \otimes \hat{\boldsymbol{x}} - \hat{\boldsymbol{y}} \otimes \hat{\boldsymbol{y}} \\ \hat{\mathbf{N}} &= \hat{\boldsymbol{x}} \otimes \hat{\boldsymbol{y}} + \hat{\boldsymbol{y}} \otimes \hat{\boldsymbol{x}} \end{aligned} \tag{C.2}$$

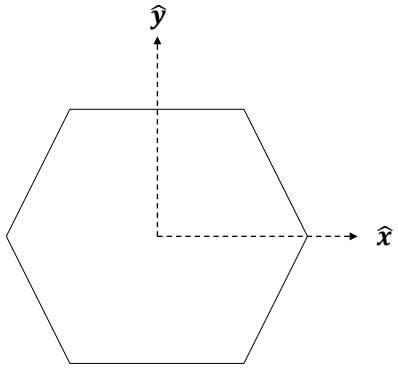

Figure C.1: Orthogonal vectors $\hat{\boldsymbol{x}}$ and $\hat{\boldsymbol{y}}$, for graphene structure where $\hat{\boldsymbol{x}}$ represents the armchair direction and $\hat{\boldsymbol{y}}$ represents the zigzag direction

As mentioned in chapter 3, graphene inherits a 6 -fold rotational symmetry. Therefore the symmetry group consists of 14 operations and those are an identity mapping, an inversion, six mirror planes and six rotations. Now putting n=6 in equation C.1 we get the structural tensor as

$$\mathbb{H}_6 = \left[\hat{\mathbf{M}} \otimes \hat{\mathbf{M}} \otimes \hat{\mathbf{M}} - \left(\hat{\mathbf{M}} \otimes \hat{\mathbf{N}} \otimes \hat{\mathbf{N}} + \hat{\mathbf{N}} \otimes \hat{\mathbf{M}} \otimes \hat{\mathbf{N}} + \hat{\mathbf{N}} \otimes \hat{\mathbf{N}} \otimes \hat{\mathbf{M}}\right)\right] \tag{C.3}$$

The invariants of an arbitrary tensor $\mathbf{A}$ of rank 2 can be expressed with respect to the structural tensor and $\mathbf{A}$ itself [62, 85].

$$\begin{aligned} \mathcal{J}^{+}_{1\mathbf{A}} &= \mathrm{tr}(\mathbf{A}), \\ \mathcal{J}^{+}_{2\mathbf{A}} &= \frac{1}{2}\mathrm{tr}(\mathbf{A}^2), \\ \mathcal{J}^{+}_{3\mathbf{A}} &= \frac{1}{8}\mathrm{tr}(\mathbf{\Pi}^{\mathbf{A}}_n \mathbf{A}) = \frac{1}{8}\mathbf{\Pi}^{\mathbf{A}}_n : \mathbf{A} \end{aligned} \tag{C.4}$$

can be realized as these invariants where

$$\mathbf{\Pi}^{\mathbf{A}}_n = A^{m-1}\Re\left[e^{in\theta} + i(m-1)\theta_{\mathbf{A}}\left(\hat{\mathbf{M}}^{\diamond} + i\hat{\mathbf{N}}^{\diamond}\right)\right] \text{ with } n = 2m, m = 1, 2, 3... \tag{C.5}$$

$\hat{\mathbf{M}}^{\diamond}+i\hat{\mathbf{N}}^{\diamond}$ introduced here can be formulated as $\hat{\mathbf{M}}^{\diamond}+i\hat{\mathbf{N}}^{\diamond} = e^{2i\theta}\left(\hat{\mathbf{M}} + i\hat{\mathbf{N}}\right)$ according to equation C.8. Additionally A and $\theta_{\mathbf{A}}$ introduced in equation C.5 can be obtained from the following equation:

$$2\mathbf{A} = \mathrm{tr}(\mathbf{A})\mathbf{I} + A\left[\cos(\theta_{\mathbf{A}})\hat{\mathbf{M}}^{\diamond} + \sin(\theta_{\mathbf{A}})\hat{\mathbf{N}}^{\diamond}\right]. \tag{C.6}$$

In order to find the value of A and $\theta_{\mathbf{A}}$ spectral decomposition of $\mathbf{A}$ is employed, which can be formulated as

$$\mathbf{A} = \sum_{\alpha=1}^{2} \lambda_{\alpha\mathbf{A}} \mathbf{Y}_{\alpha\mathbf{A}} \otimes \mathbf{Y}_{\alpha\mathbf{A}}, \tag{C.7}$$

where $\lambda_{\alpha\mathbf{A}}$ and $\mathbf{Y}_{\alpha\mathbf{A}}$ can eigenvalues and eigenvectors of $\mathbf{A}$ respectively. Now considering $\hat{\boldsymbol{x}}$ and $\hat{\boldsymbol{y}}$ are to be rotated by an angle θ to $\hat{\boldsymbol{x}}^{\diamond}$ and $\hat{\boldsymbol{y}}^{\diamond}$, we get

$$\begin{aligned}\hat{\boldsymbol{x}}^{\diamond} + i\hat{\boldsymbol{y}}^{\diamond} &= e^{-i\theta}\left(\hat{\boldsymbol{x}} + i\hat{\boldsymbol{y}}\right),\\ \hat{\boldsymbol{M}}^{\diamond} + i\hat{\boldsymbol{N}}^{\diamond} &= e^{-2i\theta}\left(\hat{\boldsymbol{M}} + i\hat{\boldsymbol{N}}\right).\end{aligned} \tag{C.8}$$

θ can be chosen in such a way that $\hat{\boldsymbol{x}}^{\diamond}$ and $\mathbf{Y}_{\mathbf{1A}}$ are in the same orientation and consequently $A = \lambda_{\mathbf{1A}} - \lambda_{\mathbf{2A}}$ $(\lambda_{\mathbf{1A}} > \lambda_{\mathbf{2A}})$ and $\theta_{\mathbf{A}} = 0$.

C.2 Invariants of logarithmic strain

Logarithmic strain strain tensor is used as the basis of strain energy formulation in the work of Kumar and Parks [45]. Logarithmic strain is a very good candidate for strain energy formulation because it can be decomposed in a volumetric and elastic strain part. It can also include the micro-mechanical attributes of a material, as shown in [86, 87, 87, 88]. Therefore putting $\mathbf{A} = \mathbf{E}^{(0)}$ in equation C.4 we get,

$$\begin{aligned}\mathcal{J}_{1\mathbf{E}^{(0)}} &= \mathrm{tr}(\mathbf{E}^{(\mathbf{0})}) = \ln(J),\\ \mathcal{J}^{\vdash}_{2\mathbf{E}^{(0)}} &= \frac{1}{2}\mathrm{tr}(\mathbf{E}^{(\mathbf{0})^2}) = \frac{1}{4}\ln(J) + \frac{1}{2}\mathbf{E}^{(\mathbf{0})}_{\mathbf{dev}} : \mathbf{E}^{(\mathbf{0})}_{\mathbf{dev}},\\ \mathcal{J}_{3\mathbf{E}^{(0)}} &= \frac{1}{8}\mathbb{H}\left(\mathbf{E}^{(\mathbf{0})}, \mathbf{E}^{(\mathbf{0})}, \mathbf{E}^{(\mathbf{0})}\right) = \left(\ln\left(\frac{\lambda_1}{\lambda_2}\right)\right)^3 \cos(6\theta),\end{aligned} \tag{C.9}$$

where $\lambda_\alpha (\alpha = 1, 2)$ are eigenvalues of $\mathbf{E}^{(\mathbf{0})}$ and $\mathbf{E}^{(\mathbf{0})}_{\mathbf{dev}} = \mathbf{E}^{(\mathbf{0})} - \frac{1}{2}\ln(J)\mathbf{I} + \mathbf{E}^{(\mathbf{0})}_{\mathbf{dev}}$ is the deviatoric part of the logarithmic strain. The invariants from equation C.9 can be further simplified as

$$\begin{aligned}\mathcal{J}_{1\mathbf{E}^{(0)}} &= \ln(J),\\ \mathcal{J}_{2\mathbf{E}^{(0)}} &= \frac{1}{2}\mathbf{E}^{(\mathbf{0})}_{\mathbf{dev}} : \mathbf{E}^{(\mathbf{0})}_{\mathbf{dev}} = \left(\ln(\lambda)\right)^2,\\ \mathcal{J}_{3\mathbf{E}^{(0)}} &= \frac{1}{8}\mathbb{H}\left(\mathbf{E}^{(\mathbf{0})}, \mathbf{E}^{(\mathbf{0})}, \mathbf{E}^{(\mathbf{0})}\right) = \left(\ln(\lambda)\right)^3 \cos(6\theta),\end{aligned} \tag{C.10}$$

where $\lambda = \sqrt{\frac{\lambda_1}{\lambda_2}}$ and $\lambda_1 > \lambda_2$.

C.3 Invariants of right Cauchy-Green Tensor

Although logarithmic strain $\mathbf{E}^{(\mathbf{0})}$ has significant advantages interms of development of material model but for the calculation of stress and elasticity tensor chain rule has to be applied. In case of an isotropic material, the stress and the elasticity can directly be obtained without using chain rule, see [89]. However for an anisotropic material, the chain rule has to be applied. Therefore right Cauchy Tensor ($\mathbf{C}$) become a better candidate for developing a anisotropic material model instead of logarithmic strain. There for the invariants for right Cauchy-Green tensor can be

formulated as

$$\begin{aligned}
\mathcal{J}^{\vdash}_{1\mathbf{C}} &= \mathrm{tr}(\mathbf{C}),\\
\mathcal{J}^{\vdash}_{2\mathbf{C}} &= \frac{1}{2}\mathbf{C}:\mathbf{C} = \frac{1}{2}\left(\Lambda_1^2+\Lambda_2^2\right),\\
\mathcal{J}^{\vdash}_{3\mathbf{C}} &= \frac{1}{8}\mathbb{H}(\mathbf{C},\mathbf{C},\mathbf{C}) = \frac{1}{8}\left(\Lambda_1-\Lambda_2\right)^3\cos(6\theta),
\end{aligned} \tag{C.11}$$

where Λ_α ($\alpha = 1, 2$) are the eigen values of $\mathbf{C}$. However for the purpose of further simplification the right Cauchy-Green Tensor is further decomposed into a area changing and area invariant part, Which can be realized as

$$\begin{aligned}
J &= \det(\mathbf{F}),\\
\bar{\mathbf{C}} &= \frac{1}{J}\mathbf{C}
\end{aligned} \tag{C.12}$$

respectively, where $\mathbf{F}$ is the deformation gradient. Therefore assuming J as an additional invariant, the list of invariants become

$$\begin{aligned}
\bar{\mathcal{J}}^{\vdash}_{1\mathbf{C}} &= \mathrm{tr}(\bar{\mathbf{C}}),\\
\bar{\mathcal{J}}^{\vdash}_{2\mathbf{C}} &= \frac{1}{2}\bar{\mathbf{C}}:\bar{\mathbf{C}} = \frac{1}{2}\left(\frac{\Lambda_1}{\Lambda_2}+\frac{\Lambda_2}{\Lambda_1}\right),\\
\bar{\mathcal{J}}^{\vdash}_{3\mathbf{C}} &= \frac{1}{8}\mathbb{H}(\bar{\mathbf{C}},\bar{\mathbf{C}},\bar{\mathbf{C}}) = \frac{1}{8}\left(\frac{\lambda_1}{\lambda_2}+\frac{\lambda_2}{\lambda_1}\right)^3\cos(6\theta),\\
\bar{\mathcal{J}}^{\vdash}_{4\mathbf{C}} &= J,
\end{aligned} \tag{C.13}$$

where $\lambda_\alpha = \sqrt{\Lambda_\alpha}$. Within this set of invariants, $\bar{\mathcal{J}}^{\vdash}_{1\mathbf{C}}$ can be expressed in terms of $\bar{\mathcal{J}}^{\vdash}_{2\mathbf{C}}$ as

$$(\bar{\mathcal{J}}^{\vdash}_{1\mathbf{C}})^2 = \frac{1}{2}\bar{\mathcal{J}}^{\vdash}_{2\mathbf{C}} + 2. \tag{C.14}$$

Therefore $\bar{\mathcal{J}}^{\vdash}_{1\mathbf{C}}$ can be eliminated from the set of invariants. Additionally $\bar{\mathcal{J}}^{\vdash}_{2\mathbf{C}}$ can be expressed in terms of traceless part of $\mathbf{C}$. The traceless part can be realised as

$$\bar{\mathbf{C}}^{\perp} = \left(\bar{\mathbf{C}} - \frac{1}{2}\mathrm{tr}(\bar{\mathbf{C}})\mathbf{I}\right). \tag{C.15}$$

The invariant $\bar{\mathcal{J}}^{\vdash}_{2\mathbf{C}}$ can be changed to

$$\mathcal{J}_{2\mathbf{C}} = \frac{1}{2}\left(\bar{\mathcal{J}}^{\vdash}_{2\mathbf{C}} - 1\right). \tag{C.16}$$

Finally the proposed set of invariants for right Cauchy-Green tensor can be realised as

$$\begin{aligned}
\mathcal{J}_{1\mathbf{C}} &= \sqrt{\det(\mathbf{C})} = J,\\
\mathcal{J}_{2\mathbf{C}} &= \frac{1}{2}\bar{\mathbf{C}}^{\perp}:\bar{\mathbf{C}}^{\perp} = \frac{1}{4}\left(\frac{\Lambda_1}{\Lambda_2}+\frac{\Lambda_2}{\Lambda_1}-2\right),\\
\mathcal{J}_{3\mathbf{C}} &= \frac{1}{8}\mathbb{H}\left(\bar{\mathbf{C}},\bar{\mathbf{C}},\bar{\mathbf{C}}\right) = \frac{1}{8}\left(\frac{\lambda_1}{\lambda_2}+\frac{\lambda_2}{\lambda_1}\right)^3\cos(6\theta),
\end{aligned} \tag{C.17}$$

Appendix D

Stress and elasticity tensor for graphene model

In this section, the calculation of stress tensor and elastic tensor is discussed for the anisotropic strain energy function. The derivatives required to calculate the stress and elasticity tensor is shown here step by step

D.1 Calculation of stress tensor

D.1.1 Elementary derivatives

As per [47] following derivatives can be written.

$$\frac{\partial J^{\alpha}}{\partial \mathbf{C}} = \frac{\alpha}{2} J^{\alpha} \mathbf{C}^{-1}, \tag{D.1}$$

$$\frac{\partial}{\partial \mathbf{C}} (f\mathbf{G}) = \mathbf{G} \odot \frac{\partial f}{\partial \mathbf{A}} + f \frac{\partial \mathbf{G}}{\partial \mathbf{A}}, \tag{D.2}$$

$$\frac{\partial \mathbf{C}}{\partial \mathbf{C}} = (\mathbf{I} \otimes \mathbf{I})^{s} = \mathcal{J}_{s}, \tag{D.3}$$

$$\frac{\partial (\mathbf{G} : \mathbf{H})}{\partial \mathbf{A}} = \mathbf{H} : \frac{\partial \mathbf{G}}{\partial \mathbf{A}} + \mathbf{G} : \frac{\partial \mathbf{H}}{\partial \mathbf{A}}, \tag{D.4}$$

$$\frac{\partial (\mathrm{tr}\mathbf{C})}{\partial \mathbf{C}} = \mathbf{I}, \tag{D.5}$$

$$\frac{\partial \mathbf{I}}{\partial \mathbf{A}} = \mathbf{0}, \tag{D.6}$$

where J is determinant of deformation gradient, α is a scalar number, $\mathbf{C}$ is a right Cauchy-Green tensor, f is scalar function of $\mathbf{A}$, $\mathbf{A}$ is an arbitrary tensor, $\mathbf{I}$ is identity tensor, $(\bullet)^{s}$ is the symmetric part of $(\bullet)$, $\mathcal{J}_{s}$ is the super symmetric identity tensor, $\mathbf{G}$ and $\mathbf{H}$ are two different tensor function of $\mathbf{A}$, $\mathrm{tr}(\mathbf{C})$ is the trace of $\mathbf{C}$ and $\mathbf{0}$ is the zero tensor. Now Putting $\alpha = -1,\ 1$ in equation D.1 we get the following,

$$\frac{\partial}{\partial \mathbf{C}} \left(\frac{1}{J} \right) = -\frac{1}{2J} \mathbf{C}^{-1} \tag{D.7}$$

$$\frac{\partial J}{\partial \mathbf{C}} = \frac{1}{2} J \mathbf{C}^{-1} \tag{D.8}$$

Additionally following formulas can be formulated. Using equation 3.15

$$\bar{\mathbf{C}}^{\perp} : \mathbf{I} = \mathbf{0}. \tag{D.9}$$

Using equation 3.15

$$\bar{\mathbf{C}}^{\perp} : \mathbf{C} = J\bar{\mathbf{C}}^{\perp} : \bar{\mathbf{C}}^{\perp}. \tag{D.10}$$

Two additional parameter $a_{\hat{\mathbf{M}}}$ and $a_{\hat{\mathbf{N}}}$ can formulated as

$$\begin{aligned} a_{\hat{\mathbf{M}}} &= 3\left[\left(\hat{\mathbf{M}} : \bar{\mathbf{C}}\right)^2 - \left(\hat{\mathbf{N}} : \bar{\mathbf{C}}\right)^2\right], \\ a_{\hat{\mathbf{N}}} &= -6\left[\left(\hat{\mathbf{M}} : \bar{\mathbf{C}}\right)\left(\hat{\mathbf{N}} : \bar{\mathbf{C}}\right)\right]. \end{aligned} \tag{D.11}$$

Using equation 3.14 and D.11 we get,

$$a_{\hat{\mathbf{M}}}\left(\hat{\mathbf{M}} : \mathbf{C}\right) + a_{\hat{\mathbf{N}}}\left(\hat{\mathbf{N}} : \mathbf{C}\right) = 24J\mathcal{J}_{3\mathbf{C}} \tag{D.12}$$

D.1.2 Calculation of stress tensor

For calculation of stress chain rule has been applied, refer [47]. Therefore using equation 3.14 and D.4 we get,

$$\frac{\partial \mathcal{J}_{2\mathbf{c}}}{\partial \mathbf{C}^{\perp}} = \mathbf{C}^{\perp}. \tag{D.13}$$

Using equation 3.15, D.2, D.3, D.5, D.6 and D.7 we get

$$\frac{\partial \bar{\mathbf{C}}^{\perp}}{\partial \mathbf{C}} = -\frac{1}{2J}\mathbf{C} \odot \mathbf{C}^{-1} + \frac{1}{4J}\mathrm{tr}(\mathbf{C})\mathbf{I} \odot \mathbf{C}^{-1} + \frac{1}{J}(\mathbf{I} \otimes \mathbf{I})^{s} - \frac{1}{2J}(\mathbf{I} \odot \mathbf{I}) \tag{D.14}$$

Using equation 3.14 D.3 and D.4 we get

$$\frac{\partial \mathcal{J}_{3\mathbf{c}}}{\partial \bar{\mathbf{C}}} = \frac{3}{8}\left[3\left\{\left(\hat{\mathbf{M}} : \bar{\mathbf{C}}\right)^2 - \left(\hat{\mathbf{N}} : \bar{\mathbf{C}}\right)^2\right\}\hat{\mathbf{M}} - 2\left(\hat{\mathbf{M}} : \bar{\mathbf{C}}\right)\left(\hat{\mathbf{N}} : \bar{\mathbf{C}}\right)\hat{\mathbf{N}}\right] \tag{D.15}$$

Using equation 3.15, D.2 and D.7 we get

$$\frac{\partial \bar{\mathbf{C}}}{\partial \mathbf{C}} = -\frac{1}{2J}\mathbf{C} \odot \mathbf{C}^{-1} + \frac{1}{J}(\mathbf{I} \otimes \mathbf{I})^{s} \tag{D.16}$$

Now, Using equation D.8, D.11 and D.13 to D.16

$$\frac{\partial \mathcal{J}_{1\mathbf{c}}}{\partial \mathbf{C}} = \frac{\partial J}{\partial \mathbf{C}} = \frac{1}{2}J\mathbf{C}^{-1} \tag{D.17}$$

$$\frac{\partial \mathcal{J}_{2\mathbf{c}}}{\partial \mathbf{C}} = \frac{\partial \mathcal{J}_{2\mathbf{c}}}{\partial \mathbf{C}^{\perp}} : \frac{\partial \mathbf{C}^{\perp}}{\partial \mathbf{C}} = -\mathcal{J}_{2\mathbf{c}}\mathbf{C}^{-1} + \frac{1}{J}\mathbf{C}^{\perp} \tag{D.18}$$

$$\frac{\partial \mathcal{J}_{3\mathbf{c}}}{\partial \mathbf{C}} = \frac{\partial \mathcal{J}_{3\mathbf{c}}}{\partial \bar{\mathbf{C}}} : \frac{\partial \bar{\mathbf{C}}}{\partial \mathbf{C}} = -\frac{3}{2}\mathcal{J}_{3\mathbf{c}}\mathbf{C}^{-1} + \frac{1}{8J}\left(a_{\hat{\mathbf{M}}}\hat{\mathbf{M}} + a_{\hat{\mathbf{N}}}\hat{\mathbf{N}}\right) \tag{D.19}$$

Following derivatives can be obtained by normal scalar derivative laws.

$$\frac{\partial W}{\partial \mathcal{J}_{1\mathbf{c}}} = \frac{\epsilon\hat{\alpha}^2}{J}\ln(J)e^{-\hat{\alpha}\ln J} - 2\mu_1\hat{\beta}J^{\hat{\beta}-1}f_1 + f_2\frac{2\eta_1}{J}\ln J \tag{D.20}$$

$$\frac{\partial W}{\partial \mathcal{J}_{2\mathbf{c}}} = 2\mu\left[e_1 - 2e_2\mathcal{J}_{2\mathbf{c}}\right] + g_2\eta\mathcal{J}_{3\mathbf{c}} \tag{D.21}$$

$$\frac{\partial W}{\partial \mathcal{J}_{3\mathbf{c}}} = \eta\left(g_1 - g_2\mathcal{J}_{2\mathbf{c}}\right) \tag{D.22}$$

Finally using equation D.17 to D.22, the second kirchhoff-Piola stress $\mathbf{S}$ can formulated as

$$\begin{aligned}\mathbf{S} = \frac{\partial W}{\partial \mathbf{C}} &= \frac{\partial W}{\partial \mathcal{J}_{1\mathbf{c}}}\frac{\partial \mathcal{J}_{1\mathbf{c}}}{\partial \mathbf{C}} + \frac{\partial \mathcal{J}_{2\mathbf{c}}}{\partial \mathbf{C}}\frac{\partial W}{\partial \mathcal{J}_{2\mathbf{c}}} + \frac{\partial \mathcal{J}_{3\mathbf{c}}}{\partial \mathbf{C}}\frac{\partial W}{\partial \mathcal{J}_{3\mathbf{c}}} \\ &= H_1\mathbf{C}^{-1} + \frac{H_2}{J}\bar{\mathbf{C}}^{\perp} + \frac{H_3}{4J}\left(a_{\hat{\mathbf{M}}}\hat{\mathbf{M}} + a_{\hat{\mathbf{N}}}\hat{\mathbf{N}}\right),\end{aligned} \tag{D.23}$$

where the constants H_1, H_2 and H_3 can be formulated as

$$\begin{aligned}H_1 &= \varepsilon\hat{\alpha}^2\ln(J)e^{-\hat{\alpha}\ln(J)} - 2\mu_1\hat{\beta}J^{\hat{\beta}}f_1 - 2\eta_1\ln(J)f_2 - H_2\mathcal{J}_{2\mathbf{C}} - 3H_3\mathcal{J}_{3\mathbf{C}}, \\ H_2 &= 2\left(2\mu\left(e_1 - 2e_2\mathcal{J}_{2\mathbf{C}}\right) - g_2\eta\mathcal{J}_{3\mathbf{C}}\right), \\ H_3 &= \eta\left(g_1 - g_2\mathcal{J}_{2\mathbf{C}}\right).\end{aligned} \tag{D.24}$$

D.2 Calculation of elasticity tensor

For calculation of elasticity tensor, the derivatives of constants from equation D.24 with respect to invariants of $\mathbf{C}$ has to be formulated. These formulas are

$$\begin{aligned}\frac{\partial H_1}{\partial \mathcal{J}_{1\mathbf{C}}} &= \frac{\varepsilon\hat{\alpha}^2}{J}\left\{1 - \hat{\alpha}\ln(J)\right\}e^{-\hat{\alpha}\ln(J)} - 2\mu_1\hat{\beta}^2J^{\hat{\beta}-1}f_1 - 2\frac{\eta_1}{J}f_2 - \frac{\partial H_2}{\partial \mathcal{J}_{1\mathbf{C}}}\mathcal{J}_{2\mathbf{C}} - 3\frac{\partial H_3}{\partial \mathcal{J}_{1\mathbf{C}}}\mathcal{J}_{3\mathbf{C}} \\ \frac{\partial H_2}{\partial \mathcal{J}_{1\mathbf{C}}} &= 2\left[2\left\{-\mu_1\hat{\beta}J^{\hat{\beta}-1}\left(e_1 - 2e_2\mathcal{J}_{2\mathbf{C}}\right)\right\}2\frac{g_2\eta_1}{J}\ln(J)\mathcal{J}_{3\mathbf{C}}\right] \\ \frac{\partial H_3}{\partial \mathcal{J}_{1\mathbf{C}}} &= -\frac{\eta_1}{J}\ln(J)\left(g_1 - g_2\mathcal{J}_{2\mathbf{C}}\right)\end{aligned} \tag{D.25}$$

$$\begin{aligned}\frac{\partial H_1}{\partial \mathcal{J}_{2\mathbf{C}}} &= -2\mu_1\hat{\beta}J^{\hat{\beta}}\left(e_1 - 2e_2\mathcal{J}_{2\mathbf{C}}\right) + 2g_2\eta_1\ln(J)\mathcal{J}_{3\mathbf{C}} - H_2 - \frac{\partial H_2}{\partial \mathcal{J}_{2\mathbf{C}}}\mathcal{J}_{2\mathbf{C}} - 3\frac{\partial H_3}{\partial \mathcal{J}_{2\mathbf{C}}}\mathcal{J}_{3\mathbf{C}} \\ \frac{\partial H_2}{\partial \mathcal{J}_{2\mathbf{C}}} &= -8\mu e_2 \\ \frac{\partial H_3}{\partial \mathcal{J}_{2\mathbf{C}}} &= -\eta g_2\end{aligned} \tag{D.26}$$

$$\begin{aligned}\frac{\partial H_1}{\partial \mathcal{J}_{3\mathbf{C}}} &= -2\eta_1 \left(g_1 - g_2 \mathcal{J}_{2\mathbf{C}}\right) \ln(J) - \frac{\partial H_2}{\partial \mathcal{J}_{3\mathbf{C}}} \mathcal{J}_{2\mathbf{C}} - 3H_3 \\ \frac{\partial H_2}{\partial \mathcal{J}_{3\mathbf{C}}} &= -2g_2\eta \end{aligned} \tag{D.27}$$

Additionally using equation D.11 derivatives of $a_{\hat{\mathbf{M}}}$, $a_{\hat{\mathbf{N}}}$ with respect to $\mathbf{C}$ can be defined as

$$\begin{aligned}\frac{\partial a_{\hat{\mathbf{M}}}}{\partial \mathbf{C}} &= \frac{6}{J}\left[\left(\hat{\mathbf{M}} : \bar{\mathbf{C}}\right)\hat{\mathbf{M}} - \left(\hat{\mathbf{N}} : \bar{\mathbf{C}}\right)\hat{\mathbf{N}}\right] - a_{\hat{\mathbf{M}}}\mathbf{C}^{-1}, \\ \frac{\partial a_{\hat{\mathbf{N}}}}{\partial \mathbf{C}} &= -\frac{6}{J}\left[\left(\hat{\mathbf{M}} : \bar{\mathbf{C}}\right)\hat{\mathbf{N}} + \left(\hat{\mathbf{N}} : \bar{\mathbf{C}}\right)\hat{\mathbf{M}}\right] - a_{\hat{\mathbf{N}}}\mathbf{C}^{-1}. \end{aligned} \tag{D.28}$$

Refering [70, 71], following derivatives can also be calculated as

$$\begin{aligned}\frac{\partial \mathbf{C}^{-1}}{\oplus \partial \mathbf{C}} &= -\frac{1}{2}\left(\mathbf{I}\otimes\mathbf{I} + \mathbf{I}\boxtimes\mathbf{I}\right), \\ \frac{\partial \bar{\mathbf{C}}^{\perp}}{\oplus \partial \mathbf{C}} &= -\frac{1}{2}\bar{\mathbf{C}}^{\perp}\oplus\mathbf{C}^{-1} + \frac{1}{2J}\left(\mathbf{I}\otimes\mathbf{I} + \mathbf{I}\boxtimes\mathbf{I} - \mathbf{I}\oplus\mathbf{I}\right), \end{aligned} \tag{D.29}$$

where $\dfrac{\partial(\bullet)}{\oplus\partial(\bullet)}$ can be defined as

$$\frac{\partial \mathbf{A}}{\oplus \partial \mathbf{B}} = \frac{\partial A^{\alpha\beta}}{\partial B_{\gamma\delta}} \mathbf{A}_\alpha \otimes \mathbf{A}_\gamma \otimes \mathbf{A}_\delta \otimes \mathbf{A}_\beta. \tag{D.30}$$

Now considering the method of calculating defining elasticity tensor from Kintzel and Baar [71] and Kintzel [70], the elasticity tensor for the membrane formulation can be defined as

$$\mathbb{C}^{\mathrm{L}} = \frac{\partial^2 W}{\partial \mathbf{C} \oplus \partial \mathbf{C}} = \frac{\partial^2 W}{\partial C_{\alpha\beta} \partial C_{\gamma\delta}} \mathbf{A}_\alpha \otimes \mathbf{A}_\gamma \otimes \mathbf{A}_\delta \otimes \mathbf{A}_\beta, \tag{D.31}$$

which can be formulated as

$$\begin{aligned}\mathbb{C}^{\mathrm{L}} \;=\; & 2\left\{\left(\frac{J}{2}\frac{\partial H_1}{\partial \mathcal{J}_{1\mathbf{C}}} - \mathcal{J}_{2\mathbf{C}}\frac{\partial H_1}{\partial \mathcal{J}_{2\mathbf{C}}} - \frac{3}{2}\mathcal{J}_{3\mathbf{C}}\frac{\partial H_1}{\partial \mathcal{J}_{3\mathbf{C}}}\right)\mathbf{C}^{-1}\oplus\mathbf{C}^{-1} + \frac{1}{J^2}\frac{\partial H_2}{\partial \mathcal{J}_{2\mathbf{C}}}\bar{\mathbf{C}}^{\perp}\oplus\bar{\mathbf{C}}^{\perp}\right. \\ & + \frac{2}{J}\frac{\partial H_1}{\partial \mathcal{J}_{2\mathbf{C}}}\left[\mathbf{C}^{-1}\oplus\bar{\mathbf{C}}^{\perp}\right]^S + \frac{1}{4J}\frac{\partial H_1}{\partial \mathcal{J}_{3\mathbf{C}}}\left[\mathbf{C}^{-1}\oplus\mathbf{Z}\right]^S + \frac{1}{2J^2}\frac{\partial H_3}{\partial \mathcal{J}_{2\mathbf{C}}}\left[\mathbf{Z}\oplus\bar{\mathbf{C}}^{\perp}\right]^S \\ & - \frac{1}{2}H_1\left(\mathbf{C}^{-1}\otimes\mathbf{C}^{-1} + \mathbf{C}^{-1}\boxtimes\mathbf{C}^{-1}\right) + \frac{H_2}{2J^2}\left(\mathbf{I}\otimes\mathbf{I} + \mathbf{I}\boxtimes\mathbf{I} - \mathbf{I}\oplus\mathbf{I}\right) \\ & \left.\frac{3H_3}{2J^2}\left[\left(\hat{\mathbf{M}} : \bar{\mathbf{C}}\right)\left(\hat{\mathbf{M}}\oplus\hat{\mathbf{M}} - \hat{\mathbf{N}}\oplus\hat{\mathbf{N}}\right) - \left(\hat{\mathbf{N}} : \bar{\mathbf{C}}\right)\left(\hat{\mathbf{M}}\oplus\hat{\mathbf{N}} + \hat{\mathbf{N}}\oplus\hat{\mathbf{M}}\right)\right]\right\}, \end{aligned} \tag{D.32}$$

where

$$\mathbf{Z} = a_{\hat{\mathbf{M}}}\hat{\mathbf{M}} + a_{\hat{\mathbf{N}}}\hat{\mathbf{N}} \tag{D.33}$$

$$(\mathbf{A}\oplus\mathbf{B})^S = \frac{1}{2}\left(\mathbf{A}\oplus\mathbf{B} + \mathbf{B}\oplus\mathbf{A}\right) \tag{D.34}$$

However, for implementation in a FE formulation the components of $\mathbb{C}^{\mathrm{L}}$ must be rearranged. This rearrangement can be done as Kintzel and baar [71] and Kintzel [70], which can be formulated as

$$\mathbb{C} = \left(\mathbb{C}^{\mathrm{L}}\right)^{\mathrm{R}} = \left(\mathbb{C}^{\mathrm{L}\alpha\beta\gamma\delta}\boldsymbol{A}_{\alpha}\otimes\boldsymbol{A}_{\beta}\otimes\boldsymbol{A}_{\gamma}\otimes\boldsymbol{A}_{\delta}\right)^{\mathrm{R}} = \mathbb{C}^{\mathrm{L}\alpha\gamma\delta\beta}\boldsymbol{A}_{\boldsymbol{\alpha}}\otimes\boldsymbol{A}_{\beta}\otimes\boldsymbol{A}_{\gamma}\otimes\boldsymbol{A}_{\delta} \tag{D.35}$$

Now considering following standard derivatives, refer [70, 71], we get

$$(\mathbf{A}\oplus\mathbf{B})^{\mathrm{R}} = \mathbf{A}\oplus\mathbf{B}, \tag{D.36}$$
$$(\mathbf{A}\otimes\mathbf{B})^{\mathrm{R}} = \mathbf{A}\boxtimes\mathbf{B}^{\mathrm{T}}, \tag{D.37}$$
$$(\mathbf{A}\boxtimes\mathbf{B})^{\mathrm{R}} = \mathbf{A}\oplus\mathbf{B}^{\mathrm{T}}, \tag{D.38}$$
$$\left[(\bullet)^{\mathrm{R}}\right]^{\mathrm{L}} = \left[(\bullet)^{\mathrm{L}}\right]^{\mathrm{R}} = (\bullet), \tag{D.39}$$

where $\mathbf{A}$ and $\mathbf{B}$ are two second order tensors. Therefore the elasticity tensor for FE formulation can be defined as

$$\begin{aligned}\mathbb{C} \;=\; & 2\left\{\left(\frac{J}{2}\frac{\partial H_1}{\partial \mathcal{J}_{1\mathbf{C}}} - \mathcal{J}_{2\mathbf{C}}\frac{\partial H_1}{\partial \mathcal{J}_{2\mathbf{C}}} - \frac{3}{2}\mathcal{J}_{3\mathbf{C}}\frac{\partial H_1}{\partial \mathcal{J}_{3\mathbf{C}}}\right)\mathbf{C}^{-1}\otimes\mathbf{C}^{-1} + \frac{1}{J^2}\frac{\partial H_2}{\partial \mathcal{J}_{2\mathbf{C}}}\bar{\mathbf{C}}^{\perp}\otimes\bar{\mathbf{C}}^{\perp}\right.\\
& + \frac{2}{J}\frac{\partial H_1}{\partial \mathcal{J}_{2\mathbf{C}}}\left[\mathbf{C}^{-1}\otimes\bar{\mathbf{C}}^{\perp}\right]^{S} + \frac{1}{4J}\frac{\partial H_1}{\partial \mathcal{J}_{3\mathbf{C}}}\left[\mathbf{C}^{-1}\otimes\mathbf{Z}\right]^{S} + \frac{1}{2J^2}\frac{\partial H_3}{\partial \mathcal{J}_{2\mathbf{C}}}\left[\mathbf{Z}\otimes\bar{\mathbf{C}}^{\perp}\right]^{S}\\
& - \frac{1}{2}H_1\left(\mathbf{C}^{-1}\boxtimes\mathbf{C}^{-1} + \mathbf{C}^{-1}\oplus\mathbf{C}^{-1}\right) + \frac{H_2}{2J^2}\left(\mathbf{I}\boxtimes\mathbf{I} + \mathbf{I}\oplus\mathbf{I} - \mathbf{I}\otimes\mathbf{I}\right)\\
& \left.\frac{3H_3}{2J^2}\left[\left(\hat{\mathbf{M}}:\bar{\mathbf{C}}\right)\left(\hat{\mathbf{M}}\otimes\hat{\mathbf{M}} - \hat{\mathbf{N}}\otimes\hat{\mathbf{N}}\right) - \left(\hat{\mathbf{N}}:\bar{\mathbf{C}}\right)\left(\hat{\mathbf{M}}\otimes\hat{\mathbf{N}} + \hat{\mathbf{N}}\otimes\hat{\mathbf{M}}\right)\right]\right\}.\end{aligned} \tag{D.40}$$

where

$$\begin{aligned}&\mathbf{Z} = a_{\hat{\mathbf{M}}}\hat{\mathbf{M}} + a_{\hat{\mathbf{N}}}\hat{\mathbf{N}},\\
&(\mathbf{A}\otimes\mathbf{B}) = \frac{1}{2}\left(\mathbf{A}\otimes\mathbf{B} + \mathbf{B}\otimes\mathbf{A}\right).\end{aligned} \tag{D.41}$$

Considering Kintzel [70] and Kintzel and Baar [71], the tensor products $\otimes$, $\boxtimes$ and $\oplus$[1] can be realised as

$$\begin{aligned}&\mathbf{A}\otimes\mathbf{B} = A^{\alpha\beta}A^{\gamma\delta}\boldsymbol{A}_{\boldsymbol{\alpha}}\otimes\boldsymbol{A}_{\boldsymbol{\beta}}\otimes\boldsymbol{A}_{\boldsymbol{\gamma}}\otimes\boldsymbol{A}_{\boldsymbol{\delta}},\\
&\mathbf{A}\oplus\mathbf{B} = A^{\alpha\beta}A^{\gamma\delta}\boldsymbol{A}_{\boldsymbol{\alpha}}\otimes\boldsymbol{A}_{\boldsymbol{\gamma}}\otimes\boldsymbol{A}_{\boldsymbol{\delta}}\otimes\boldsymbol{A}_{\boldsymbol{\beta}} = A^{\alpha\delta}A^{\beta\gamma}\boldsymbol{A}_{\boldsymbol{\alpha}}\otimes\boldsymbol{A}_{\boldsymbol{\beta}}\otimes\boldsymbol{A}_{\boldsymbol{\gamma}}\otimes\boldsymbol{A}_{\boldsymbol{\delta}},\\
&\mathbf{A}\boxtimes\mathbf{B} = A^{\alpha\beta}A^{\gamma\delta}\boldsymbol{A}_{\boldsymbol{\alpha}}\otimes\boldsymbol{A}_{\boldsymbol{\gamma}}\otimes\boldsymbol{A}_{\boldsymbol{\beta}}\otimes\boldsymbol{A}_{\boldsymbol{\delta}} = A^{\alpha\gamma}A^{\beta\delta}\boldsymbol{A}_{\boldsymbol{\alpha}}\otimes\boldsymbol{A}_{\boldsymbol{\beta}}\otimes\boldsymbol{A}_{\boldsymbol{\gamma}}\otimes\boldsymbol{A}_{\boldsymbol{\delta}},\end{aligned} \tag{D.42}$$

The components of $\mathbb{C}$ can be calculated using following formula.

$$\mathbb{C}^{\alpha\beta\gamma\delta} = \boldsymbol{A}^{\boldsymbol{\alpha}}\otimes\boldsymbol{A}^{\boldsymbol{\beta}} : \mathbb{C} : \boldsymbol{A}^{\boldsymbol{\gamma}}\otimes\boldsymbol{A}^{\boldsymbol{\delta}}. \tag{D.43}$$

[1] In [70] and [71] $\times$ is used instead of $\oplus$

Bibliography

[1] M. Yoshida, "Nanotube modeler," 2005.

[2] Mathworks, "Matlab," 1984.

[3] V. I. Merkulov, M. A. Guillorn, D. H. Lowndes, M. L. Simpson, and E. Voelkl, "Shaping carbon nanostructures by controlling the synthesis process," *Applied Physics Letters*, vol. 79, no. 8, pp. 1178–1180, 2001.

[4] A. K. Geim and K. S. Novoselov, "The rise of graphene," in *Nanoscience and Technology: A Collection of Reviews from Nature Journals*, pp. 11–19, World Scientific, 2010.

[5] M. Yudasaka, S. Iijima, and V. H. Crespi, "Single-wall carbon nanohorns and nanocones," in *Carbon nanotubes*, pp. 605–629, Springer, 2007.

[6] S. N. Naess, A. Elgsaeter, G. Helgesen, and K. D. Knudsen, "Carbon nanocones: wall structure and morphology," *Science and Technology of advanced materials*, vol. 10, no. 6, p. 065002, 2009.

[7] I. Ovidko, "Review on grain boundaries in graphene. curved poly-and nanocrystalline graphene structures as new carbon allotropes," *Rev. Adv. Mater. Sci*, vol. 30, no. 3, pp. 201–224, 2012.

[8] S. Alwarappan and A. Kumar, *Graphene-based materials: science and technology*. CRC Press, 2013.

[9] V. V. Mokashi, D. Qian, and Y. Liu, "A study on the tensile response and fracture in carbon nanotube-based composites using molecular mechanics," *Composites science and technology*, vol. 67, no. 3-4, pp. 530–540, 2007.

[10] B. Javvaji, P. R. Budarapu, V. Sutrakar, D. R. Mahapatra, M. Paggi, G. Zi, and T. Rabczuk, "Mechanical properties of graphene: Molecular dynamics simulations correlated to continuum based scaling laws," *Computational Materials Science*, vol. 125, pp. 319–327, 2016.

[11] A. Khoei and M. Khorrami, "Mechanical properties of graphene oxide: A molecular dynamics study," *Fullerenes, Nanotubes and Carbon Nanostructures*, vol. 24, no. 9, pp. 594–603, 2016.

[12] A. A. Balandin, "Thermal properties of graphene and nanostructured carbon materials," *Nature materials*, vol. 10, no. 8, p. 569, 2011.

[13] E. Pop, V. Varshney, and A. K. Roy, "Thermal properties of graphene: Fundamentals and applications," *MRS bulletin*, vol. 37, no. 12, pp. 1273–1281, 2012.

[14] T. Y. Kim, C.-H. Park, and N. Marzari, "The electronic thermal conductivity of graphene," *Nano letters*, vol. 16, no. 4, pp. 2439–2443, 2016.

[15] Z. Fan, L. F. C. Pereira, P. Hirvonen, M. M. Ervasti, K. R. Elder, D. Donadio, T. Ala-Nissila, and A. Harju, "Thermal conductivity decomposition in two-dimensional materials: Application to graphene," *Physical Review B*, vol. 95, no. 14, p. 144309, 2017.

[16] A. C. Neto, F. Guinea, N. M. Peres, K. S. Novoselov, and A. K. Geim, "The electronic properties of graphene," *Reviews of modern physics*, vol. 81, no. 1, p. 109, 2009.

[17] P. Ulloa, A. Latgé, L. E. Oliveira, and M. Pacheco, "Cone-like graphene nanostructures: electronic and optical properties," *Nanoscale research letters*, vol. 8, no. 1, p. 384, 2013.

[18] D. Qian, "A multiscale approach to the influence of geometry and deformation on the electronic properties of carbon nanotubes," in *IUTAM Symposium on Surface Effects in the Mechanics of Nanomaterials and Heterostructures*, pp. 247–255, Springer, 2013.

[19] J. Baringhaus, M. Ruan, F. Edler, A. Tejeda, M. Sicot, A. Taleb-Ibrahimi, A.-P. Li, Z. Jiang, E. H. Conrad, C. Berger, *et al.*, "Exceptional ballistic transport in epitaxial graphene nanoribbons," *Nature*, vol. 506, no. 7488, p. 349, 2014.

[20] T. Natsuki, "Theoretical analysis of vibration frequency of graphene sheets used as nanomechanical mass sensor," *Electronics*, vol. 4, no. 4, pp. 723–738, 2015.

[21] J. Liu, "Charging graphene for energy," *Nature nanotechnology*, vol. 9, no. 10, p. 739, 2014.

[22] K. Kostarelos and K. S. Novoselov, "Graphene devices for life," *Nature nanotechnology*, vol. 9, no. 10, p. 744, 2014.

[23] S. Böhm, "Graphene against corrosion," *Nature nanotechnology*, vol. 9, no. 10, p. 741, 2014.

[24] B. Marinho, M. Ghislandi, E. Tkalya, C. E. Koning, and G. de With, "Electrical conductivity of compacts of graphene, multi-wall carbon nanotubes, carbon black, and graphite powder," *Powder Technology*, vol. 221, pp. 351–358, 2012.

[25] B. Galindo, S. G. Alcolea, J. Gómez, A. Navas, A. O. Murguialday, M. P. Fernandez, and R. Puelles, "Effect of the number of layers of graphene on the electrical properties of tpu polymers," in *IOP Conference Series: Materials Science and Engineering*, vol. 64, p. 012008, IOP Publishing, 2014.

[26] K. Spanos, S. Georgantzinos, and N. Anifantis, "Mechanical properties of graphene nanocomposites: A multiscale finite element prediction," *Composite Structures*, vol. 132, pp. 536–544, 2015.

[27] R. Atif, I. Shyha, and F. Inam, "Mechanical, thermal, and electrical properties of graphene-epoxy nanocompositesa review," *Polymers*, vol. 8, no. 8, p. 281, 2016.

[28] X. Xia, J. Hao, Y. Wang, Z. Zhong, and G. J. Weng, "Theory of electrical conductivity and dielectric permittivity of highly aligned graphene-based nanocomposites," *Journal of Physics: Condensed Matter*, vol. 29, no. 20, p. 205702, 2017.

[29] J. Lee and B. Lee, "Modal analysis of carbon nanotubes and nanocones using fem," *Computational Materials Science*, vol. 51, no. 1, pp. 30–42, 2012.

[30] Z. ZHOU, D. QIAN, V. K. VASUDEVAN, and R. S. RUOFF, "Folding mechanics of bi-layer graphene sheet," *Nano LIFE*, vol. 2, no. 02, p. 1240007, 2012.

[31] M. Arroyo and T. Belytschko, "Finite crystal elasticity of carbon nanotubes based on the exponential cauchy-born rule," *Physical Review B*, vol. 69, no. 11, p. 115415, 2004.

[32] X. Guo, J. Wang, and H. Zhang, "Mechanical properties of single-walled carbon nanotubes based on higher order cauchy–born rule," *International Journal of Solids and Structures*, vol. 43, no. 5, pp. 1276–1290, 2006.

[33] J. Wang, X. Guo, H. Zhang, L. Wang, and J. Liao, "Energy and mechanical properties of single-walled carbon nanotubes predicted using the higher order cauchy-born rule," *Physical Review B*, vol. 73, no. 11, p. 115428, 2006.

[34] J. Yan, K. M. Liew, and L. He, "Predicting mechanical properties of single-walled carbon nanocones using a higher-order gradient continuum computational framework," *Composite Structures*, vol. 94, no. 11, pp. 3271–3277, 2012.

[35] V. Shenoy, R. Miller, E. Tadmor, D. Rodney, R. Phillips, and M. Ortiz, "An adaptive finite element approach to atomic-scale mechanicsthe quasicontinuum method," *Journal of the Mechanics and Physics of Solids*, vol. 47, no. 3, pp. 611–642, 1999.

[36] J. Yan, K. Liew, and L. He, "Buckling and post-buckling of single-wall carbon nanocones upon bending," *Composite Structures*, vol. 106, pp. 793–798, 2013.

[37] X. Wang, J. Wang, and X. Guo, "Finite deformation of single-walled carbon nanocones under axial compression using a temperature-related multiscale quasi-continuum model," *Computational Materials Science*, vol. 114, pp. 244–253, 2016.

[38] R. Firouz-Abadi, M. Fotouhi, and H. Haddadpour, "Free vibration analysis of nanocones using a nonlocal continuum model," *Physics Letters A*, vol. 375, no. 41, pp. 3593–3598, 2011.

[39] R. Firouz-Abadi, M. Fotouhi, and H. Haddadpour, "Stability analysis of nanocones under external pressure and axial compression using a nonlocal shell model," *Physica E: Low-dimensional Systems and Nanostructures*, vol. 44, no. 9, pp. 1832–1837, 2012.

[40] M. R. Gandomani, M. Noorian, H. Haddadpour, and M. Fotouhi, "Dynamic stability analysis of single walled carbon nanocone conveying fluid," *Computational Materials Science*, vol. 113, pp. 123–132, 2016.

[41] D. Sfyris, G. Sfyris, and C. Galiotis, "Curvature dependent surface energy for free standing monolayer graphene: Geometrical and material linearization with closed form solutions," *International Journal of Engineering Science*, vol. 85, pp. 224–233, 2014.

[42] M. Delfani and H. Shodja, "An exact analysis for the hoop elasticity and pressure-induced twist of cnt-nanovessels and cnt-nanopipes," *Mechanics of Materials*, vol. 82, pp. 47–62, 2015.

[43] M. Delfani and H. Shodja, "A large-deformation thin plate theory with application to one-atom-thick layers," *Journal of the Mechanics and Physics of Solids*, vol. 87, pp. 65–85, 2016.

[44] M. Delfani, H. Shodja, and F. Ojaghnezhad, "Mechanics and morphology of single-walled carbon nanotubes: from graphene to the elastica," *Philosophical Magazine*, vol. 93, no. 17, pp. 2057–2088, 2013.

[45] S. Kumar and D. M. Parks, "On the hyperelastic softening and elastic instabilities in graphene," *Proceedings of the Royal Society A: Mathematical, Physical and Engineering Sciences*, vol. 471, no. 2173, p. 20140567, 2015.

[46] R. Ghaffari, T. X. Duong, and R. A. Sauer, "A new shell formulation for graphene structures based on existing ab-initio data," *International Journal of Solids and Structures*, vol. 135, pp. 37–60, 2018.

[47] M. Itskov, *Tensor algebra and tensor analysis for engineers*. Springer, 2007.

[48] R. A. Sauer and T. X. Duong, "On the theoretical foundations of thin solid and liquid shells," *Mathematics and Mechanics of Solids*, vol. 22, no. 3, pp. 343–371, 2017.

[49] H. H. Pérez-Garza, E. W. Kievit, G. F. Schneider, and U. Staufer, "Highly strained graphene samples of varying thickness and comparison of their behaviour," *Nanotechnology*, vol. 25, no. 46, p. 465708, 2014.

[50] H. Tomori, A. Kanda, H. Goto, Y. Ootuka, K. Tsukagoshi, S. Moriyama, E. Watanabe, and D. Tsuya, "Introducing nonuniform strain to graphene using dielectric nanopillars," *Applied physics express*, vol. 4, no. 7, p. 075102, 2011.

[51] K. S. Kim, Y. Zhao, H. Jang, S. Y. Lee, J. M. Kim, K. S. Kim, J.-H. Ahn, P. Kim, J.-Y. Choi, and B. H. Hong, "Large-scale pattern growth of graphene films for stretchable transparent electrodes," *nature*, vol. 457, no. 7230, p. 706, 2009.

[52] C. Lee, X. Wei, J. W. Kysar, and J. Hone, "Measurement of the elastic properties and intrinsic strength of monolayer graphene," *science*, vol. 321, no. 5887, pp. 385–388, 2008.

[53] G. Cao, "Atomistic studies of mechanical properties of graphene," *Polymers*, vol. 6, no. 9, pp. 2404–2432, 2014.

[54] Q. Lu, W. Gao, and R. Huang, "Atomistic simulation and continuum modeling of graphene nanoribbons under uniaxial tension," *Modelling and Simulation in Materials Science and Engineering*, vol. 19, no. 5, p. 054006, 2011.

[55] Q. Lu, M. Arroyo, and R. Huang, "Elastic bending modulus of monolayer graphene," *Journal of Physics D: Applied Physics*, vol. 42, no. 10, p. 102002, 2009.

[56] M. Xu, J. T. Paci, J. Oswald, and T. Belytschko, "A constitutive equation for graphene based on density functional theory," *International Journal of Solids and Structures*, vol. 49, no. 18, pp. 2582–2589, 2012.

[57] H. M. Shodja, F. Ojaghnezhad, A. Etehadieh, and M. Tabatabaei, "Elastic moduli tensors, ideal strength, and morphology of stanene based on an enhanced continuum model and first principles," *Mechanics of Materials*, vol. 110, pp. 1–15, 2017.

[58] X. Wei, B. Fragneaud, C. A. Marianetti, and J. W. Kysar, "Nonlinear elastic behavior of graphene: Ab initio calculations to continuum description," *Physical Review B*, vol. 80, no. 20, p. 205407, 2009.

[59] H. Hencky, "The elastic behavior of vulcanized rubber," *Rubber Chemistry and Technology*, vol. 6, no. 2, pp. 217–224, 1933.

[60] H. Hencky, "The law of elasticity for isotropic and quasi-isotropic substances by finite deformations," *Journal of Rheology (1929-1932)*, vol. 2, no. 2, pp. 169–176, 1931.

[61] R. Ghaffari and R. A. Sauer, "A new efficient hyperelastic finite element model for graphene and its application to carbon nanotubes and nanocones," *Finite Elements in Analysis and Design*, vol. 146, pp. 42–61, 2018.

[62] Q.-S. Zheng, "Two-dimensional tensor function representation for all kinds of material symmetry," *Proceedings of the Royal Society of London. Series A: Mathematical and Physical Sciences*, vol. 443, no. 1917, pp. 127–138, 1993.

[63] J. Boehler, "On irreducible representations for isotropic scalar functions," *ZAMM-Journal of Applied Mathematics and Mechanics/Zeitschrift für Angewandte Mathematik und Mechanik*, vol. 57, no. 6, pp. 323–327, 1977.

[64] J.-P. Boehler, "A simple derivation of representations for non-polynomial constitutive equations in some cases of anisotropy," *ZAMM-Journal of Applied Mathematics and Mechanics/Zeitschrift für Angewandte Mathematik und Mechanik*, vol. 59, no. 4, pp. 157–167, 1979.

[65] E. Kiral and G. Smith, "On the constitutive relations for anisotropic materialstriclinic, monoclinic, rhombic, tetragonal and hexagonal crystal systems," *International Journal of Engineering Science*, vol. 12, no. 6, pp. 471–490, 1974.

[66] G. Smith, M. Smith, and R. Rivlin, "Integrity bases for a symmetric tensor and a vectorthe crystal classes," *Archive for Rational Mechanics and Analysis*, vol. 12, no. 1, pp. 93–133, 1963.

[67] J. H. Rose, J. Ferrante, and J. R. Smith, "Universal binding energy curves for metals and bimetallic interfaces," *Physical Review Letters*, vol. 47, no. 9, p. 675, 1981.

[68] J. H. Rose, J. R. Smith, and J. Ferrante, "Universal features of bonding in metals," *Physical review B*, vol. 28, no. 4, p. 1835, 1983.

[69] T. X. Duong, F. Roohbakhshan, and R. A. Sauer, "A new rotation-free isogeometric thin shell formulation and a corresponding continuity constraint for patch boundaries," *Computer Methods in Applied Mechanics and Engineering*, vol. 316, pp. 43–83, 2017.

[70] O. Kintzel, "Fourth-order tensors–tensor differentiation with applications to continuum mechanics. part ii: Tensor analysis on manifolds," *ZAMM-Journal of Applied Mathematics and Mechanics/Zeitschrift für Angewandte Mathematik und Mechanik: Applied Mathematics and Mechanics*, vol. 86, no. 4, pp. 312–334, 2006.

[71] O. Kintzel and Y. Başar, "Fourth-order tensors–tensor differentiation with applications to continuum mechanics. part i: Classical tensor analysis," *ZAMM-Journal of Applied Mathematics and Mechanics/Zeitschrift für Angewandte Mathematik und Mechanik: Applied Mathematics and Mechanics*, vol. 86, no. 4, pp. 291–311, 2006.

[72] P. Wriggers, *Nonlinear finite element methods*. Springer Science & Business Media, 2008.

[73] B. J. Alder and T. E. Wainwright, "Phase transition for a hard sphere system," *The Journal of chemical physics*, vol. 27, no. 5, pp. 1208–1209, 1957.

[74] J. Kołoczek, Y.-K. Kwon, and A. Burian, "Characterization of spatial correlations in carbon nanotubes-modelling studies," *Journal of Alloys and Compounds*, vol. 328, no. 1-2, pp. 222–225, 2001.

[75] J. A. Jaszczak, G. W. Robinson, S. Dimovski, and Y. Gogotsi, "Naturally occurring graphite cones," *Carbon*, vol. 41, no. 11, pp. 2085–2092, 2003.

[76] C.-T. Lin, C.-Y. Lee, H.-T. Chiu, and T.-S. Chin, "Graphene structure in carbon nanocones and nanodiscs," *Langmuir*, vol. 23, no. 26, pp. 12806–12810, 2007.

[77] D. Pettifor and I. Oleinik, "Analytic bond-order potentials beyond tersoff-brenner. i. theory," *Physical Review B*, vol. 59, no. 13, p. 8487, 1999.

[78] D. Pettifor and I. Oleinik, "Bounded analytic bond-order potentials for σ and π bonds," *Physical review letters*, vol. 84, no. 18, p. 4124, 2000.

[79] D. Pettifor and I. Oleinik, "Analytic bond-order potential for open and close-packed phases," *Physical Review B*, vol. 65, no. 17, p. 172103, 2002.

[80] D. Murdick, X. Zhou, H. Wadley, D. Nguyen-Manh, R. Drautz, and D. Pettifor, "Analytic bond-order potential for the gallium arsenide system," *Physical Review B*, vol. 73, no. 4, p. 045206, 2006.

[81] D. K. Ward, X. W. Zhou, B. M. Wong, F. Doty, and J. Zimmerman, "Analytical bond-order potential for the cadmium telluride binary system," *Physical Review B*, vol. 85, no. 11, p. 115206, 2012.

[82] LAMMPS, "Lammps documentation," 2019.

[83] NIST, "nteratomic potentials repository."

[84] E. B. Tadmor and R. E. Miller, *Modeling materials: continuum, atomistic and multiscale techniques*. Cambridge University Press, 2011.

[85] Q.-S. Zheng, "Theory of representations for tensor functionsa unified invariant approach to constitutive equations," *Applied Mechanics Reviews*, vol. 47, no. 11, pp. 545–587, 1994.

[86] P. Neff and I.-D. Ghiba, "The exponentiated hencky-logarithmic strain energy: part iiicoupling with idealized multiplicative isotropic finite strain plasticity," *Continuum Mechanics and Thermodynamics*, vol. 28, no. 1-2, pp. 477–487, 2016.

[87] P. Neff, I.-D. Ghiba, and J. Lankeit, "The exponentiated hencky-logarithmic strain energy. part i: Constitutive issues and rank-one convexity," *Journal of Elasticity*, vol. 121, no. 2, pp. 143–234, 2015.

[88] P. Neff, B. Eidel, F. Osterbrink, and R. Martin, "The hencky strain energy log u 2 measures the geodesic distance of the deformation gradient to so (n) in the canonical left-invariant riemannian metric on gl (n)," *PAMM*, vol. 13, no. 1, pp. 369–370, 2013.

[89] J. Bonet, A. J. Gil, and R. D. Wood, *Nonlinear solid mechanics for finite element analysis: statics*. Cambridge University Press, 2016.